Australian Water Availability Project (AWAP): CSIRO Marine and Atmospheric Research Component: Final Report for Phase 3

M.R. Raupach, P.R. Briggs, V. Haverd, E.A. King, M. Paget and C.M. Trudinger

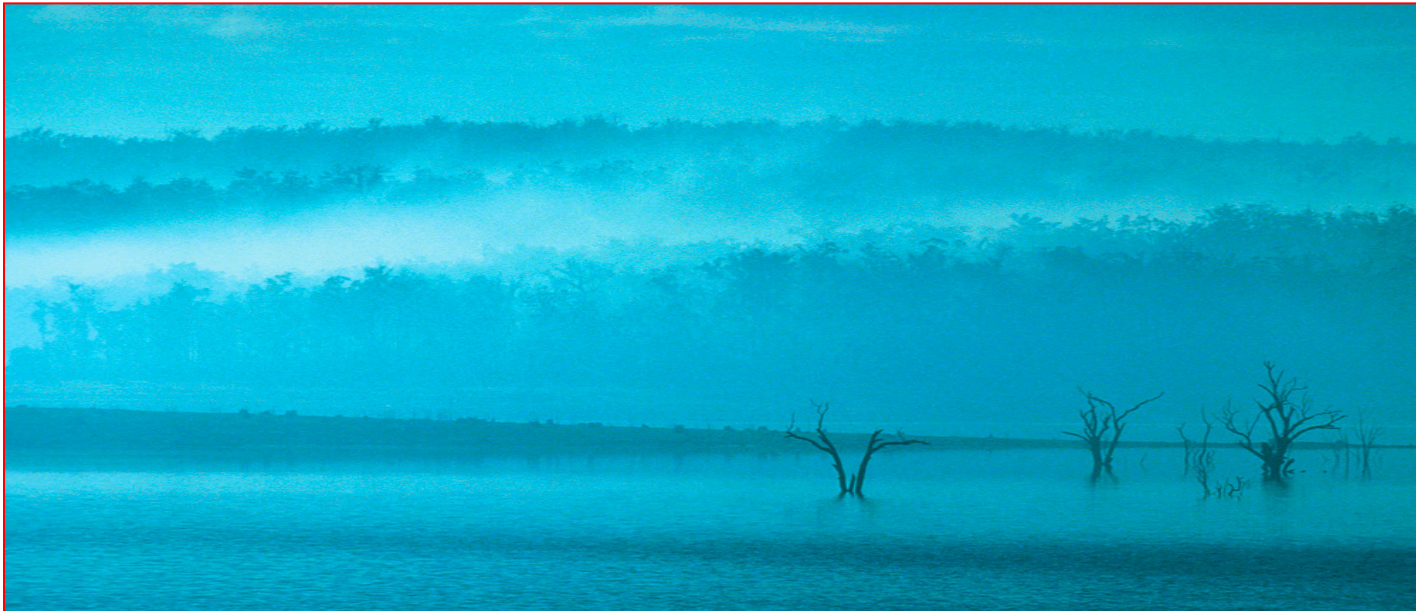**CAWCR Technical Report No. 013**

July 2009

www.cawcr.gov.au

Australian Water Availability Project (AWAP): CSIRO Marine and Atmospheric Research Component: Final Report for Phase 3

M.R. Raupach, P.R. Briggs, V. Haverd, E.A. King, M. Paget and C.M. Trudinger

CAWCR Technical Report No. 013

July 2009

Centre for Australian Weather and Climate Research, a Partnership between the Bureau of Meteorology and CSIRO, Melbourne, Australia

Enquiries should be addressed to:
Dr Michael Raupach
CSIRO Marine and Atmospheric Research
Global Carbon Project
GPO Box 3023, Canberra ACT 2601
Australia

Michael.Raupach@csiro.au

Copyright and Disclaimer

Australian Water Availability Project (AWAP)

CSIRO Marine and Atmospheric Research Component: Final Report for Phase 3

**M.R. Raupach, P.R. Briggs, V. Haverd, E.A. King,
M. Paget, C.M. Trudinger**

Percent Rank Relative Soil Moisture (Lower Layer) [%]   2007/01/01 to 2007/12/31
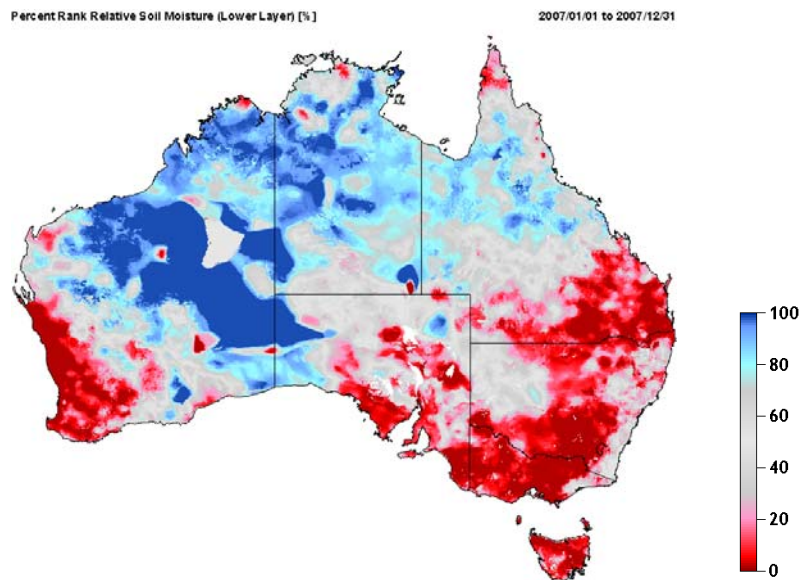
Mean percentile rank of relative water content in lower soil layer, Jan-Dec 2007
Grey = median, red = dry anomaly, blue = wet anomaly

**CSIRO Marine and Atmospheric Research, Canberra, Australia
9 September 2008**

www.csiro.au/awap

1

Contents

Cover photo: Storm clouds near Goulburn, NSW, by Greg Heath. Used with appreciation.

Summary

Context: The aim of the Australian Water Availability Project (AWAP) is to monitor the state and trend of the terrestrial water balance of the Australian continent, using model-data fusion methods to combine measurements and model predictions. The project determines the past history and present state of soil moisture and all water fluxes contributing to changes in soil moisture (rainfall, transpiration, soil evaporation, surface runoff and deep drainage), across the entire Australian continent at a spatial resolution of 5 km. Information is provided through a web interface in three forms: (1) weekly near-real-time reporting, (2) historical monthly time series (1900 to present), and (3) monthly climatologies.

AWAP is a joint effort by CSIRO Marine and Atmospheric Research (CMAR), the Bureau of Meteorology (BoM) and the Bureau of Rural Science (BRS).

This report describes the CMAR contribution to Phase 3 (2007-08) of AWAP, and also provides a consolidated description of CMAR work through the entire project, thereby summarising and in some areas superseding previous CMAR reports on Phase 1 (2005-06) and Phase 2 (2006-07).

Overall achievements: Development of the AWAP water balance framework has yielded the following overall achievements (with Phase 3 components identified):

- *Model:* A simple, robust water balance model has been developed in a way which facilitates model-data fusion. Specifically in Phase 3, the model has been provided with an option to use observed vegetation greenness (as remotely-sensed Fraction of Absorbed Photosynthetically Active Radiation, FAPAR) instead of model predictions for vegetation cover. This option has produced a significant improvement in water balance predictions.

- *Near-real-time operational system:* The operational system is now delivering publicly available operational water balance products at (http://www.csiro.au/awap/), including near-real-time information at weekly intervals from March 2007 to the present, and monthly historic information from 1900 to 2007. In phase 3, the prototype operational system from Phase 2 has been streamlined, made more robust, and documented. Work is under way to transfer the CMAR operational system for water balance products to BoM as the primary operational agency, where it will work alongside the BoM operational system for daily gridded meteorological fields.

- *Water balance history and climatology:* Using the simplified model with monthly climatological vegetation greenness, Phase 3 has delivered a 108-year (1900 to present) historic record of the full terrestrial water balance for the Australian continent, at 5 km spatial and monthly time resolution (aggregated from daily calculations). Quantities determined include soil moisture in two layers and terrestrial water fluxes due to rainfall, transpiration, soil evaporation, surface runoff and deep drainage. Results have been tested successfully against multi-decadal streamflow data in 200 unimpaired catchments.

Scientific contributions: New research opportunities are offered by the AWAP water balance framework and results, especially the 108-year record of the Australian terrestrial water balance. This report outlines first steps in four such investigations:

- *Drivers of recent water balance trends:* AWAP water balance results have been used to quantify the amplification of rainfall perturbations in total runoff perturbations. In particular, we have analysed the drivers of the recent (post 2002) decline in gauged flow in the Murray-Darling Basin (gauged at Wentworth on the River Murray), to just 23% of its pre-2002 average value. This was caused by three sequential factors: (1) a decrease in precipitation, to 81% of its pre-2002 average; (2) a decrease in the fraction of precipitation appearing runoff, to 41% of its pre-2002 average; and (3) a decrease in the fraction of runoff reaching the river gauge, to 68% of its pre-2002 average. These factors combine multiplicatively ($0.23 = 0.81 \times 0.41 \times 0.68$). It is concluded that the largest contributor to the recent decline in river flow is a strong decrease in the fraction of precipitation appearing as runoff, followed in significance by a decline in the fraction of runoff reaching the river gauge, and finally by a decline in the precipitation itself.

- *Climate-water connections:* The AWAP water balance dataset, extending from 1900 to present, provides an improved tool for investigating climatological relationships between terrestrial water stores and fluxes and climate modes influencing Australian hydrology, including ENSO (El Nino-Southern Oscillation), IOD (Indian Ocean Dipole), SAM (Southern Annular Mode) and others. Here we report an enhancement of the correlation between ENSO and properties of the water balance when soil moisture is used as the water balance property rather than precipitation.

- *Assimilation of remotely sensed land surface temperature:* A new approach has been developed to overcome earlier difficulties in the assimilation of remotely sensed land surface temperature (LST), in which observed LST perturbations are used with a data-derived mean aerodynamic conductance to constrain water balance fluctuations.

- *Testing CABLE:* The AWAP water balance framework (including continental datasets and modelling environment) has been used to test and improve CABLE, the land surface module for ACCESS, the new climate and earth system model being developed jointly by CSIRO and BoM through the Centre for Australian Weather and Climate Research (CAWCR). This work has identified a significant hydrological issue in that CABLE overestimates total runoff. A new soil hydrology scheme to fix the problem has been developed and is under test in the AWAP framework.

Future development: There are a number of areas where further development is required, including: (1) dynamic model development to incorporate a comprehensive treatment of plant carbon dynamics, better treatment of different land cover types, and a better treatment of soil evaporation; (2) improvement of the observation model for vegetation greenness; (3) access to more diverse remotely sensed data streams; (4) access to more timely hydrological data; (5) implementation of the Ensemble Kalman Filter in operational mode.

1   Introduction

The aim of the Australian Water Availability Project (AWAP) is to monitor the state and trend of the terrestrial water balance of the Australian continent, using model-data fusion methods to combine measurements and model predictions. The project determines the past history and present state of soil moisture and all water fluxes contributing to changes in soil moisture (rainfall, transpiration, soil evaporation, surface runoff and deep drainage), across the entire Australian continent at a spatial resolution of 5 km. With a single framework, the project provides soil moistures and water fluxes over the Australian continent in three forms: weekly in near-real-time, historical monthly time series (1900 to present), and monthly climatologies.

The long-term intention is to contribute to integrated monitoring and understanding of the dynamics of Australian landscape systems, especially responses to climate variability and change, and thus to assist adaptive, system-wide management.

The approach is based on model-data fusion, the combination of information from both data and models to maximise knowledge about the system (Raupach *et al.* 2005b; Raupach *et al.* 2006, Trudinger *et al.* 2007; Trudinger *et al.* 2008). Figure 1 shows the seven main components of a generic model-data fusion application: (1) forcing data, (2) data for assimilation, (3) the model, (4) prior information, (5) the model-data fusion process, (6) a product interface (here the operational system), and (7) mechanisms for product utilisation. Later sections of this report show how the present work utilises this framework.

Organisationally, AWAP is a partnership between CSIRO Marine and Atmospheric Research (CMAR), the Bureau of Meteorology (BoM) and the Bureau of Rural Science (BRS). Their respective primary roles are to provide water balance products (CMAR), high-resolution meteorological data (BoM) and policy uptake (BRS). The project has run since 2005 in three phases: Phase 1 from January 2005 to June 2006 (Raupach *et al.* 2006), Phase 2 to June 2007 (Raupach *et al.* 2007), and Phase 3 from to June 2008 (reported here).

The two milestones for AWAP Phase 3 (from the Collaborative Research and Development Agreement for AWAP Phase 3, CMAR component) are: (1) to consolidate advances made in 2005-07 through further development of dynamic and observation models and further development of the model-data fusion methodology; and (2) write up of the system in appropriate documentation and scientific papers. Delivery against the milestones is represented by: (1) this report, which provides system documentation and descriptions of progress in several areas detailed below; (2) published papers (Raupach 2007; Trudinger *et al.* 2007; Trudinger *et al.* 2008) and five papers in preparation emanating from the results presented below; and (3) the AWAP operational system (http://www.csiro.au/awap/).

The report is structured into two parts, augmented by Appendices. The first part, comprising Sections 1 to 4, describes the model framework and basic results. After the present introductory Section 1, Section 2 outlines the water balance model and the model-data fusion framework, Section 3 describes parameter estimation methods and model tests, and Section 4 describes results on current and historic Australian water balances.

The second part, comprising Sections 5 to 8, reports initial explorations in four scientific areas opened by the AWAP framework. Section 5 applies AWAP results to diagnose drivers of

recent declines in Murray River flow, Section 6 describes observed relationships between ENSO and the Australian water balance, Section 7 outlines a novel approach for the assimilation of remotely sensed land surface temperature (LST), and Section 8 describes application of the AWAP framework to test and improve CABLE (Kowalczyk *et al.* 2006), the land surface module for ACCESS, the new climate and earth system model being developed jointly by CSIRO and BoM.

Six Appendices provide technical detail: Appendix A covers the dynamic model; Appendix B the observation models, Appendix C the model parameters and forcing data; Appendix D the land surface temperature algorithm; Appendix E the remote sensing data sources; and Appendix F briefly describes the operational system.

Through the above structure, this report serves three purposes. First, it delivers on the CMAR contribution to AWAP Phase 3. Second (in Sections 1 to 4 and Appendices) it provides a consolidated description of CMAR work through the entire project, thereby summarising and superseding previous CMAR reports on Phases 1 and 2. Third (in Sections 5 to 8) it provides a forward perspective on research opportunities opened by the AWAP framework and results.
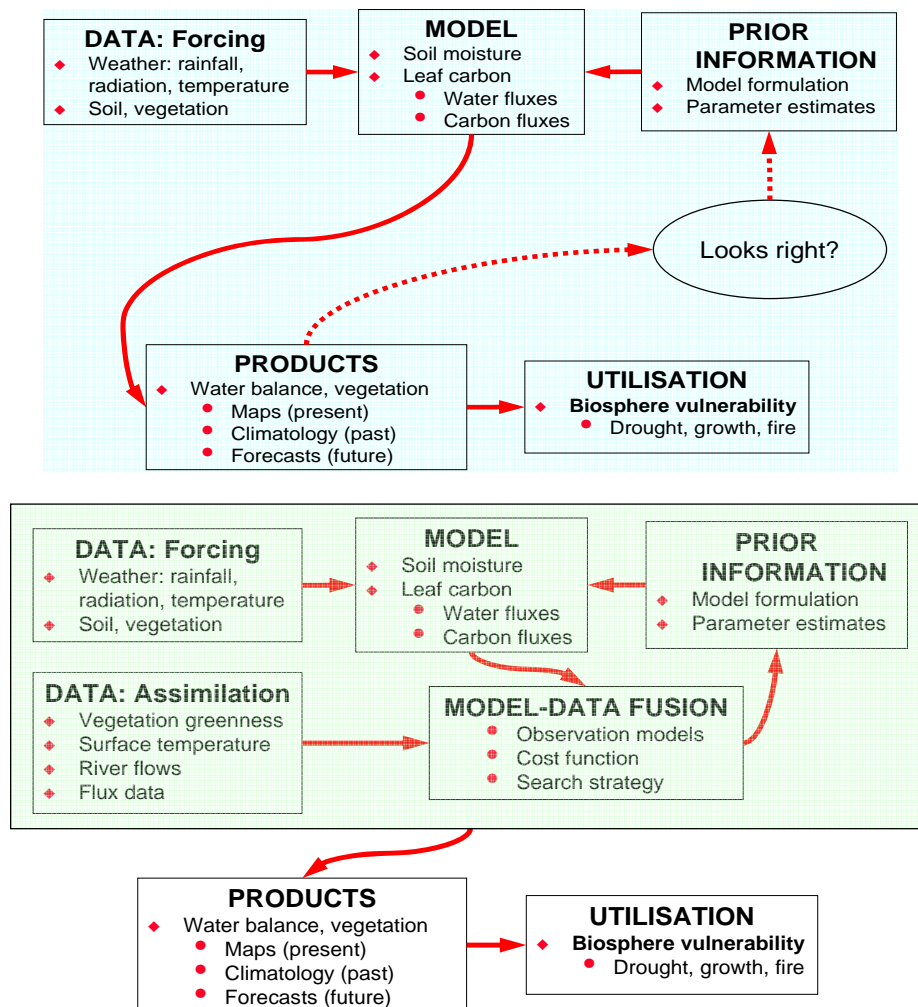

Figure 1: Schematic representation of components of a terrestrial-biosphere data assimilation system. Upper panel: without data assimilation; lower panel: with data assimilation.

2 Modelling Framework

2.1 Water balance model

State variables and water balance equations: The terrestrial water balance considered in this work applies to water in the (mainly) unsaturated soil column, spatially resolved across the Australian continent. This is defined using two control volumes consisting of "shallow" (typically to depth 0.2 m) and "deep" (typically 0.2 to 1.5 m) soil layers. The model state variables are the water stores (W_1, W_2) in these layers, or equivalently the relative soil water contents (w_1, w_2). A mass balance of water equates the change in the soil water store in each control volume to the sum of the water fluxes across the boundaries of the volume:

$$dW_1/dt \;=\; F_{WPrec} \;-\; F_{WTra1} \;-\; F_{WSoil} \;-\; F_{WRun} \;-\; F_{WLch1} \qquad \text{(M1)}$$

| Change of soil water in layer 1 | Precipitation | Transpiration from layer 1 | Soil Evaporation | Surface Runoff | Leaching from layer 1 to 2 |

$$dW_2/dt \;=\; F_{WLch1} \;-\; F_{WLch2} \;-\; F_{WTra2} \qquad \text{(M2)}$$

| Change of soil water in layer 2 | Leaching from layer 1 to 2 | Deep Drainage | Transpiration from layer 2 |

Blue and red colours identify input and output fluxes, respectively. Equations in the main report are numbered (M1), (M2), … to distinguish them from equations in appendices.

Note that liquid water in aquifers, rivers and reservoirs is governed by mass balances in different control volumes, outside those for soil water. Some of the outflow fluxes in Equations (M1) and (M2), such as surface runoff and deep drainage, are inputs to liquid-water control volumes.

Phenomenological equations: It is necessary to specify the water fluxes (F_W) on the right hand side of Equations (M1) and (M2) in terms of the state variables (the water stores W_1, W_2), forcing meteorological variables, and numerical parameters. We refer to these specifications generically as "phenomenological equations"; the term is borrowed from thermodynamics, where similar specifications are needed (Prigogine 1961; Raupach *et al.* 2005a; Raupach *et al.* 2005b). The term is also a reminder that these specifications are almost always partly phenomenological in character, even in the most process-based of models.

The phenomenological equations used here are described fully in Appendix A. They are based on the following principles.

1. *Precipitation* (F_{WPrec}) is an external input.

2. *Transpiration* (F_{WTra}), made up of contributions from each soil layer (F_{WTra1}, F_{WTra2}), is defined as the lesser of energy-limited and water-limited transpiration rates. The energy-limited rate is defined by the Priestley-Taylor evaporation rate attenuated by the vegetation cover fraction (v), for reasons of both physics (Raupach 2000, Raupach 2001) and simplicity. The water-limited transpiration rate in each soil layer is specified using a rate parameter k_E which controls the decay of water extraction by roots from a drying soil under water-limited transpiration and full vegetation cover.

3. *Soil evaporation* (F_{WSoil}) the product of an upper-limit value (Priestley-Taylor evaporation), the relative water content in the upper soil layer raised to power (a model parameter), and the fraction of bare soil ($1-v$).

4. *Surface runoff* (F_{WRun}) is given by a step function: all precipitation runs off when the upper-layer soil is saturated, and there is no runoff otherwise.

5. *Leaching* (F_{WLch}) or drainage downward out of each soil layer is given by the product of saturated hydraulic conductivity and a power (γ) of the relative water content in that layer.

The sum of transpiration and soil evaporation is the total evapotranspiration, denoted $F_{WE} = F_{WTra} + F_{WSoil}$. The sum of surface runoff and deep drainage is the total runoff or local discharge flux of water from the soil column, denoted $F_{WDis} = F_{WRun} + F_{WLch2}$.

Model scope and complexity: The full dynamic water balance model, called "WaterDyn", consists of Equations (M1), (M2) and the phenomenological equations, with meteorological forcing data and parameters specified below; see Appendices A to C for full details.

To indicate the scope of the model, Figure 2 shows spatially averaged monthly time series of meteorological forcing data and selected outputs over the Murrumbidgee drainage basin (see Figure 3 for a map), for the period 1981 to 2006. Model outputs include the relative soil moisture in two layers (w_1, w_2) (second panel in Figure 2), and all water fluxes appearing in Equations (M1) and (M2) (third and fourth panels). Meteorological forcing data (top panel of Figure 2) include precipitation, downward solar irradiance, and maximum and minimum air temperatures, and soil, vegetation and process parameters described below.

The model is deliberately kept as simple as possible for three reasons: to maximise robustness, to facilitate parameterisation at continental scale, and to provide the greatest possible numerical efficiency to expedite repeated tests and multi-member ensemble runs. To maximise efficiency, the WaterDyn code (in Fortran 95) performs parallel calculations for all grid cells in a computational domain. Overheads from read and write operations are kept low by optimising disk access procedures. On a typical workstation (2 Gflops s^{-1}) a continental run of 278000 grid cells for 100 years takes about 60 hr of processing time.

Process descriptions in this model are simple in comparison with many terrestrial biosphere models, including the land surface components of most Global Climate Models (GCMs). Nevertheless, all major water fluxes are represented by phenomenological equations which are appropriate at aggregation of several kilometres, using a minimal number of parameters. These choices reflect the outcome of tradeoffs between simplicity and complexity in terrestrial biosphere modelling, arising from two basic issues. First, large-scale parameterisations for strongly nonlinear processes such as drainage and surface runoff need to be different from those at small scales, such as the Richards equation for soil water movement, because interactions between nonlinearity and small-scale variability do not allow phenomenological equations to be scale-invariant (Raupach *et al.* 2005a). The second issue arises from the problem of "equifinality" (Beven 1995) in which parameters are effectively unresolvable because multiple parameter choices yield similar model performance. This is a strong argument for keeping model complexity as low as possible.
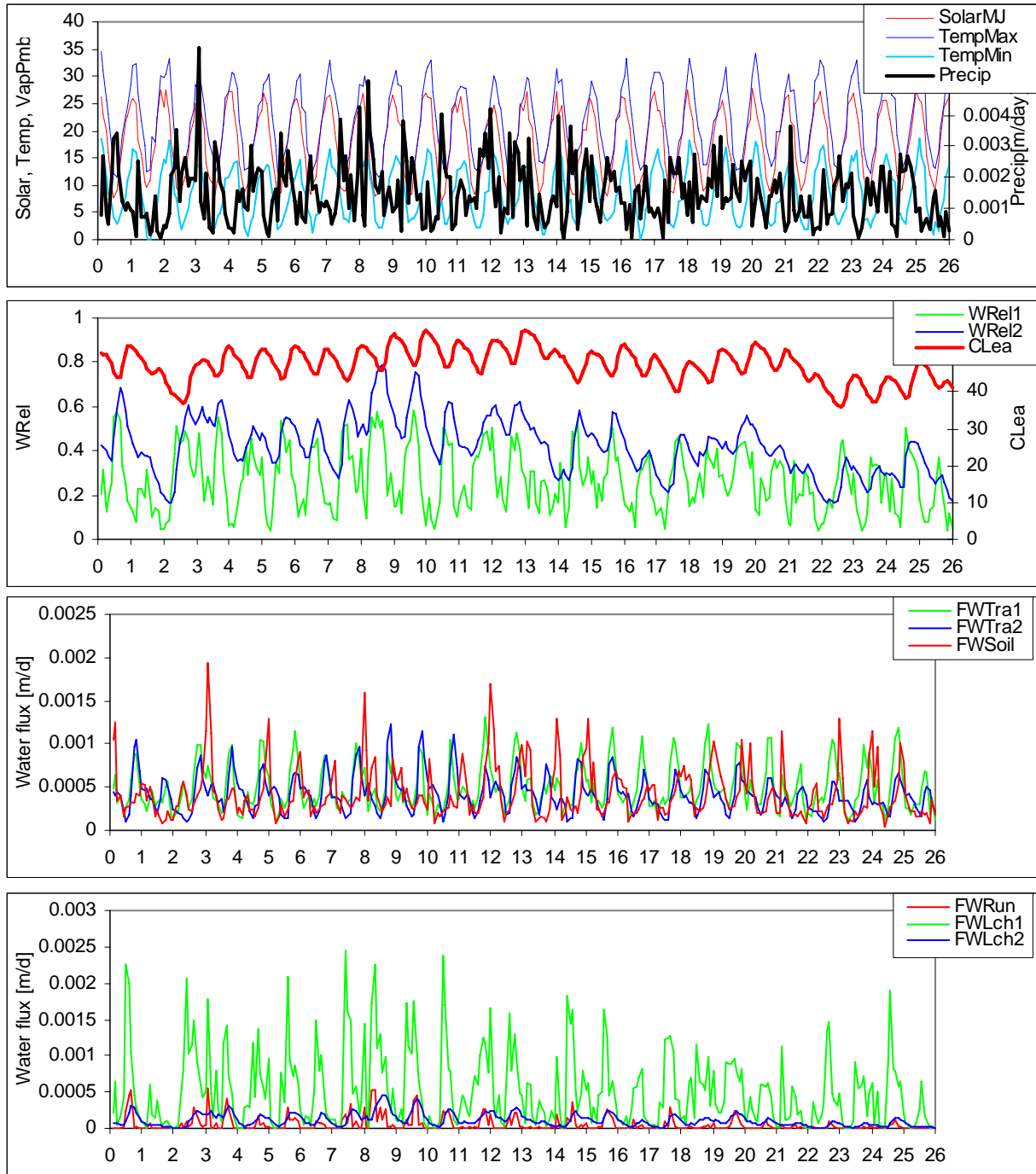
Figure 2: Spatially averaged monthly time series of WaterDyn inputs and selected outputs over the Murrumbidgee catchment. Time axis (0 to 26 years) runs from 1-jan-1981 to 31-dec-2006. Top panel: meteorological forcing, including precipitation, solar irradiance and daily maximum and minimum air temperatures; second panel: computed state variables, consisting of relative soil moisture in two layers ($w_{1,2}$) and green-leaf carbon store C_L (molC m^{-2}) (note that the computed store C_L is not used for water balance calculations); third panel: water fluxes contributing to evapotranspiration (including transpiration from upper and lower soil layers and soil evaporation); fourth panel: fluxes contributing to total runoff (including surface runoff, drainage from layer 1 to layer 2, deep drainage out of layer 2). Model version and run: WaterDyn25M, Murrumbidgee25b2.

Development and operational systems: The modelling framework is implemented in two systems which both use the same core model (WaterDyn): a development system is used for model tests and long-term historic runs, and an operational system for near-real-time products. In the operational system, the core model is run on a weekly cycle in a script environment (written in PERL) which automatically carries out tasks associated with data acquisition, pre-processing, model execution, post-processing and web display; see Appendix F for more detail.

The model and runs are version-controlled[1]; version numbers are given for all results.

2.2   *Data*

The model requires meteorological forcing data, specifications of soil and vegetation properties, and data for parameter estimation and model testing. These are described briefly below, with further details in Appendix C.

Meteorological forcing: Gridded daily meteorological forcing data are required for precipitation, downward solar irradiance, and maximum and minimum air temperatures. Historic data (mainly from 1900 to present), gridded across the Australian continent at 0.05 deg spatial resolution, are available from two sources: BoM (Jones *et al.* 2007), and SILO (Jeffrey *et al.* 2001). BoM data are used in this report, unless indicated otherwise.

Soil and vegetation properties: Spatially explicit soil properties for the two soil layers in the model are defined by maps obtained from interpretations of the digital Atlas of Australian Soils (McKenzie and Hook 1992; McKenzie *et al.* 2000). This atlas classifies Australian soils into about 700 soil types, which are translated into soil physical properties using pedotransfer functions.

The vegetation cover fraction (v) is determined either externally or from a leaf carbon submodel. When v is externally prescribed (as for all results in this report) it is given from a remotely-sensed vegetation greenness obtained from a monthly climatology of Fraction of Absorbed Photosynthetically Active Radiation (FAPAR) from the SeaWiFS satellite.

Observations for parameter estimation and data assimilation: Two main kinds of observational data are used for parameter estimation and model testing: outflow or discharge from unimpaired catchments, and remotely sensed Land Surface Temperature (LST).

- Multidecadal records of daily outflow from approximately 200 nominally unimpaired gauged catchments, mostly in southeast Australia, have been consolidated and quality-controlled by Dr Francis Chiew and colleagues, CSIRO Land and Water. An unimpaired catchment is defined here as one in which there is no significant water extraction for human use or retention by dams, and where there is no subsurface horizontal water movement across the catchment boundaries. For such a catchment, the flow through the catchment gauge is approximately equal to the sum over the catchment area of the total

---

[1] A typical model version name is "WaterDyn25M", where "25" is the version number and "M" denotes the mode of operation (M for the forward model without model-data fusion). Version documentation is included in the code. In the development system a typical run identifier is "Australia25a", where "Australia" denotes the spatial domain, "25" is the model version number, and "a" distinguishes a run with unique, archived control file.

runoff ($F_{WDis} = F_{WRun} + F_{WLch2}$) from each land element, averaged over a time long enough that transmission delays from each land element to the gauge are negligible, and subsurface water storage changes are small compared with time integrated fluxes. Figure 3 shows the nominally unimpaired catchments in SE Australia for which outflow data are available; they cover a total of about 1.6% of the Australian land area. These data need to be used with two cautions in mind: first, they represent a biased sample (the mean precipitation on unimpaired catchments is over 900 mm y^{-1} compared with 465 mm y^{-1} for the whole Australian continent). Second, nominally unimpaired catchments may not actually satisfy the above definition of an unimpaired catchment (see Section 3.4). Nevertheless, the outflow data set from unimpaired catchments represents an invaluable resource for model testing and provides a primary constraint on the model water balance.

- Land Surface Temperature (LST) data provide a constraint on the surface energy balance. We use data on LST and Brightness Temperature (BT) for the Australian continent, from two sensors: NOAA-AVHRR and AATSR. Algorithmic details are given in Appendix D, and details of sensors and satellite platforms in Appendix E.
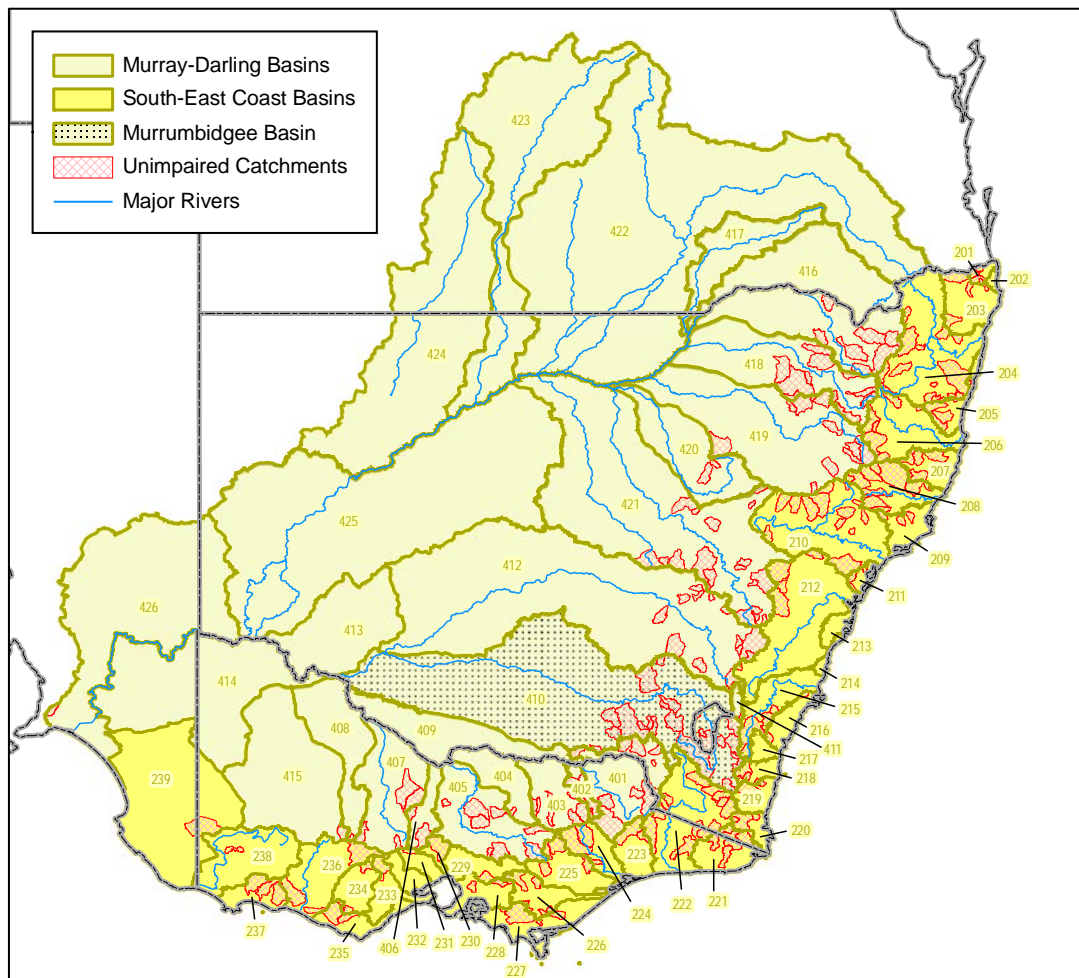

Figure 3: Nominally unimpaired catchments in southeast Australia (hatched red areas), superimposed on spatial domain maps for the Murray-Darling Basin (light olive) and South-East Coast Drainage Divisions as defined by the Australian National Resources Audit (ANRA) (NLWRA 2001a; NLWRA 2001b). The Murrumbidgee basin (410) is stippled in black.

3 Parameter estimation and model testing

3.1 *Parameter estimation methodology*

Most phenomenological equations for terrestrial biosphere models (including water balance models) contain parameters which have to be prescribed or estimated. In general, parameter estimation may be done either heuristically or with formal model-data fusion methods. The term "model-data fusion" describes a suite of techniques for combining measurements and models, broadly including both classical parameter estimation and data assimilation; see (Raupach *et al.* 2005b; Trudinger *et al.* 2007) for descriptions in the present context. All model-data fusion techniques involve four essential components: (1) a dynamic model (here the water balance model described above and in Appendix A); (2) a set of observations, together with observation models which project the predictions of the dynamic model into predictions of quantities for which measurements are available (as described in Appendix B); (3) a cost function measuring disagreement between model and observations (here a weighted sum of squared model-measurement differences); (4) a search strategy to find best estimates of "target variables", equal to the values which minimise the cost function. All formal model-data fusion methods yield not only the best estimates of the target variables but also about the uncertainty in those estimates. Figure 1 sketches the way that these elements fit into a system.

A long-term goal in AWAP is the operational implementation of a sequential (for example, Ensemble Kalman Filter) data assimilation system for terrestrial hydrology and biospheric dynamics, using the data described in the previous section and other sources. While parts of such a system have been developed, the present operational system does not yet use this system. Instead, it is based on batch-mode model-data fusion to estimate model parameters, as described in detail below.

In terrestrial biosphere modelling, parameter estimation faces two basic problems: The first is horizontal heterogeneity in parameter values, introduced by landscape variability. Because it is not possible to capture all this variability in practice, unrepresented variability is a source of spatial scatter in predictions. Second, "equifinality" (Beven 1995) occurs when a model performs similarly well against observations with multiple parameter sets, so that parameters are unresolvable. A single cost-function minimum in parameter space is surrounded by an effectively equifinal region if the minimum is at the bottom of a shallow valley.

In this work, the primary parameter estimation strategy involved three steps. First, a reference parameter set was determined using formal parameter estimation with a down-gradient search algorithm, applied to a limited set of training data. Second, sensitivities of key model outputs (water fluxes) to parameter values were determined to assess the extent to which parameter uncertainty affects results. Third, the model with the evaluated reference parameter set was subjected to several tests against a much broader set of observations. The latter two steps together indicate the implications of horizontal heterogeneity and equifinality.

3.2 *Reference parameter set*

Parameters in the present model are of two classes, spatially uniform (UU) and spatially explicit (VV), where the notation refers to the generic arrays used to hold the two parameter classes in the model code. The UU parameters are mainly process parameters. The VV parameters consist mainly of surface radiative, soil and vegetation properties specified in map form. A full list of all parameters in both classes is given in Appendix C.

For practical reasons all estimated parameters are located in the spatially uniform (UU) array. To admit some flexibility in the spatially explicit (VV) parameters while retaining the information in available maps, we introduced spatially uniform multipliers in the UU array for selected VV parameters; see Appendix C for details.

Formal parameter estimation was used to estimate nine of the UU parameters: (RateEW1, RateEW2, PwrFWSoil, PwrFWLch, ZSoil1Mult, ZSoil2Mult, HySat1Mult, HySat2Mult) = (k_{E1}, k_{E2}, β, γ, m_{Z1}, m_{Z2}, m_{K1}, m_{K2}). Appendix A and Table C1 describe the physical meanings of these quantities. The search algorithm was the Levenberg-Marquardt (LM) method implemented in the PEST software package (http://www.sspa.com/PEST/). To keep the dimension of the search space as low as possible (which helps both the speed and stability of the search), we did not estimate parameters which are immaterial for the water balance or for which good prior knowledge is available so that parameter estimation is unnecessary.

The cost function to be minimised was the sum of squared differences between monthly measured catchment outflows and monthly aggregates of modelled total runoff ($F_{WDis} = F_{WRun} + F_{WLch2}$), for the period 1981 to 2006, in six unimpaired gauged catchments in the Murrumbidgee basin. Table 1 gives basic properties of the six catchments used to providing this training data set.

Catchment	Catchment ID number	Area (km^2)	Rainfall (F_{WPrec}) (mm y^{-1})	Total runoff (F_{WDis}) (mm y^{-1})	Actual ET (F_{WE}) (mm y^{-1})	Potential ET ($F_{W(PT)}$) (mm y^{-1})
Adelong Creek @ Batlow Road	410061	155	1018	245	773	1237
Adjungbilly Creek @ Darbalara	410038	411	1044	203	841	1210
Billabong Creek @ Aberfeldy	410097	331	663	58	604	1277
Goobarragandra River @ Lacmalac	410057	673	1123	402	722	1176
Muttama Creek @ Coolac	410044	1025	648	47	601	1284
Tarcutta Creek @ Old Borambola	410047	1660	764	100	663	1279
Murrumbidgee basin	-	80 000	543	63	480	1328

Table 1: Properties of the 6 catchments used to provide training data, together with the Murrumbidgee basin (last line, grey highlight). All fluxes are averages over the period 1981 to 2006. Rainfall (F_{WPrec}) is aggregated from the gridded meteorological forcing data used throughout this work. Total runoff (F_{WDis}) is the observed catchment outflow, except for the Murrumbidgee basin where it is the aggregated model prediction for F_{WDis}. Actual ET figures in this table are differences ($F_{WPrec} - F_{WDis}$). Potential ET is Priestley-Taylor (Appendix A).

Figure 4 shows seven different estimates for each of the nine target parameters: one estimate from each the six individual catchments taken separately; and an estimate from the aggregate of all six catchments taken together (denoted Murrum6). The bars represent 95% confidence intervals derived from standard statistical methods (eg Press *et al.* 1992) implemented in the PEST software. The best-estimate parameter values vary among catchments, with some of the variability being statistically significant. Therefore, noise is introduced in model predictions because true, spatially varying parameter values are replaced by spatially uniform

values in the UU array. However, this is not as serious as it may appear at first sight because the sensitivities of most fluxes to most of the estimated parameters are relatively low (as shown below), so large relative errors in parameter values translate into smaller relative errors in predicted fluxes and soil moistures.
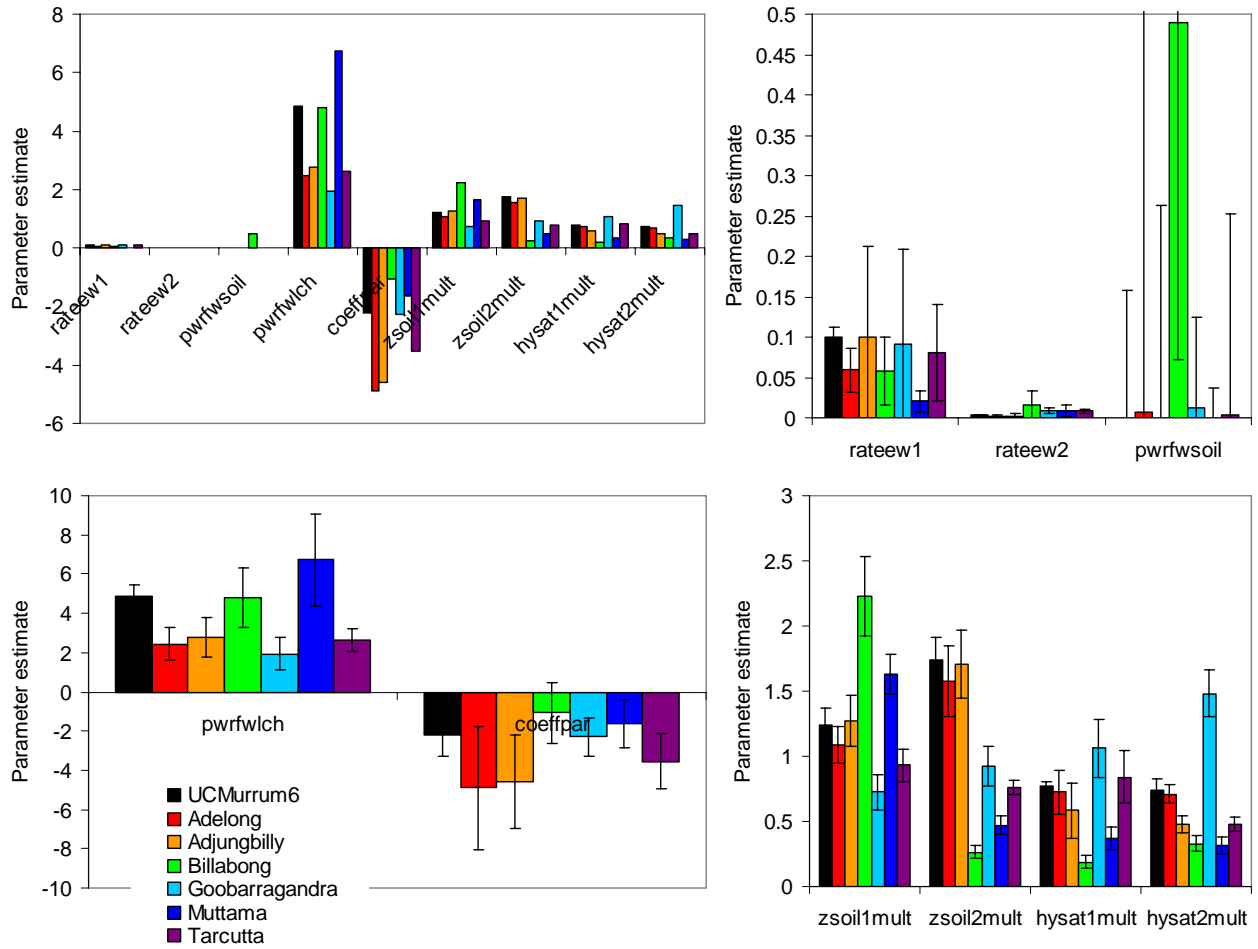
Figure 4: Estimates of 9 parameters (RateEW1, RateEW2, PwrFWSoil, PwrFWLch, CoeffPAR, ZSoil1Mult, ZSoil2Mult, HySat1Mult, HySat2Mult) = (k_{E1}, k_{E2}, β, γ, c_{PAR}, m_{Z1}, m_{Z2}, m_{K1}, m_{K2}) in 6 individual unimpaired catchments (coloured bars), and in all 6 catchments taken in aggregate (UCMurrum6, black bars). Top left panel shows estimates of all 9 parameters on the same scale; other panels show groups of parameters on suitably expanded scales. Parameter estimation is by the down-gradient Levenberg-Marquardt (LM) method implemented in the PEST software package (http://www.sspa.com/PEST/). Error bars denote 95% confidence intervals. Run: UCMurrum25 (PEST mode).

We determined a reference set of spatially uniform (UU) parameters by taking approximate averages across the spatially variable parameter estimates in Figure 4. This reference parameter set, given in Appendix C, was used in all subsequent work reported here.

In the reference parameter set we used map (Digital Atlas of Australian Soils) data for both soil depths and saturated volumetric water contents. However, we did not use the corresponding data for saturated hydraulic conductivities, because the map values of saturated hydraulic conductivity led to deterioration in model performance; map values had to be reduced by factors between 20 and 50 to recover reasonable model predictions. Possible reasons are: (1) landscape-scale properties associated with soil hydraulic conductivity in this

14

model are likely to differ from the small-scale soil physical definition of hydraulic conductivity, because of complications arising from upscaling in strongly heterogeneous media; and (2) inappropriate pedotransfer functions were used to derive soil hydraulic conductivities from soil types in the Digital Atlas of Australian Soils.

Figure 5 compares predicted and observed long-term mean outflow using the reference parameter set, for the six catchments in Table 1 over the period 1981 to 2006. The departure of the points from the 1:1 line is a measure of the scatter introduced by the use of single values for spatially uniform (UU) parameters, rather than values which are tuned for each catchment individually (which would force all points to lie on the 1:1 line).
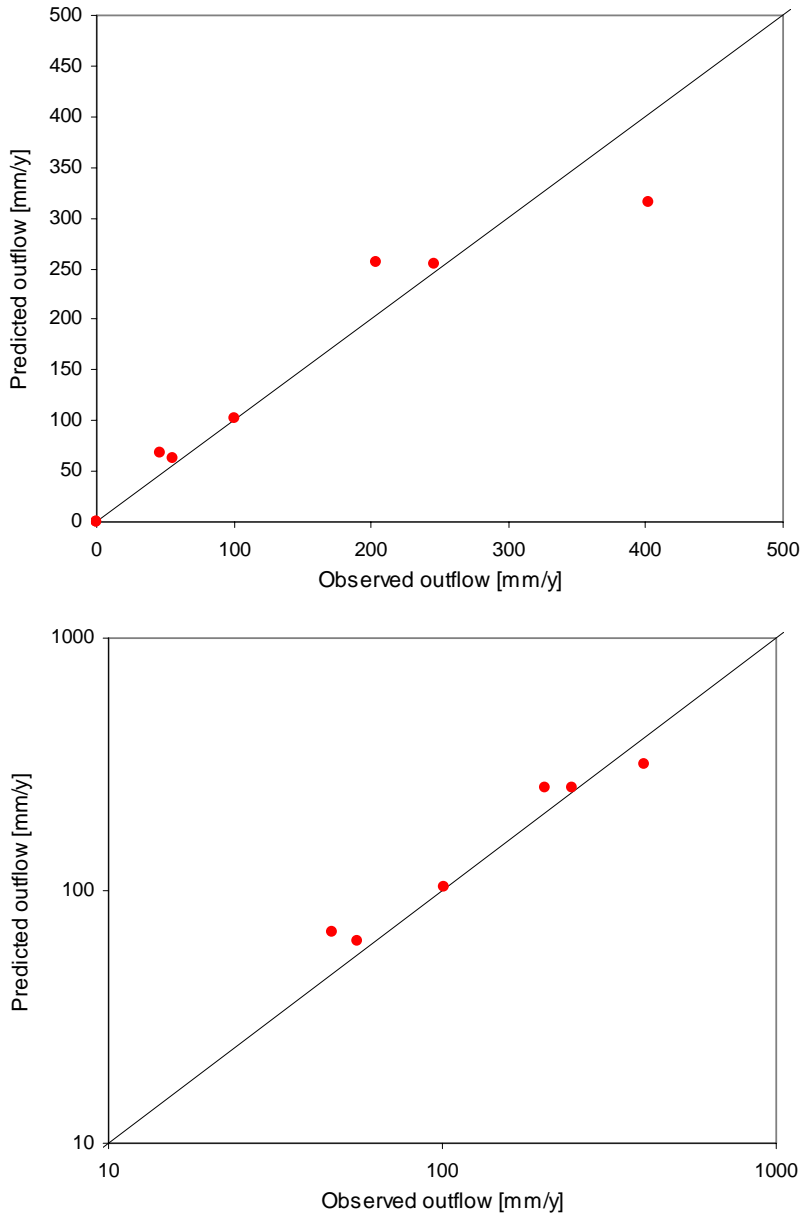

Figure 5: Predicted versus observed mean outflow (over available observations from 1981 to 2006 inclusive) for six nominally unimpaired gauged catchments in the Murrumbidgee basin (Table 1). Upper and lower panels use linear and logarithmic axes, respectively. Model version and run: WaterDyn25M, Murrumbidgee25b2.

3.3 Sensitivity analysis

The sensitivity of a model output variable (such as a water flux F_i) to a given parameter (p_j) is a dimensionless number, defined as

$$\text{Sensitivity}\left(F_i \text{ to } p_j\right) = \frac{\text{fractional change in } F_i}{\text{fractional change in } p_j} = \frac{p_j}{F_i}\frac{\partial F_i}{\partial p_j} \qquad \text{(M3)}$$

The partial derivatives are evaluated at a point in parameter space. Figures 6a and 6b show the sensitivities of selected fluxes to variation of significant model parameters, for the Adelong Creek catchment and the Murrumbidgee basin respectively. The Murrumbidgee basin includes the Adelong Creek catchment as a small subset, and is much larger and drier in spatial average (Table 1).

In Figure 6, each upper panel shows sensitivities of evapotranspiration ($F_{WE} = F_{WTra} + F_{WSoil}$) and its components, transpiration (F_{WTra}) and soil evaporation (F_{WSoil}). The lower panel shows the sensitivities of total runoff ($F_{WDis} = F_{WRun} + F_{WLch2}$) and its components, surface runoff (F_{WRun}) and deep drainage (F_{WLch2}). Sensitivities were calculated using small perturbations of parameters about their values in the reference parameter set. Sensitivities to spatially variable (VV) parameters were determined by the use of multipliers in the UU array.

Figure 6 reveals several aspects of the sensitivity of the model to its parameters. First, the broad behaviour of the sensitivities is similar in the Adelong Creek catchment and the Murrumbidgee basin, despite the Murrumbidgee basin on average being drier (runoff/rainfall ≈ 0.11) than the Adelong Creek catchment (runoff/rainfall ≈ 0.24).

Second, for variation of most parameters, the sensitivity of total runoff and its contributing fluxes is opposite to the sensitivity of evapotranspiration and its contributing fluxes, and larger in magnitude by a factor of 3 or more. This is a consequence of the relative magnitudes of the total runoff and evapotranspiration fluxes. The long-term mean water balance is $F_{WPrec} = F_{WE} + F_{WDis}$. Differentiating with respect to p_j (and noting that $\partial F_{WPrec}/\partial p_j = 0$ because F_{WPrec} is independent of parameters) we have $\partial F_{WDis}/\partial p_j = -\partial F_{WE}/\partial p_j$. It follows that the sensitivities of total runoff and evapotranspiration to a parameter p_j are related by

$$\text{Sensitivity}\left(F_{WDis} \text{ to } p_j\right) = \frac{F_{WE}}{F_{WDis}}\text{Sensitivity}\left(F_{WE} \text{ to } p_j\right)$$

The ratio of evapotranspiration to total runoff (F_{WE}/F_{WDis}) is about 3.5 in the Adelong Creek catchment and 8 in the Murrumbidgee basin (Table 1), consistent with the larger sensitivities of runoff than evapotranspiration fluxes to parameter variations in Figure 6.

Third, Figure 6 shows that most sensitive parameters are:
- the Priestley-Taylor coefficient (c_{PT}), albedo (a) and emissivity (e), which together influence the available energy and potential evaporation;
- FAPAR, which influences both energy-limited and water-limited transpiration.
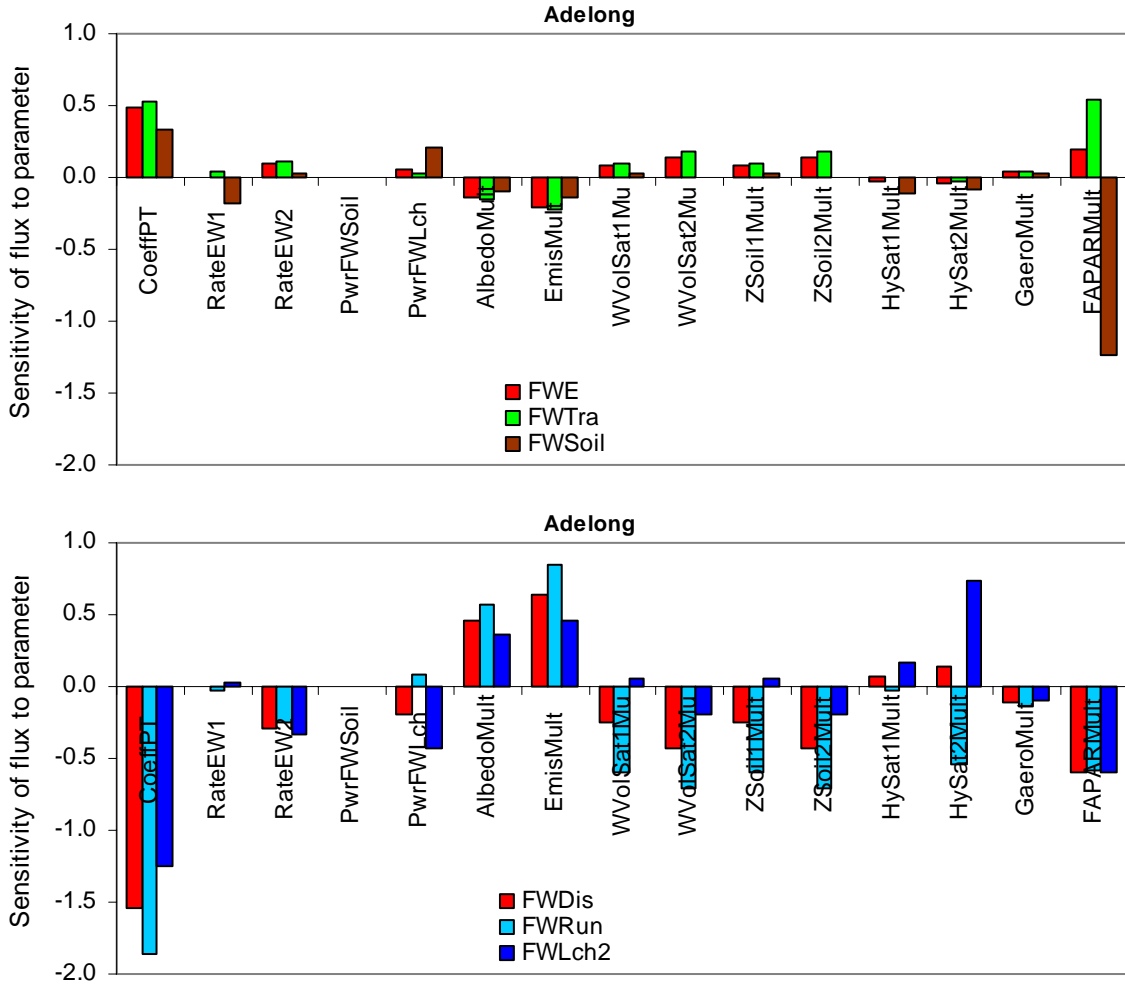
Figure 6a: Sensitivities of fluxes to parameters for the Adelong Creek catchment. Upper panel: total evapotranspiration ($F_{WE} = F_{WTra} + F_{WSoil}$) and its components, transpiration (F_{WTra}) and soil evaporation (F_{WSoil}). Lower panel: total runoff ($F_{WDis} = F_{WRun} + F_{WLch2}$) and its components, surface runoff (F_{WRun}) and deep drainage (F_{WLch2}). See Table C1 for parameter code names. Run: Adelong25b.
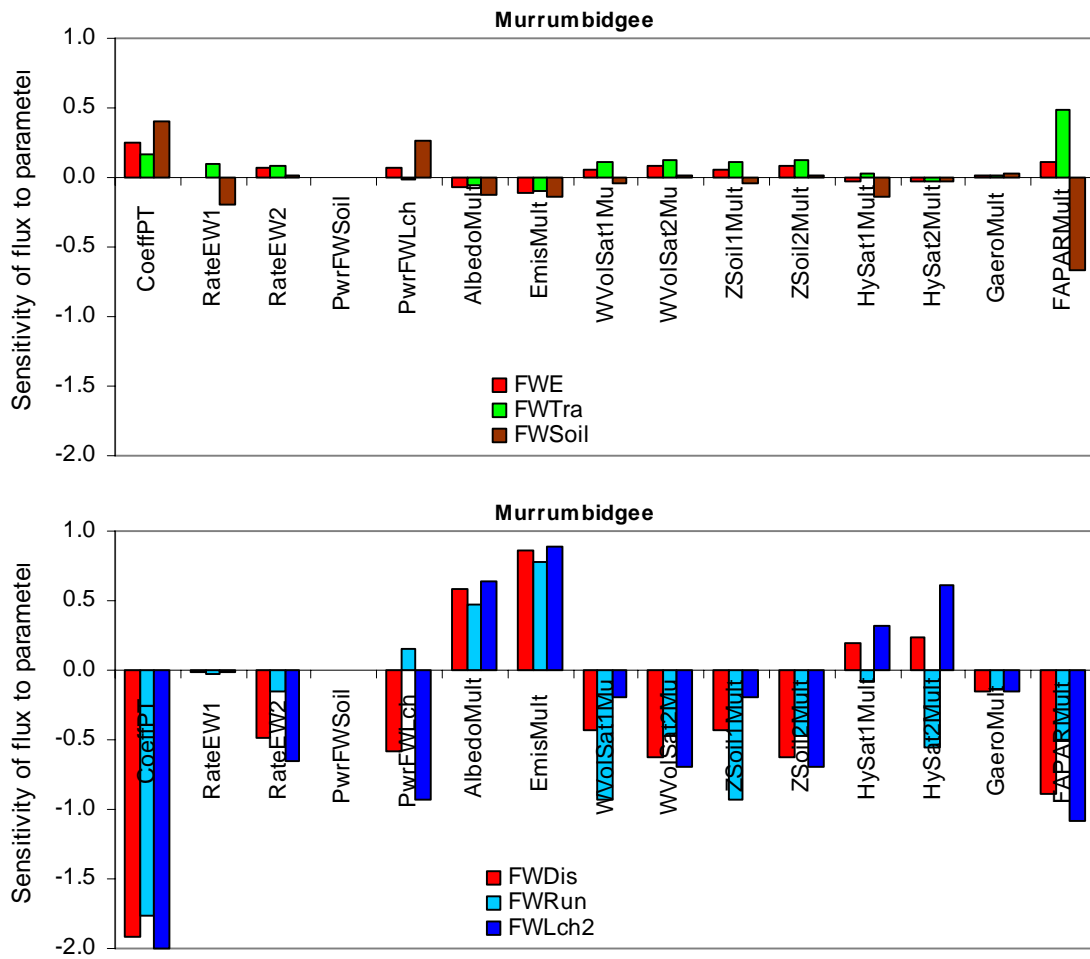
Figure 6b: Sensitivities of fluxes to parameters for the Murrumbidgee basin, with other details as for Figure 6a. Run: Murrumbidgee25b2.

3.4 Model tests

The full model, with the reference parameter set, has been subjected to several tests. The results indicate present strengths, limitations and directions for improvement of the model.

Long-term mean outflow: Figure 7 compares predicted and observed long-term mean outflow for the full available set of 200 unimpaired gauged catchments. This test is independent of the parameter estimation process because almost all of the points represent catchments not used for parameter estimation. There is spatial scatter (as anticipated above) but little evidence of bias across the range from dry to wet catchments. The main systematic departure of predictions from observations is a tendency for the model to overpredict measured outflows from dry (low-flow) catchments, evident in the lower panel of Figure 7 where logarithmic axes are used to expand the low-flow region. Two different possible causes for this trend are (1) model failure in low-flow environments, and (2) water extraction, so that some nominally unimpaired catchments do not satisfy the criteria for an unimpaired catchment given in Section 2.2, causing predicted total runoff to exceed gauged catchment outflow. These possibilities cannot presently be distinguished.

Monthly outflow: Figure 8a compares predicted and observed monthly outflow over the period 1981 to 2006 for four of the six test catchments in Table 1 (Goobarragandra, Adelong, Tarcutta and Muttama, in order of decreasing mean rainfall). The comparison is not independent of the parameter estimation process because these catchment data were used for that purpose, but it does indicate the effect of using spatially uniform rather than spatially varying parameters. In general, model performance at this monthly time scale is quite good.

Daily outflow: Figure 8b shows a similar comparison to Figure 8a, but for daily outflow over three years rather than monthly outflow. This test is independent of model parameterisation because daily outflow data were not used there in disaggregated form. The agreement at daily scale is not as good as for monthly outflow; the model tends to overpredict baseflow relative to peak daily flow in the Muttama catchment, and to underpredict in Goobarragandra, while in Adelong and Tarcutta the baseflow is relatively well predicted and daily peak flows are statistically reproduced, but specific peak daily flow events are often not predicted well. These results indicate two possible forms of model failure: (1) saturation in the upper soil layer water store in the model (which controls surface runoff) is not occurring at exactly the right times; and (2) the simple parameterisation for surface runoff (that runoff only occurs when the upper soil layer saturates) neglects infiltration excess runoff occurring when the instantaneous rainfall rate exceeds the local saturated hydraulic conductivity.

Inferior model performance at daily time scales relative to monthly and long-term time scales is expected, both because model parameterisations are not designed to simulate short-term dynamics, especially in surface runoff.

Aerodynamic conductance: A further model test is described in Section 7, where an estimate of long-term mean aerodynamic conductance from modelled sensible heat fluxes and observed surface-air temperature differences provides an indirect test of modelled spatial patterns of sensible heat flux.
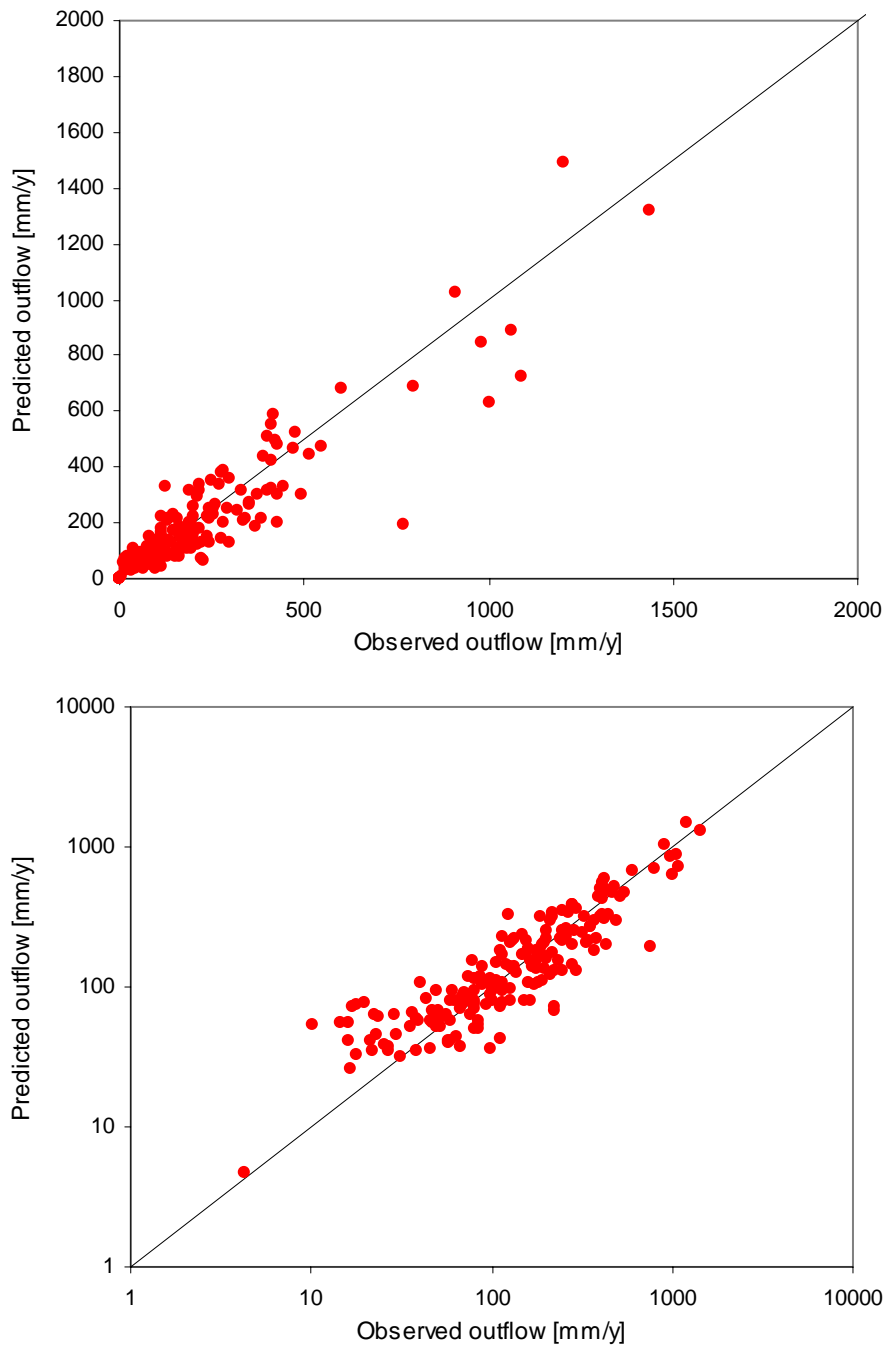
Figure 7: Predicted versus observed mean outflow (over available observations from 1981 to 2006 inclusive) for 200 unimpaired gauged catchments across Australia. Upper and lower panels use linear and logarithmic axes, respectively. Model version and run: WaterDyn25M, UCAll25b2.
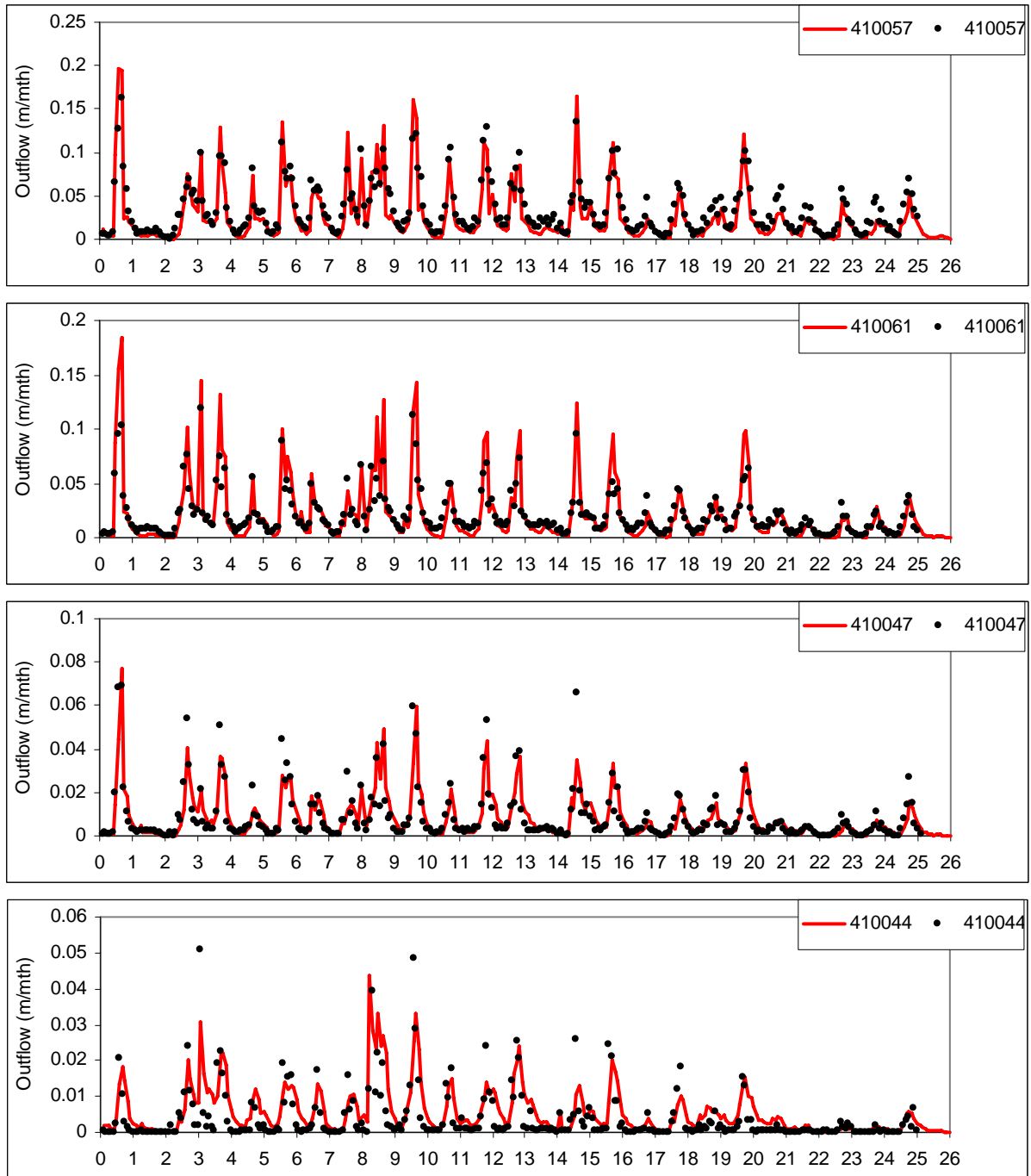
Figure 8a: Comparison of predicted (lines) and observed (points) monthly mean outflow for four unimpaired gauged catchments in the Murrumbidgee basin: Goobarragandra River at Lacmalac (410057), Adelong Creek at Batlow Road (410061), Tarcutta Creek at Old Borambola (410047) and Muttama Creek at Coolac (410044). Time axis (0 to 26 years) runs from 1-jan-1981 to 31-dec-2006. Model version and run: WaterDyn25M, Murrumbidgee25b2.
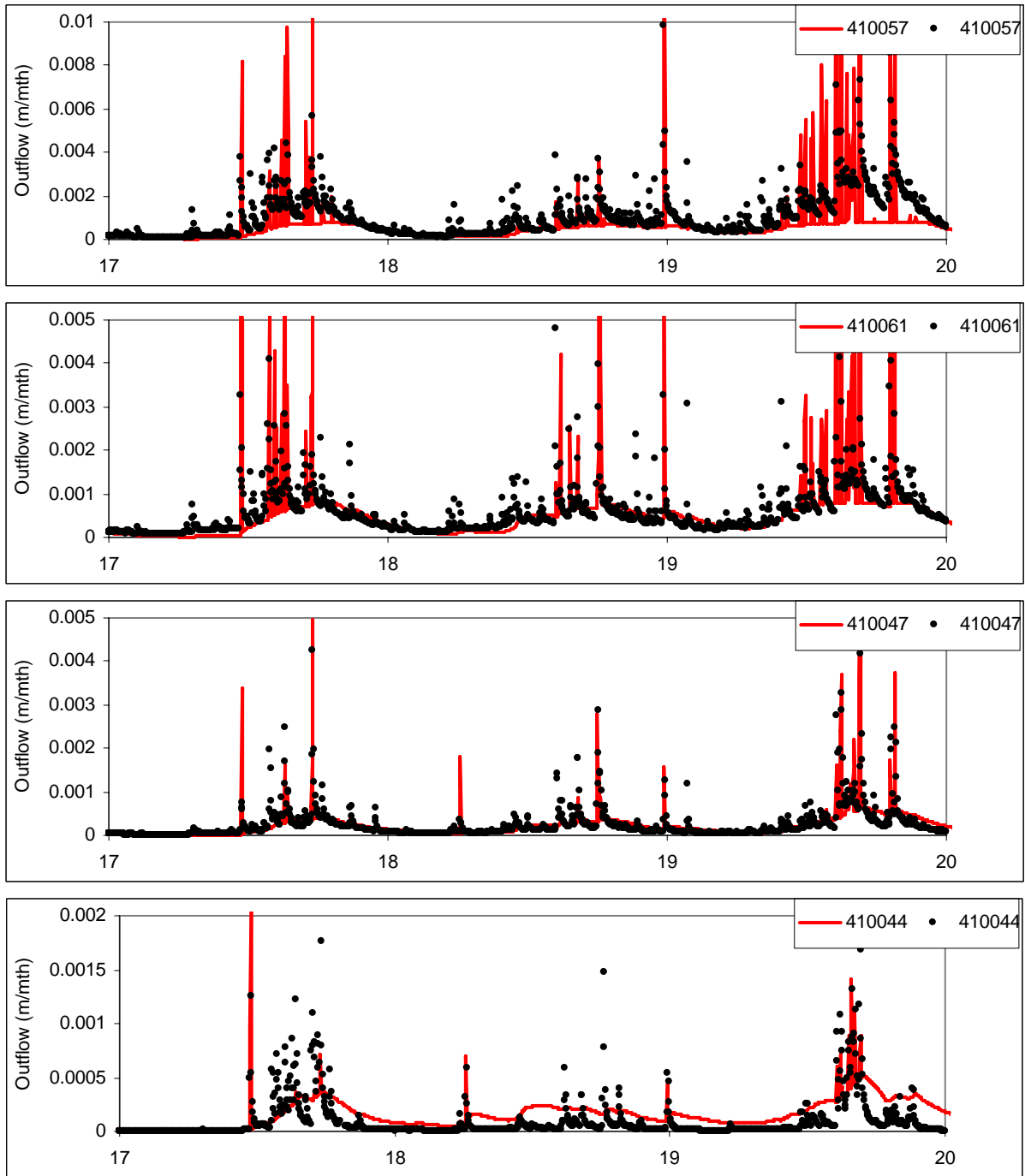
Figure 8b: As for Figure 8a, for daily outflow over 3 years. Time axis (17 to 20 years) runs from 1-jan-1998 to 31-dec-2000.

4 Australian Water Balance: Climatology and Recent Trends

A continental-scale model reference run has been used to determine the Australian terrestrial water balance at 0.05 deg scale for the 108-year period January 1900 to December 2007. This run uses BoM meteorological forcing data and reference values of spatially uniform parameters. The reference run also establishes a monthly climatology (on a reference period from 1961 to 1990) for all predicted water stores and fluxes, and meteorological forcing variables.

Figures 9a and 9b show continental time histories of the upper-layer and lower-layer relative soil moistures (w_1, w_2), as continental monthly map sequences from 1990 to 2007. To make dynamical variability clearer, these figures show percentile ranks about monthly climatologies (the rank of the current month in the cumulative probability distribution for that month over the climatological period 1961 to 1990, calculated separately at each 0.05 deg grid cell). Full map sequences of this kind from 1900 to 2007 are available on the AWAP website for all forcing variables (precipitation, solar irradiance and daily maximum and minimum air temperatures) and output variables (transpiration, soil evaporation, total evapotranspiration, surface runoff, deep drainage, total runoff, Priestley-Taylor potential evaporation).

Noteworthy in Figure 9 are the strong, widespread deficits in soil moisture in 1994, 2002 and 2006-07. Particularly in southern Australia, the soil moisture deficit relative to climatological average conditions has been acute for the whole period 2002 to 2007. This is due to the ongoing drought from 2002, probably coupled with higher temperatures and other stresses. Such a prolonged deep soil moisture deficit is already having ecological consequences such as increased mortality in mature native vegetation.

Figure 10 shows Australian monthly climatologies in dimensional units for all variables (precipitation, solar irradiance, daily maximum and minimum air temperatures, Priestley-Taylor potential evaporation, upper-layer and lower-layer relative water contents, total evapotranspiration, transpiration, soil evaporation, total runoff, surface runoff, and deep drainage). The climatological reference period is 1961-1990, except for solar irradiance which is a satellite-derived product available only for 1990 onward, so the climatological reference period for solar irradiance is 1990-2007.

A noteworthy feature of the climatologies, most clearly seen in upper-layer soil moisture but present in all water balance variables, is the large patch of very low rainfall in inland north of Western Australia. This region is very sparse in rainfall observations and it is possible that the rainfall gridding scheme is producing regions of near-zero long-term rainfall.
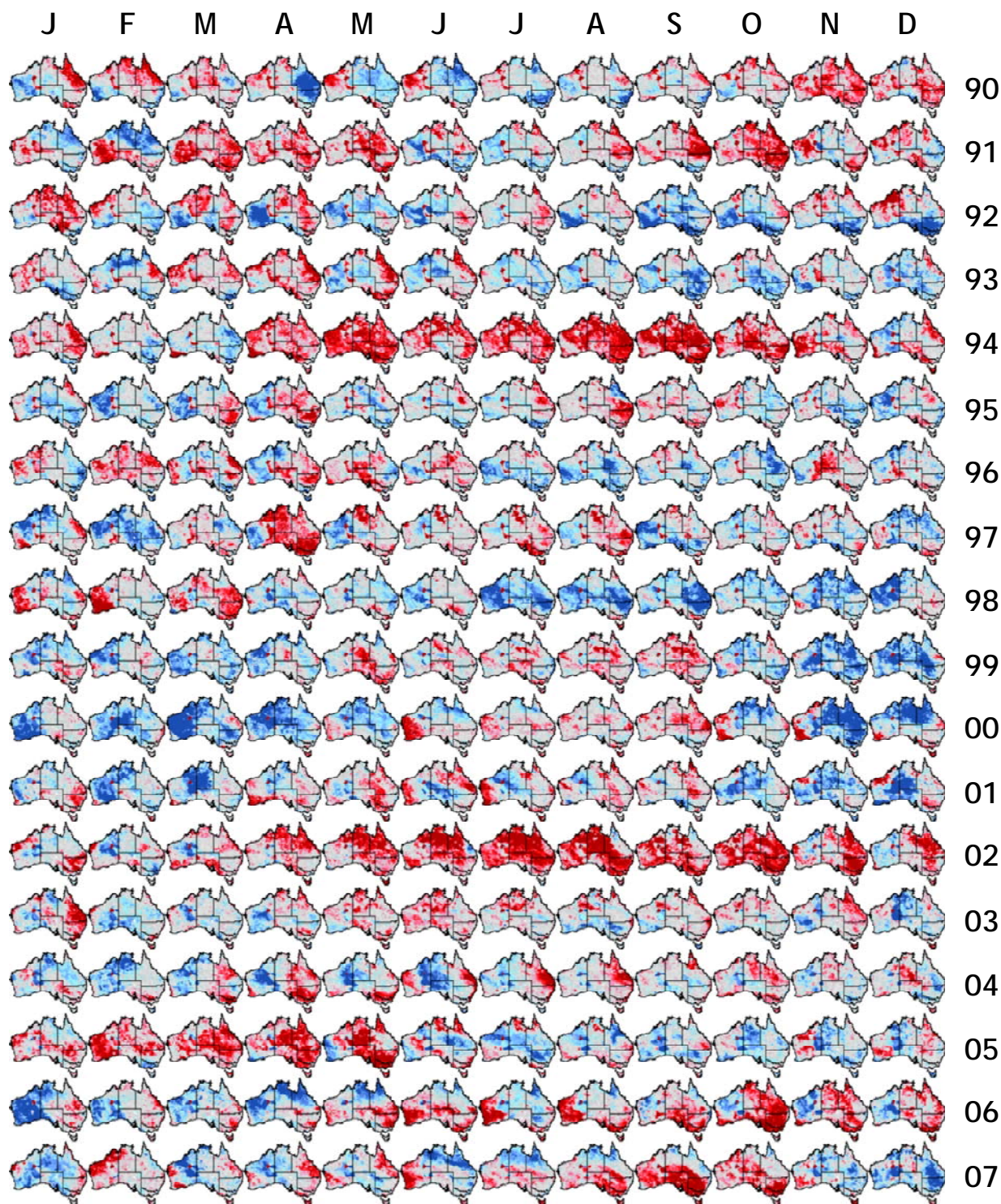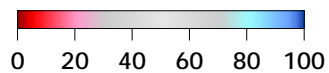
Figure 9a: Time series (1990-2007) of percentile rank of monthly upper-layer relative soil moisture (w_1) for Australia. Model version and run: WaterDyn25M, Australia25a.
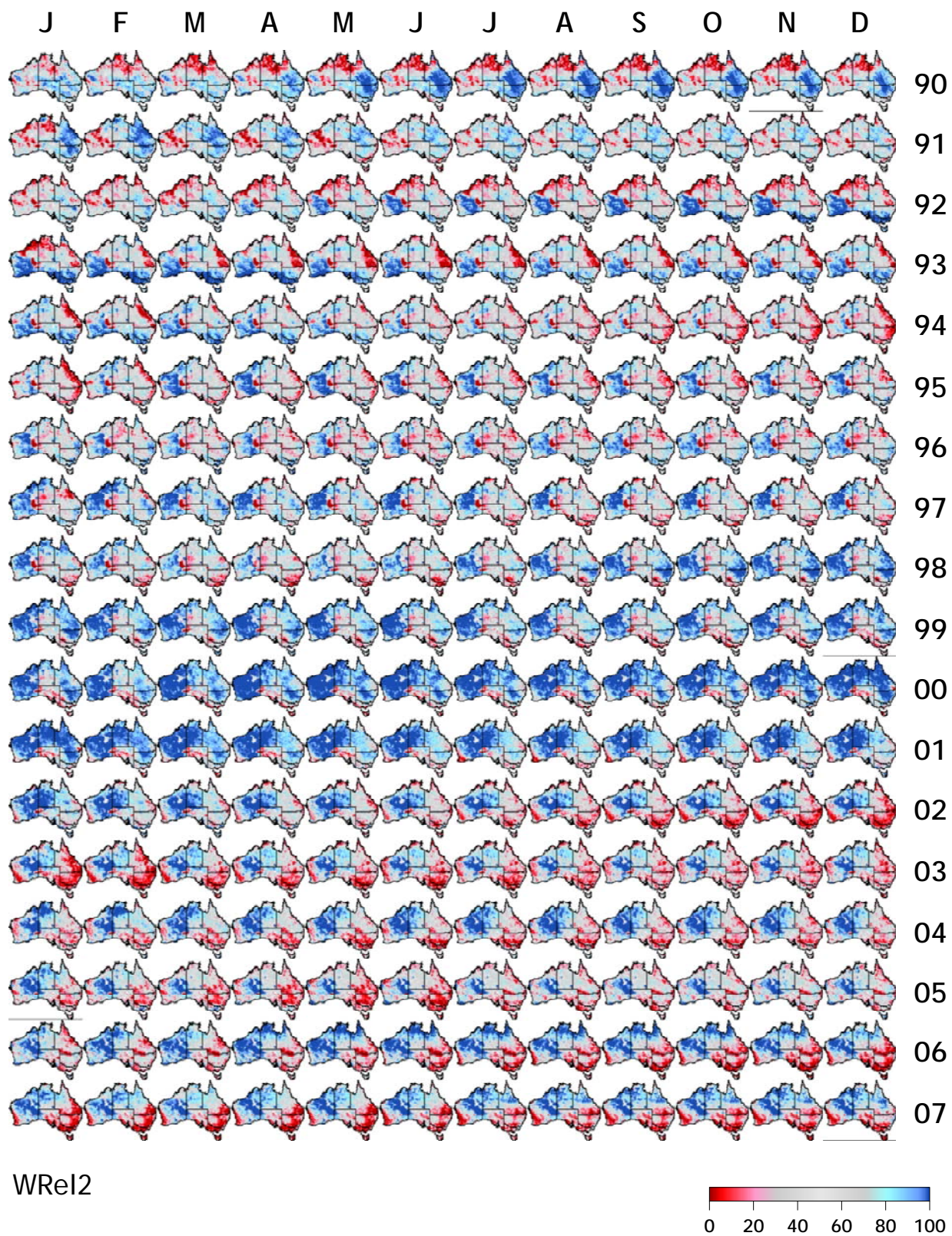
Figure 9b: As for Figure 9a, for monthly lower-layer relative soil moisture (w_2).
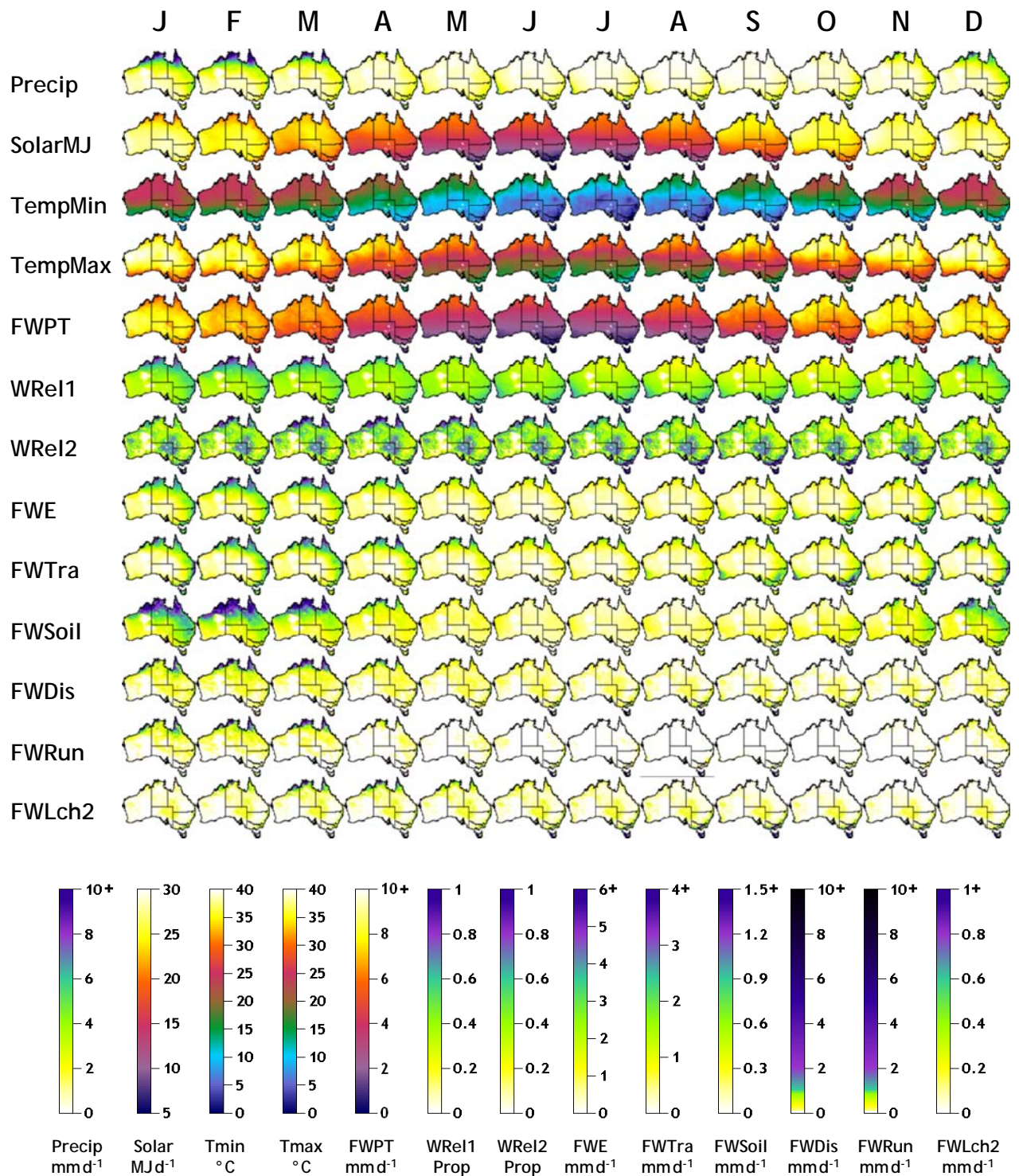
Figure 10: Australian monthly climatologies (reference period 1961-1990), except for solar irradiance (1990-2007). Variables: precipitation (Precip); solar irradiance (Solar); daily maximum and minimum air temperatures (Tmax, Tmin); Priestley-Taylor potential evaporation (FWPT); upper-layer and lower-layer relative water contents (WRel1, WRel2); total evapotranspiration (FWE); transpiration (FWTra), soil evaporation (FWSoil), total runoff (FWDis); surface runoff (FWRun), deep drainage (FWLch2). Model version and run: WaterDyn25M, Australia25a.

Legend:

- 1.1 NE Coast (Seaboard)
- 1.2 NE Coast (Burdekin-Fitzroy)
- 2 South-East Coast
- 3 Tasmania
- 4.1 MDB Wet Basins (Rain > 1000mm/y)
- 4.2 MDB Agric Basins (Rain 460mm to 1000 mm/y)
- 4.3 MDB Semi-Arid Basins (Rain < 460mm/y)
- 5 South Australian Gulfs
- 6 South-West Coast
- 7 Indian Ocean
- 8 Timor Sea
- 9 Gulf of Carpentaria
- 10 Lake Eyre
- 11 Bulloo-Bancannia
- 12 Western Plateau
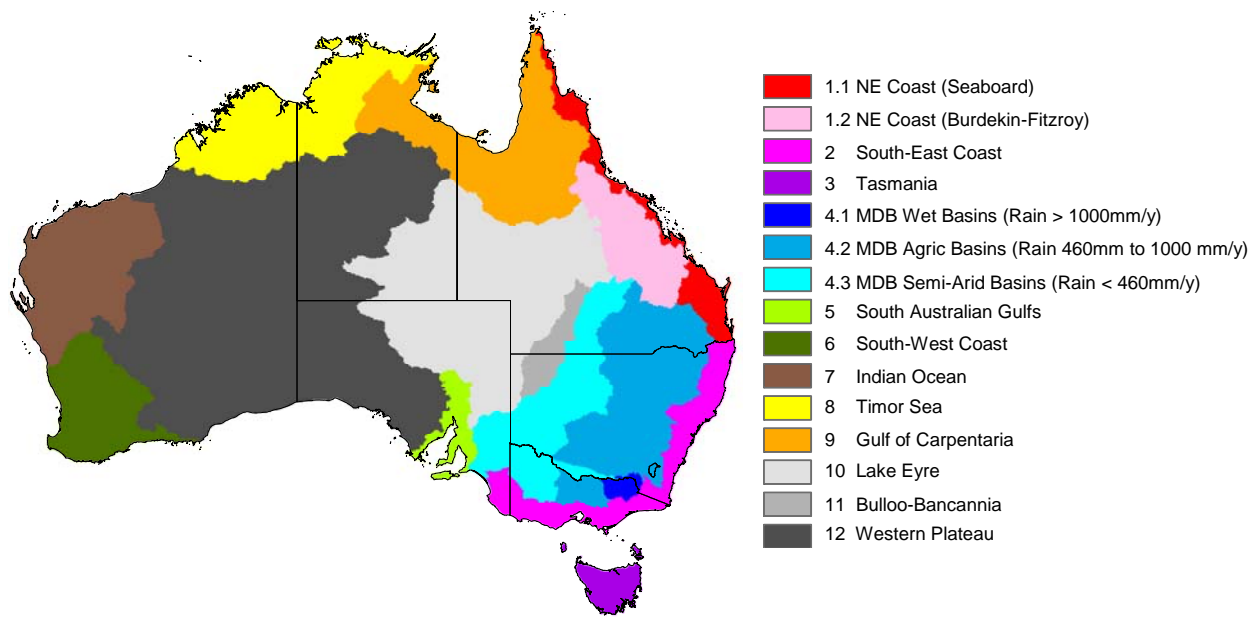
Figure 11: Regionalisation of the Australian continent into Australian National Resources Audit (ANRA) Drainage Divisions (NLWRA 2001a; NLWRA 2001b). There are 12 primary ANRA Drainage Divisions, each an aggregate of a number of Drainage Basins (see Figure 3 for examples). In the above regionalisation, two ANRA Divisions with highly diverse biogeography and hydroclimatology have been subdivided into parts which are still aggregates of Drainage Basins, as follows. The NE Coast (Division 1) has been divided into seaboard basins (denoted 1.1) and the Burdekin and Fitzroy basins (denoted 1.2) which are primarily inland and drier. The Murray-Darling Basin (Division 4) has been subdivided into wet, agricultural and semi-arid basins (respectively denoted 4.1, 4.2 and 4.3), where wet basins have mean annual rainfall exceeding 1000 mm y^{-1}, semi-arid basins have rainfall less than 460 mm y^{-1}, and agricultural basins fall between these points. The final regionalisation has 15 regions.

5   Recent Decline in Murray River Flow

It is well known that flows in the Murray-Darling Basin (MDB) have suffered major declines in recent years, accompanying the post-2002 drought. A map of the MDB is given in Figure 3. Figure 11 shows a regionalisation of the Australian continent, including the MDB, used below.

The flow in the Murray River recorded at Wentworth, just downstream of the confluence of the Murray and Darling Rivers, is shown in Figure 12 (bottom panel). Effectively all total runoff entering the MDB river system occurs upstream of this point. The average flow in the period 2002-2007 was just 23% of the average flow for the previous half century (1951-2001).

AWAP results provide some insight into the reasons for this decline. To explore this, we first construct and then apply a simple theoretical framework based on mass balances for water flows in the pathway from precipitation on land to the river at a downstream gauging station.

Theory: The mass balance for water in the river system is:

$$
\underbrace{Q_{River}}_{\substack{\text{River flow}}} = \underbrace{R_{Land}}_{\substack{\text{Total runoff}\\\text{from land}\\\text{surfaces}}} - \underbrace{E_{River}}_{\substack{\text{Evaporation}\\\text{from water}\\\text{surfaces}}} - \underbrace{D_{River}}_{\substack{\text{Diversion for}\\\text{irrigation and}\\\text{urban use}}} - \underbrace{G_{River}}_{\substack{\text{Flux from}\\\text{river to}\\\text{groundwater}}} - \underbrace{dS_{River}/dt}_{\substack{\text{Storage}\\\text{changes}}}
$$

$$
= \underbrace{R_{Land}}_{\substack{\text{Total runoff}\\\text{from land}\\\text{surfaces}}} - \underbrace{L_{River}}_{\substack{\text{Total losses}\\\text{from river}\\\text{system}}}
$$

(M4)

where Q_{River} is the flow through the river at a particular gauge, R_{Land} is the total land runoff from all contributing land elements, E_{River} is the evaporation from water surfaces in the river system, D_{River} is the total diversion from the river system for irrigation and urban use, G_{River} is the net flux to groundwater from the river system, and dS_{River}/dt is the net change in water storage (S_{River}) in the river system. The last four terms can be combined into a total loss flux of water from the river, $L_{River} = E_{River} + D_{River} + G_{River} + dS_{River}/dt$, which includes all contributions to transmission losses in the river system. All terms have dimensions (water volume)/time.

The terrestrial counterpart of Equation (M4) is the mass balance of soil water, Equations (M1) and (M2) above, which can be recast as

$$
\underbrace{R_{Land}}_{\substack{\text{Total runoff}\\\text{from land}\\\text{surfaces}}} = \underbrace{P_{Land}}_{\substack{\text{Precipitation}\\\text{from land}\\\text{surfaces}}} - \underbrace{E_{Land}}_{\substack{\text{Evapotranspiration}\\\text{from land}\\\text{surfaces}}} - \underbrace{dW_{Land}/dt}_{\substack{\text{Soil water}\\\text{storage change}}}
$$

$$
= \underbrace{P_{Land}}_{\substack{\text{Precipitation}\\\text{from land}\\\text{surfaces}}} - \underbrace{L_{Land}}_{\substack{\text{Total losses}\\\text{from land}\\\text{to river}}}
$$

(M5)

where P_{Land} is the total precipitation on all land elements in the river basin, E_{Land} is the total evapotranspiration from those land elements, and dW_{Land}/dt is the total change in soil water storage. The last two terms can be combined into a total loss flux of water in transfer from

land to river, $L_{Land} = E_{Land} + dW_{Land}/dt$. Terms in Equation (M5) are area integrals of the mass fluxes in Equations (M1) and (M2), and have dimensions (water volume)/time as in Equation (M4).

Both of these water balances constitute a relationship between a response (the left hand side) and a driver (the first term on the right hand side). The driver is the flow entering a transmission pathway and the response is the flow leaving the pathway to enter further pathways downstream. Each equation can be written in terms of a transmission fraction f, the ratio of the response to the driver, so that

$$R_{Land} = f_{Land} P_{Land} \; ; \qquad Q_{River} = f_{River} R_{Land} \qquad \text{(M6)}$$

where the transmission fractions for land (precipitation-to-runoff) and river (runoff-to-gauge) pathways are

$$f_{Land} = \frac{R_{Land}}{P_{Land}} = \left(1 - \frac{L_{Land}}{P_{Land}}\right); \qquad f_{River} = \frac{Q_{River}}{R_{Land}} = \left(1 - \frac{L_{River}}{R_{Land}}\right) \qquad \text{(M7)}$$

Because the transmission pathways are sequential, the eventual flow in the river is related to the ultimate driver (precipitation) by a transmission cascade in which losses accumulate through each successive transmission pathway:

$$Q_{River} = P_{Land} f_{Land} f_{River} \qquad \text{(M8)}$$

The overall transmission fraction from precipitation to gauge ($f_{Total} = f_{Land} f_{River} = Q_{River}/P_{Land}$) is less than either of the individual transmission fractions because all transmission fractions are between 0 and 1.

Application: Figure 12 shows time series for 1951-2007 of the precipitation P_{Land} and the total runoff R_{Land} (both integrated over the whole MDB), together with the river flow Q_{River} (gauged at Wentworth). The precipitation is derived from BoM gridded meteorological data (Jones *et al.* 2007), and the total runoff from the whole-continent 108-year run of WaterDyn discussed above.

The sharp fall in river flow since 2002 is strongly evident. There are similar falls in precipitation and total runoff, with slight increases in both series at the end of 2007 in response to the 2007-2008 La Niña event.

In addition to series for P_{Land} and R_{Land} integrated across the whole MDB (black lines in the top two panels of Figure 12), we show the contributions to P_{Land} and R_{Land} from the high, medium and low-rainfall parts of the MDB (blue, green and red lines respectively, summing to the back line). These regions were defined by aggregating Australian National Resources Audit (ANRA) (NLWRA 2001a; NLWRA 2001b) Drainage Basins, as shown in Figure 11. By volume, most of the precipitation fell on the intermediate region, with only a small contribution from the wet region because of its small area. However, the relative contribution of the wet region to total runoff was greater because a larger fraction of precipitation appears as runoff in the wet region compared with drier regions.

Figure 13 shows time series of the three transmission fractions f_{Land}, f_{River} and f_{Total}, defined above. A large decrease has occurred in recent years in the f_{Land}, while the decline in f_{River} has been less.

Table 2 shows the averages of the three fluxes P_{Land}, R_{Land} and Q_{River}, and the transmission fractions f_{Land} and f_{River}, time-averaged for the periods 1951-2001 and 2002-2007. We consider the 1951-2001 period to define a long-term average climatology for this purpose. The average river flow (Q_{River}) in the recent (2002-2007) period was just 23% of its climatological (1951-2001) value. Since the flow is given by Equation (M8) as $P_{Land}f_{Land}f_{River}$, it is possible to attribute this strong decline to changes in precipitation (P_{Land}) and the transmission fractions f_{Land} and f_{River}. The last line of Table 2 shows that the recent decline of Q_{River} to 23% of its climatological value is caused by declines in P_{Land} to 81%, f_{Land} to 41% and f_{River} to 68% of their respective climatological values ($0.23 = 0.81 \times 0.41 \times 0.68$).

It is concluded that the largest contributor to the recent decline in river flow is a strong decrease in the fraction of precipitation appearing as runoff, followed in significance by a decline in the fraction of runoff reaching the river gauge, and finally by a decline in the precipitation itself. This result is consistent with the well-known amplification of precipitation changes in total runoff changes, by a factor of order 3 for the typical semi-arid hydrological regime of the MDB: that is, a 1% change in precipitation results in about a 3% change in total runoff (Raupach and Briggs 2005).

	P_{Land} (TL/y)	R_{Land} (TL/y)	Q_{River} (TL/y)	R_{Land}/P_{Land} $= f_{Land}$	Q_{River}/R_{Land} $= f_{River}$
Period A (1951-2001)	539	51	9.04	0.094	0.18
Period B (2002-2007)	436	17	2.04	0.039	0.12
Ratio (Period B)/(Period A)	0.81	0.33	0.23	0.41	0.68

Table 2: Time-averaged values for the periods 1951-2001 and 2002-2007 of precipitation P_{Land}, total runoff R_{Land} (both integrated over the whole MDB), river flow Q_{River} (gauged at Wentworth), and the transmission fractions f_{Land}, f_{River} for transmission through precipitation-to-runoff and runoff-to-gauge pathways. Also shown is the ratio of the value of each quantity in the recent period (2002-2007) to its climatological-average value, taken to be the 1951-2001 average.
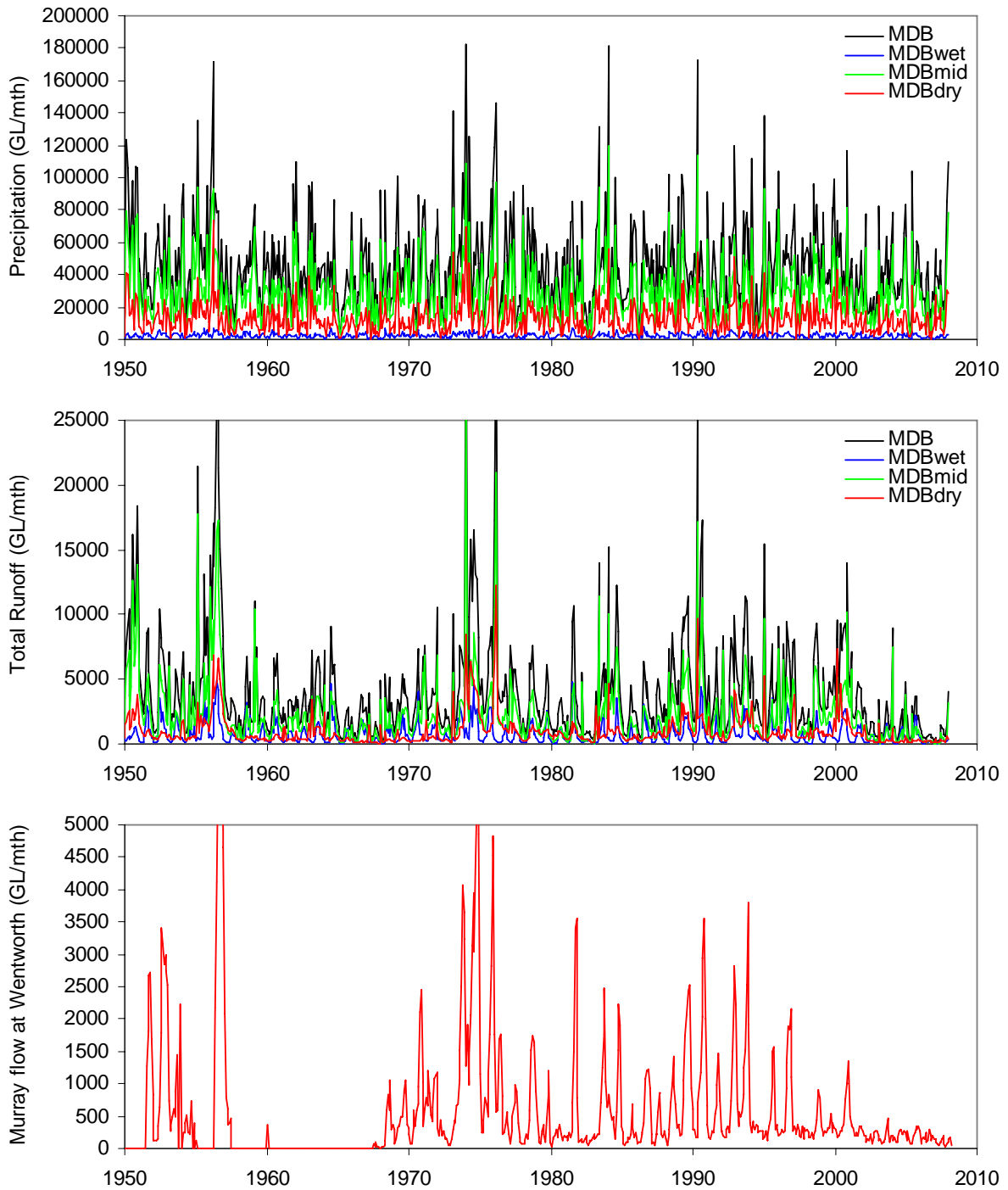
Figure 12: (top) monthly series of total precipitation (P_{Land}) falling on the MDB (black), with contributions falling on wet (blue), agricultural (green) and semi-arid (red) ANRA drainage basins in the MDB; (middle) total runoff (R_{Land}) from all land surfaces in the MDB (black), with contributions from wet (blue), agricultural (green) and semi-arid (red) drainage basins; (bottom) gauged flow in the Murray River at Wentworth (Q_{River}).
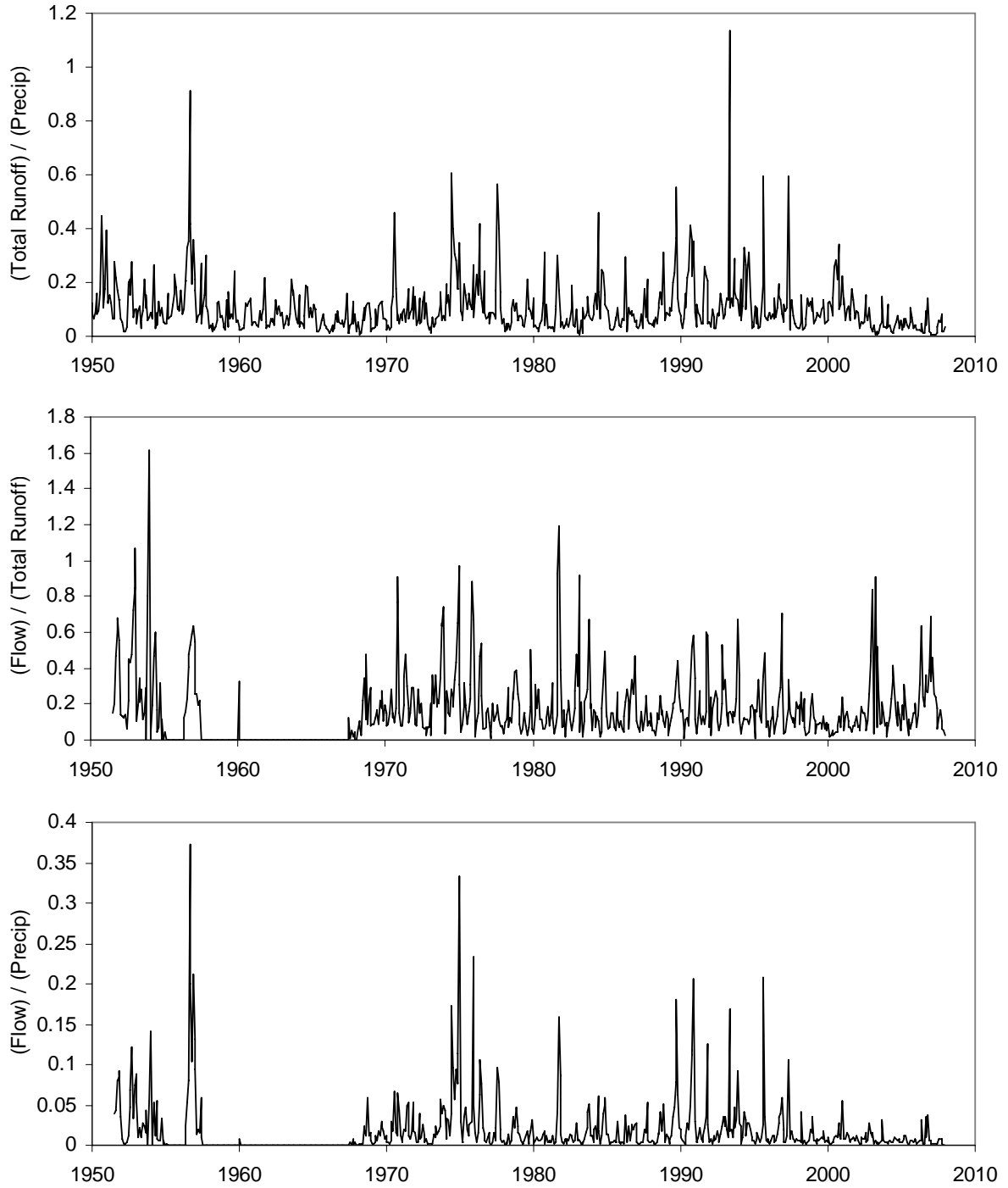
Figure 13: (top) transmission fraction $f_{Land} = R_{Land}/P_{Land}$; (middle) transmission fraction $f_{River} = Q_{River}/R_{Land}$; (bottom) total transmission fraction $f_{Total} = f_{Land}f_{River} = Q_{River}/P_{Land}$.

6 ENSO and the Australian Water Balance

It is known that the El Niño-Southern Oscillation (ENSO) climate mode is well correlated with Australian rainfall and soil moisture, especially in eastern Australia (Nicholls *et al.* 1996; Power *et al.* 1999; Nicholls 2004; Liu *et al.* 2007). ENSO is a nonperiodic oscillation recurring every 2 to 7 years with an "El Niño" phase characterised by strong warming in the eastern and central equatorial Pacific ocean, and an opposite "La Niña" phase. Eastern Australian droughts are more pronounced during the El Niño phase of ENSO, and rainfall is higher during the La Niña phase. Further, the strength of this relationship is modulated by lower-frequency climate oscillations, particularly the Interdecadal Pacific Oscillation (IPO) (Power *et al.* 1999).
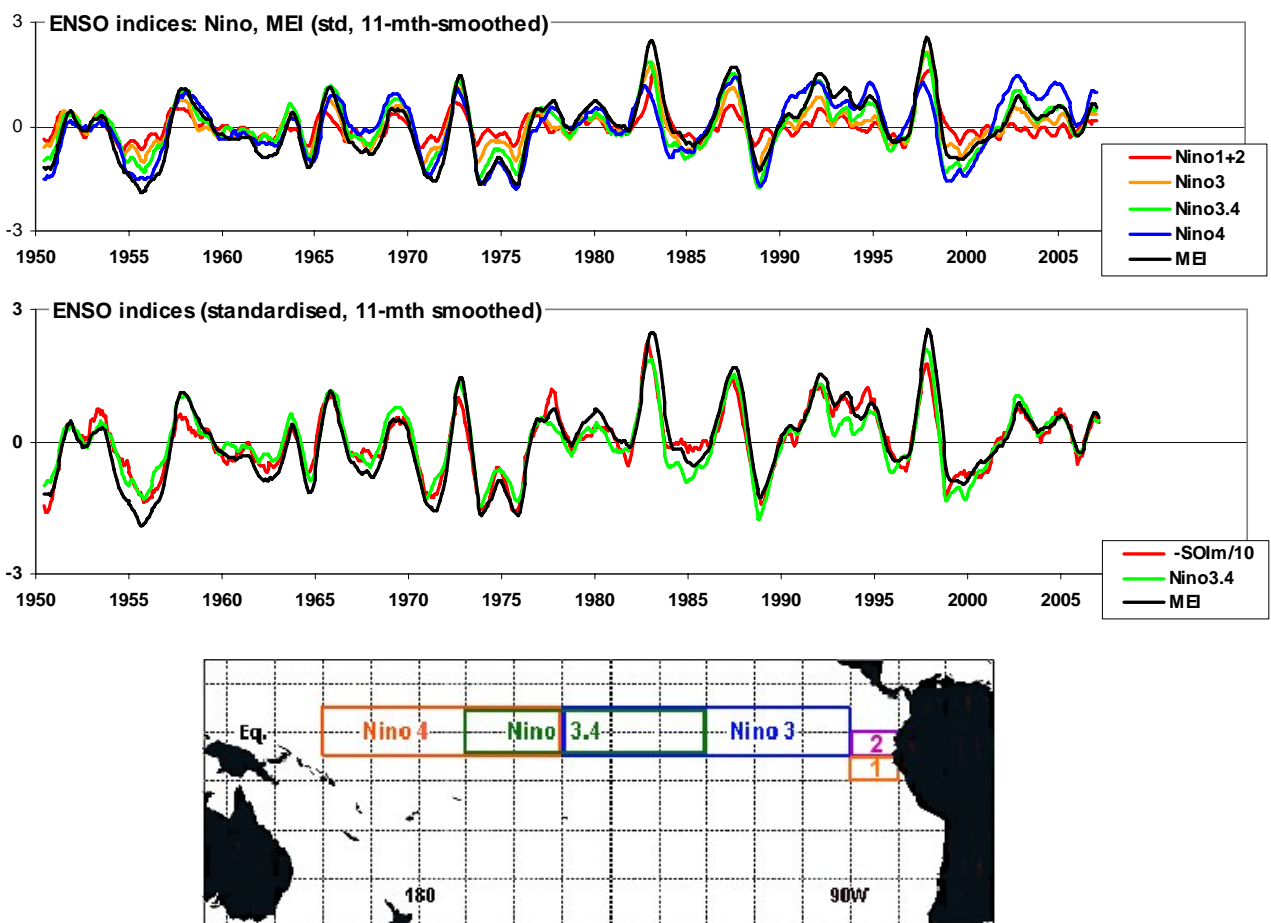
Figure 14: Time series of ENSO indices, detrended to second order and normalised to zero mean and unit variance. Top: Niño1+2 average (red), Niño3 (orange), Niño3.4 (green), Niño4 (blue), MEI (black). Middle: SOI (red), Niño3.4 (green), MEI (black). Bottom: location of ocean regions defining the Niño1, Niño2, Niño3, Niño3.4 and Niño4 sea surface temperatures. The Multivariate ENSO Index (MEI) constructed from the first principal components of sea-level pressure, zonal and meridional components of the surface wind, sea surface temperature, surface air temperature, and total sky cloudiness fraction (Wolter and Timlin 1993; Wolter and Timlin 1998). Monthly time series for Niño3, Niño3.4, Niño4 are from [http://www.cpc.ncep.noaa.gov/data/indices/sstoi.indices]. Series for the MEI are from [http://www.cdc.noaa.gov/ClimateIndices/List/]. Series for the SOI are from the Bureau of Meteorology [http://www.bom.gov.au/climate/current/soihtm1.shtml] with sign reversal and rescaling to match other indices.

Several indices are available to characterise ENSO: the far eastern (Niño1, Niño2), eastern (Niño3), central (Niño3.4) and western (Niño4) equatorial Pacific sea surface temperatures; the Southern Oscillation Index (SOI), defined from the Darwin-Tahiti pressure difference; and the Multivariate ENSO Index (MEI) (Wolter and Timlin 1993; Wolter and Timlin 1998). Figure 14 shows monthly time series of these indices, all scaled to unit variance and signed so that a positive index value is associated with the El Niño phase of ENSO (requiring a reversal of the sign convention for the SOI used by BoM).

Here we present preliminary results on the ENSO correlation in AWAP water balance outputs. We use the lagged correlation coefficient, defined for two stationary time series $X(t)$ and $Y(t)$ by

$$\mathrm{Corr}_{[X,Y]}(\tau) \; = \; \frac{\left\langle \left(X(t) - \langle X \rangle \right) \left(Y(t+\tau) - \langle Y \rangle \right) \right\rangle}{\sigma_X \sigma_Y} \tag{M9}$$

where τ is the time lag, σ_X and σ_Y are the standard deviations of the series, and $\langle \bullet \rangle$ denotes an average over time t, so that $\langle X \rangle$ and $\langle Y \rangle$ are the means of the series. At a time lag τ of zero, $\mathrm{Corr}_{[X,Y]}(0)$ is the conventional correlation coefficient between X and Y.

Figure 15 shows lagged correlation coefficients between a 61-year (1955-2006)[2] monthly time series of the SOI (series X), and corresponding monthly time series of spatially averaged precipitation (series Y). The spatial averaging of precipitation was done over the 15 regions shown in Figure 11, defined by ANRA Drainage Divisions. Consistent with the sign convention for ENSO indices including the SOI, the strongest correlations are negative, occurring at time lag zero. Correlations are larger for regions in eastern Australia (with negative peaks around −0.3 to −0.4) than in the west (peaks around −0.2). The correlation decays with time lag, reaching zero at lags (τ) around +6 months (SOI leads precipitation) and −12 months (precipitation leads SOI).

Figure 16 shows corresponding lagged correlation coefficients between the SOI (series X) and lower-layer soil moisture averaged over ANRA Drainage Divisions (series Y). There is a significant enhancement of the peak correlations, to (negative) peak values around −0.5 in eastern Australia. In contrast with precipitation the peak occurs at a nonzero time lag of around +3 months (that is, a fluctuation in SOI precedes a fluctuation in soil moisture).

The analysis has been repeated with other ENSO indices (Figure 14) in place of the SOI. The indices producing the best correlation between ENSO and lower-layer soil moisture are the SOI (Figures 15, 16) and the MEI, which give nearly identical results. Correlations with indices based on sea surface temperature (Niño4, Niño3.4 …) are somewhat lower.

These results are multidecadal correlations, and therefore do not resolve modulation of the ENSO-water balance correlation by decadal-scale modes of climate variability such as the IPO (Power *et al.* 1999). Investigation of this modulation is a subject for future work.

---

[2] The record period comes from the use in this preliminary analysis of AWAP results from Phase 2 (Raupach *et al.* 2007), model WaterDyn18M, run Australia18a, with SILO meteorological forcing data. The analysis has not yet been updated to latest AWAP results, but little change in outcome of this analysis is anticipated.

Figure 15: Lagged correlations between monthly SOI and rainfall averaged over Drainage Divisions in the eastern part of Australia (colours in upper panel) and the western part (colours in lower panel). Black lines in both panels are for lower-layer soil moisture averaged over the whole continent. Time period: 1955 to 2006. Model version and run: WaterDyn18M, Australia18a (using SILO meteorology).

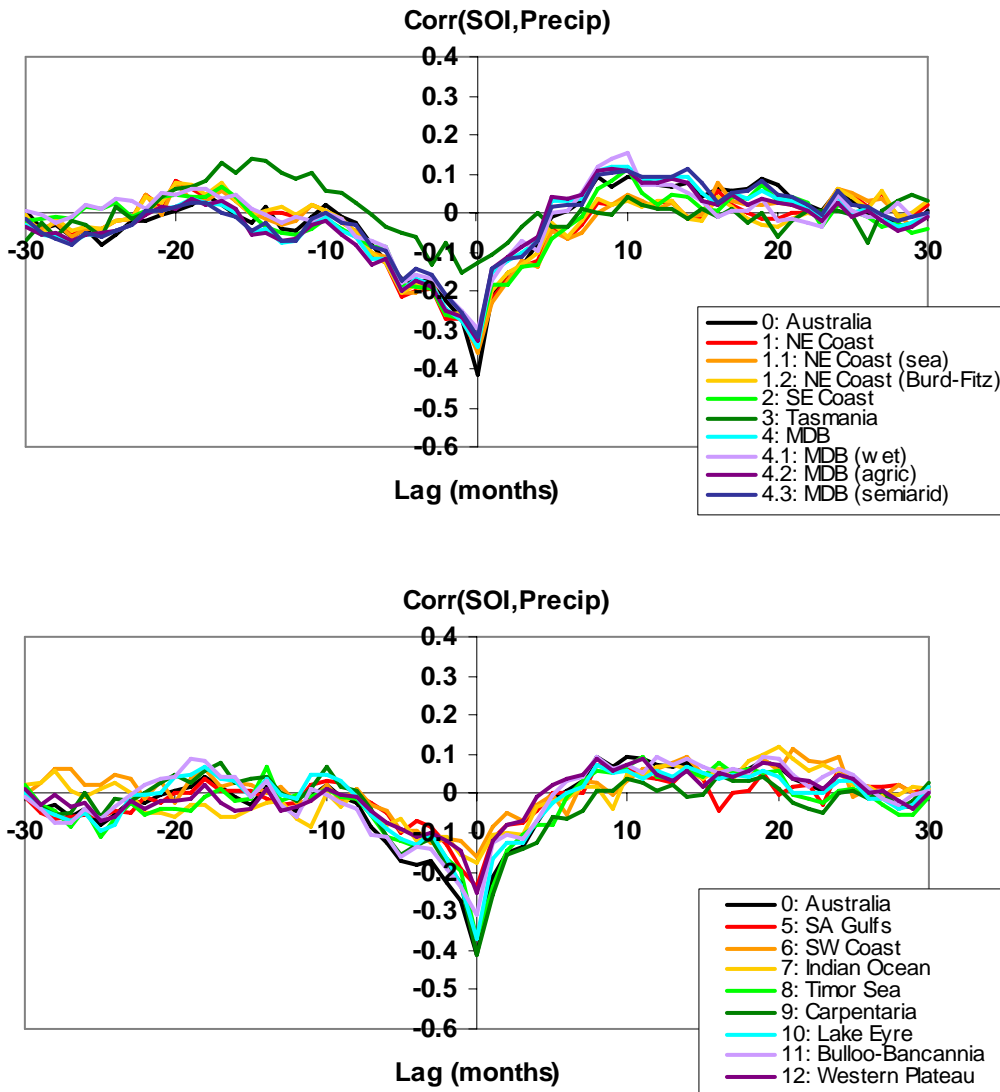Figure 16: Lagged correlation between monthly SOI and lower-layer soil moisture averaged over Drainage Divisions in the eastern part of Australia (colours in upper panel) and the western part (colours in lower panel). Black lines in both panels are for lower-layer soil moisture averaged over the whole continent. Time period: 1955 to 2006. Model version and run: WaterDyn18M, Australia18a (using SILO meteorology).
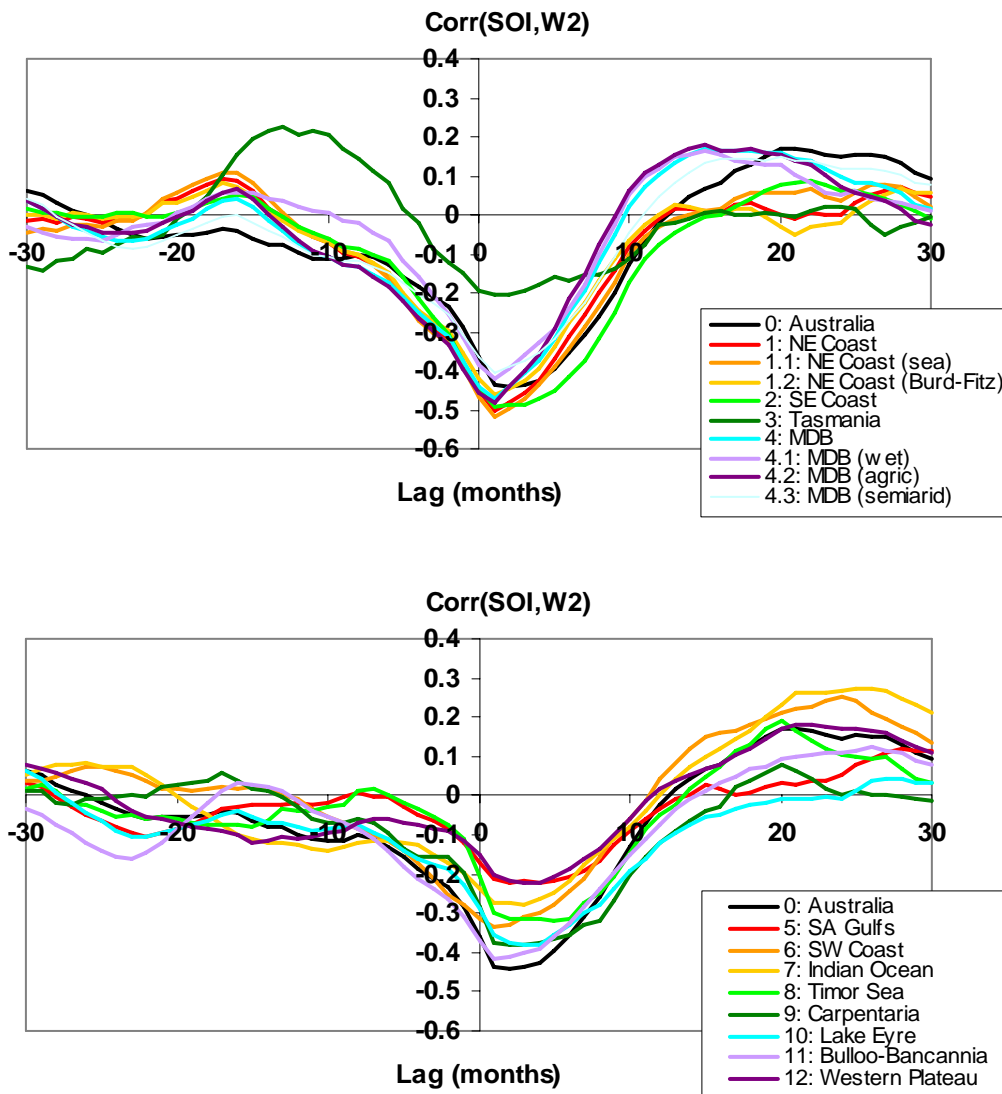
7 Assimilation of Remotely Sensed Land Surface Temperature

A long-term goal of this project has been the assimilation of Land Surface Temperature (LST) with the Ensemble Kalman Filter (EnKF), for estimation of either model state (soil moistures) or parameters. Although this is not yet fully achieved, some aspects of progress to date are described here.

Observation model for LST: Model-data fusion requires an observation model to produce a model-based estimate of the observed quantity from the state variables predicted by the dynamic model. The observation model for LST (T_s) is the relationship between T_s at satellite overpass time (t_p) and the air temperature (T_a) and sensible heat flux (Φ_H) at that time:

$$T_s\left(t_p\right) = T_a\left(t_p\right) + \frac{\Phi_H\left(t_p\right)}{\rho_A c_{PA} G_a\left(t_p\right)} \tag{M10}$$

where G_a is the aerodynamic conductance for heat transfer from the surface to the air, ρ_A is the air density, and c_{PA} is the specific heat of air at constant pressure. Appendix B gives the expressions used here to account for the difference between conditions at the overpass time (t_p) and the average diurnal conditions described by the dynamic model. Algorithms for deriving LST from satellite-measured thermal radiances are given in Appendix D.

Determination of aerodynamic conductance: A major issue in the use of Equation (M10) is the assignment of the aerodynamic conductance (G_a). This quantity is influenced by at least five factors (Raupach 1998): (1) surface roughness, determined in turn by vegetation height and cover fraction; (2) the distribution of heat sources between ground surface and vegetation, also determined (on time scales longer than daily) by vegetation cover fraction; (3) the characteristic leaf dimension; (4) wind speed; and (5) atmospheric stability. Fully process-based models which include all these factors exist, but they are complex and require meteorological inputs not available in the AWAP framework, especially historic wind speed estimates.

We are exploring a different approach to estimate G_a. The principle is to divide the above five factors influencing G_a into influences with slow and fast variability. The slowly-varying influences are those related to vegetation structure, including (1), (3) and long-term aspects of (2). Rapidly-varying influences are those related to short-term meteorology, including (4), (5) and short-term aspects of (2). If the vegetation structure is steady, the former influences are all steady. The latter are rapidly varying.

We work with the inverse of G_a, the aerodynamic resistance $R_a = 1/G_a$, and decompose R_a into a slowly-varying component $\langle R_a \rangle$ dependent on vegetation structure, and a fluctuating component R_a' dependent on short-term meteorology. Putting this into Equation (M10), we obtain

$$T_s\left(t_p\right) - T_a\left(t_p\right) = \frac{\Phi_H\left(t_p\right)}{\rho_A c_{PA}}\left(\langle R_a \rangle + R_a'\right) = \frac{\Phi_H\left(t_p\right)}{\rho_A c_{PA}}\langle R_a \rangle + \text{noise} \tag{M11}$$

The last equality treats the contribution from R_a' as high-frequency noise. If the vegetation structure is steady in time, $\langle R_a \rangle$ is given by the long-term average of the *observed* surface-air temperature difference $T_s - T_a$, modulated by the inverse of the sensible heat flux:

$$\langle R_a \rangle = \left\langle \frac{\rho_A c_{PA} \left(\text{LST}_{Obs}\left(t_p\right) - T_a\left(t_p\right) \right)}{\Phi_H\left(t_p\right)} \right\rangle; \quad \langle G_a \rangle = \langle R_a \rangle^{-1} \quad (M12)$$

We compute a time-independent estimate of $\langle R_a \rangle$ in this way and take G_a to be its inverse.

The approach is based on the fact that, from Equation (M11), the observed $T_s - T_a$ contains information from three sources: vegetation structure through $\langle R_a \rangle$, local meteorology through R_a', and the surface energy and water balances through Φ_H. The second is treated as noise, the first provides a near-steady but strongly spatially varying signal obtained with Equation (M12), and the third provides temporal structure to $T_s - T_a$ which constrains the surface energy and water balances, and thence soil moisture.

Figure 17 illustrates this approach for the Murrumbidgee basin, using LST data from AVHRR satellites (Appendix D) for the period 1992 to 2006. The top panel shows the average over this 15-year period of the observed surface-air temperature difference ($T_s - T_a$) at satellite overpass time, from AVHRR data on T_s and BoM gridded data for T_a (downscaled to satellite overpass time as described in Appendix B). The third and fourth panels show model output for the time-averaged latent (Φ_E) and sensible (Φ_H) heat fluxes. These are only weakly dependent on G_a, and hence can be obtained to a good approximation with a very crude prior estimate such as $G_a = 0.02$ m s^{-1} (Table C2). Combining the sensible heat flux with the observed ($T_s - T_a$) in the top panel, Equation (M12) can be used to estimate the long-term component of G_a.

The resulting estimate of G_a (bottom panel of Figure 17) is realistic, showing a spatial variability from 0.01 to 0.02 m s^{-1} in areas with short vegetation cover and up to 0.05 to 0.07 m s^{-1} in the forested areas on the Great Dividing Range, values consistent with process models for such vegetation types. This estimate of G_a is also an indirect test of the spatial patterns of sensible heat flux predicted by the model (as foreshadowed in Section 3.4).

This approach has the advantage of finding a G_a estimate which produces unbiased estimates for energy balance fluxes in the long-term average. Short-term variations in energy balance conditions, through moisture availability, will lead to modifications to the predicted LST from Equation (M10), thereby providing information to constrain the energy and water balances.
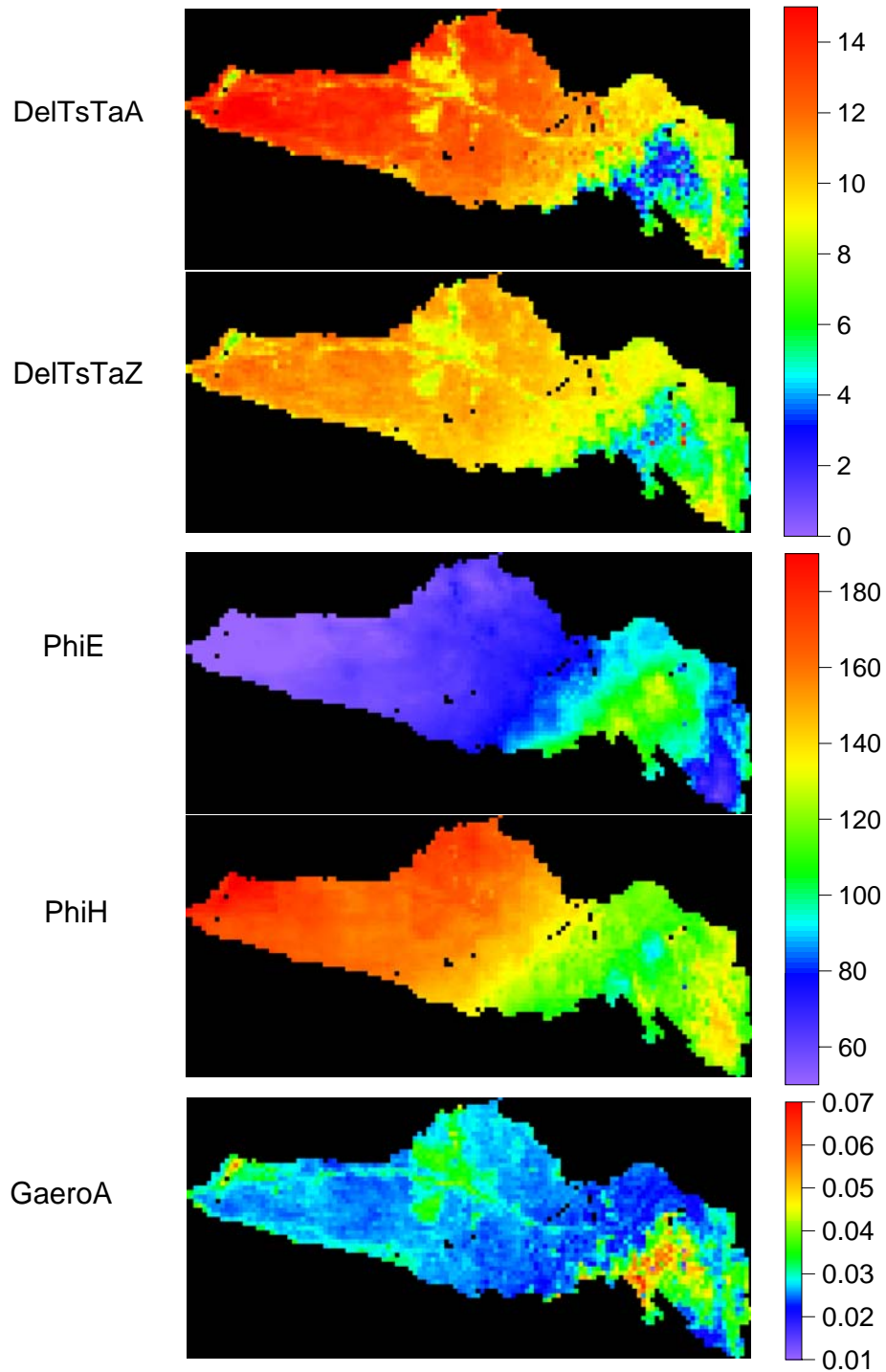
Figure 17: Illustration of determination of aerodynamic conductance G_a. First and second panels: observed and modelled surface-air temperature difference ($T_s - T_a$, degC) in the Murrumbidgee basin. Third and fourth panels: modelled latent heat flux (Φ_E, W m^{-2}) and sensible heat flux (Φ_H, W m^{-2}). Bottom panel: estimated long-term aerodynamic conductance (G_a, m s^{-1}) from Equation (M12). All quantities are long-term averages over period of available LST observations (1992 to 2006). Run: Murrumbidgee24b.

8   Use of AWAP Framework to Test CABLE

The AWAP water balance framework (including continental datasets and modelling environment) has provided an invaluable tool for testing CABLE, the land surface module for ACCESS, the new climate and earth system model being developed jointly by CSIRO and BoM through the Centre for Australian Weather and Climate Research (CAWCR). CABLE is a different, much more detailed model from WaterDyn (the water balance model used throughout AWAP and described in Appendix A).

This section describes the development and application of a test environment for CABLE, created by replacing WaterDyn with CABLE to form a model called "CableDyn". The intentions of this section are (1) to show how the AWAP framework provides opportunities for testing terrestrial biosphere models other than WaterDyn, and (2) to contribute to the development of CABLE, and thence ACCESS, by providing hydrological tests which have been unavailable hitherto. It is shown that CABLE (in the form currently used in ACCESS and associated global climate models) overestimates observed total runoff.

CableDyn: CableDyn is an extension of the WaterDyn code, in which the CSIRO Atmosphere Biosphere Land Exchange (CABLE) model (Kowalczyk *et al.* 2006) is a switchable option, so that CABLE (version 1.4) is used for all model calculations instead of WaterDyn. In addition to code replacement, this requires two additional components.

1. Initialisation: CableDyn has a CABLE initialisation subroutine which assigns initial values to CABLE state variables and sets CABLE parameter values. There are three options for setting parameters: (1) to use CABLE default values based on soil and vegetation types assigned according to latitude and longitude; (2) to read parameters directly from the CableDyn control file as single-point values, or (3) to read parameters as maps (VV arrays).

2. Meteorological downscaling: Since CABLE operates at a subdiurnal time-scale, meteorological downscaling is required. At each daily time-step, the meteorological downscaling subroutine returns 24 hourly values of each meteorological variable. CABLE is then called 24 times, with state variables being held in memory between model calls. Hourly fluxes are accumulated after each model call to produce daily fluxes. Hourly model outputs can be written directly to file. Space and time averaging of daily fluxes to produce monthly, annual and whole-of run sums and catchment-scale fluxes is done by the host AWAP framework in CableDyn.

Meteorological downscaling is performed as follows. Downward solar irradiance is distributed over the daylight hours using astronomical formulae. Downward longwave irradiance is computed from down-scaled air temperature (Swinbank 1963). Daily rainfall observations represent the amount of precipitation falling in the 24 hours leading up to 0900h local time on the date of observation, so hourly estimates of rainfall are generated by spreading 9/24 of the current day's rainfall evenly across the period 0000h to 0900h, and 15/24 of the next day's rainfall across the period 0900h to 2400h. Daily vapour pressure observations are instantaneous at 0900h and 1500h, so hourly estimates for vapour pressure are generated by linear interpolation between 1500h the previous day, 0900h and 1500h the current day, and 0900h the next day. Hourly temperature is calculated with a mixed sine and square-root curve to approximate the shape of the diurnal temperature curve (Cesaraccio *et al.* 2001), a more sophisticated version of the approach used in Appendix B. Calculation of

midnight-to-midnight hourly temperatures by this method requires the current day's minimum and maximum, the next day's minimum, and the previous day's maximum. Windspeed is not available. A 24 h mean value of 2 ms^{-1} is assumed, with constant daytime and nocturnal values in the ratio 3:1.

Initial tests: CableDyn was run for a spatial domain covering 200 unimpaired gauged catchments across Australia. Since the carbon allocation scheme in CABLE is still under development, leaf area index (LAI) must currently be prescribed. For this initial model run, LAI was set to 2.0 and CABLE default values were used for other parameters. Catchment outflow (surface runoff plus deep soil drainage) was aggregated for each catchment over the period of the model run (1/1/1981 to 31/12/2005).

The results, shown in Figure 18, indicate that CableDyn (with default parameters) is systematically overestimating catchment discharge, and hence underestimating evapotranspiration. This contrasts with the result from WaterDyn, which produces an unbiased prediction of the same catchment outflow data (Figure 5).
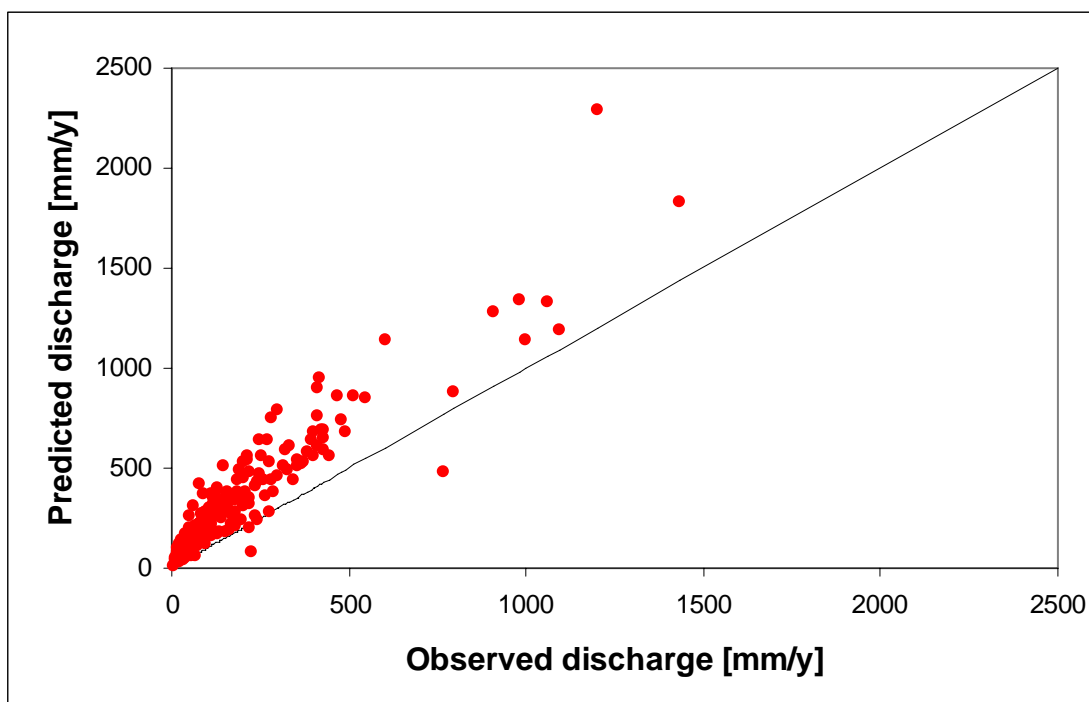
Figure 18: Comparison of CableDyn predictions and observations of discharge for 200 gauged catchments across Australia, averaged over the period (1/1/1981 to 31/12/2005).

Further offline tests: Possible reasons for the overestimation of catchment outflow in Figure 18 are currently being explored in offline tests outside the continental CableDyn environment, using observations of sensible heat, latent heat and net radiation (H, λE and R_{net}) from flux tower sites. In particular, model predictions have been made for the Tumbarumba flux site, using CABLE and an alternate soil model called "Soil-Litter".

CABLE v1.4 contains a 6-layer soil model which predicts soil temperature, liquid water and ice content (Kowalczyk *et al.* 2006). We are developing an alternate model "Soil-Litter", an

extension of a fast solution of the Richards equation by Ross (Ross 2003) which also predicts water vapour content and carries a litter layer. Although this scheme does not yet allow for ice formation and melting, it has three key advantages over the soil-model in CABLE v1.4:
- improved infiltration, consistent with the widely-tested Ross model;
- vapour phase transfer of soil-moisture, and hence more realistic soil-moisture profile, particularly near the soil surface; and
- reduced soil evaporation in the presence of litter.

Soil-Litter has been added as a switchable option in CABLE v1.4, allowing model runs to be performed either using the default soil model, or using "Soil-Litter", which accepts identical parameters to the default soil model.

Four model runs for Tumbarumba were performed for the period 1/1/2000-31/12/2006:
1. CABLE v1.4 with measured hourly meteorological forcing data from the Tumbarumba site;
2. as for run 1, using Soil-Litter in place of the 6-layer soil model in CABLE;
3. CABLE v1.4 with downscaled meteorology from BoM gridded surfaces, as used in CableDyn;
4. as for run 3, using Soil-Litter in place of the 6-layer soil model in CABLE.

CABLE default parameters were used, and LAI was set to 2.8, as determined for this site by ground-based laser measurements (Jupp *et al.* 2008). Litter depth was set to 2 cm, in accordance with field observations (H. Keith, personal communication).

Model outputs of H, λE and R_{net}, aggregated to daily and monthly averages, were compared with corresponding observations spanning the period (24/2/2001-31/12/2006). Results of linear regression analyses for daily and monthly fluxes, as well as Root Mean Squared Error (RMSE) and Bias Error (BE), are given in Tables 2 and 3 respectively, where

$$\text{RMSE} \;=\; \sqrt{\frac{\sum_{i=1}^{n}(y_i - x_i)^2}{n}} \;;\qquad \text{BE} \;=\; \frac{\sum_{i=1}^{n}(y_i - x_i)}{n} \tag{M13}$$

The most striking result from these comparisons is shown in Figure 19, which compares predictions and measurements of daily H and λE for model runs (1) and (2). It is clear that CABLE's ability to predict the latent heat flux (i.e. evapotranspiration) at Tumbarumba improves dramatically when the default soil model is replaced with Soil-Litter. While the bias error in λE is very similar for the two simulations, the scatter is much reduced when Soil-Litter is used. This is likely to be attributable to less extremely high evaporation fluxes when the surface soil is moist, because of the presence of litter, and to less extremely low transpiration fluxes because the presence of litter and the improved infiltration allow more moisture to be retained in the root zone during relatively dry periods. A similar result is shown by the comparison of monthly mean fluxes of H and λE in Figure 20.

		slope	intercept	R^2	RMSE	BE	n
CABLE v1.4 with measured hourly meteorological forcing	H	1.01	-0.88	0.62	3.09	-0.84	2023
	λE	0.80	0.31	0.40	3.34	-0.68	2023
	R_{net}	1.08	-2.58	0.94	2.63	-1.92	2023
CABLE v1.4 with Soil_Litter with measured hourly meteorological forcing	H	0.94	-0.56	0.75	2.23	-0.83	2023
	λE	0.93	-0.72	0.73	2.15	-1.09	2023
	R_{net}	1.08	-2.84	0.94	2.78	-2.12	2023
CABLE v1.4 with CableDyn meteorological forcing	H	0.94	-0.85	0.68	2.67	-1.11	2023
	λE	1.04	-0.44	0.61	2.74	-0.26	2023
	R_{net}	1.05	-1.95	0.89	2.75	-1.55	2023
CABLE v1.4 with Soil_Litter withCableDyn meteorological forcing	H	1.01	-0.64	0.76	2.23	-0.62	2023
	λE	0.80	-0.52	0.76	2.21	-1.52	2023
	R_{net}	1.04	-2.19	0.89	2.91	-1.85	2023

Table 2: Linear Regression statistics for predictions of daily fluxes (in MJ per day) (*H*, *λE* and *R_{net}*) against corresponding observations.

		slope	intercept	R^2	RMSE	BE	n
CABLE v1.4 with measured hourly meteorological forcing	H	1.31	-2.14	0.71	2.43	-0.84	65
	λE	0.78	0.47	0.45	2.43	-0.65	65
	R_{net}	1.04	-2.28	0.96	2.18	-1.91	65
CABLE v1.4 with Soil_Litter with measured hourly meteorological forcing	H	1.11	-1.27	0.83	1.55	-0.82	65
	λE	0.97	-0.94	0.85	1.55	-1.09	65
	R_{net}	1.06	-2.61	0.96	2.38	-2.11	65
CABLE v1.4 with CableDyn meteorological forcing	H	1.18	-1.88	0.79	1.97	-1.11	65
	λE	1.12	-0.86	0.70	2.01	-0.24	65
	R_{net}	1.06	-2.02	0.96	1.87	-1.54	65
CABLE v1.4 with Soil_Litter withCableDyn meteorological forcing	H	1.21	-1.48	0.87	1.43	-0.61	65
	λE	0.89	-0.97	0.90	1.75	-1.54	65
	R_{net}	1.05	-2.29	0.96	2.13	-1.84	65

Table 3: Linear Regression statistics for predictions of monthly mean fluxes (in MJ per day)(*H*, *λE* and *R_{net}*) against corresponding observations.

There are two other noteworthy aspects of the results in Tables 1 and 2. First, there is a significant negative bias in predicted net radiation (all model runs), leading to an underprediction of $H + \lambda E$. Second, and unexpectedly, CABLE predictions of λE at both daily and monthly averaging times are improved when CableDyn meteorology is used instead of hourly measurements from the site. The same is not true for simulations using "Soil-Litter". Further work is required to distinguish the effects of meteorological downscaling and source of the daily meteorological data (site vs BoM) on model predictions.

We anticipate that further model runs at other flux sites, using both CABLE v1.4 and CABLE v1.4 with Soil-Litter, will help to explain the over-prediction of discharge by CableDyn (with default parameters) shown in Figure 18.
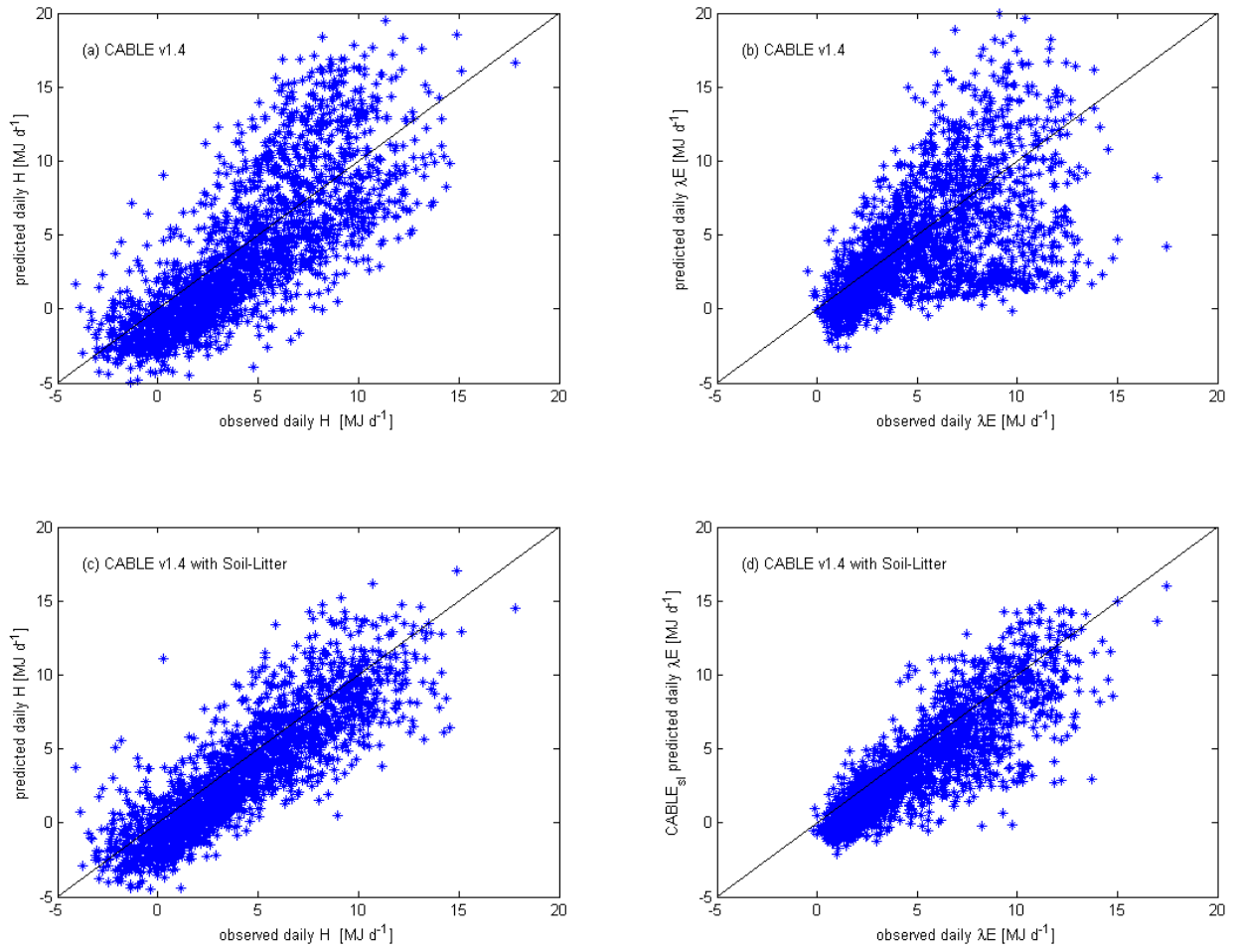
Figure 19: Comparisons of predicted and observed daily *H* and *λE* for simulations using CABLE v1.4 (a) and (b) and CABLE v1.4 with "Soil-Litter" (c) and (d).
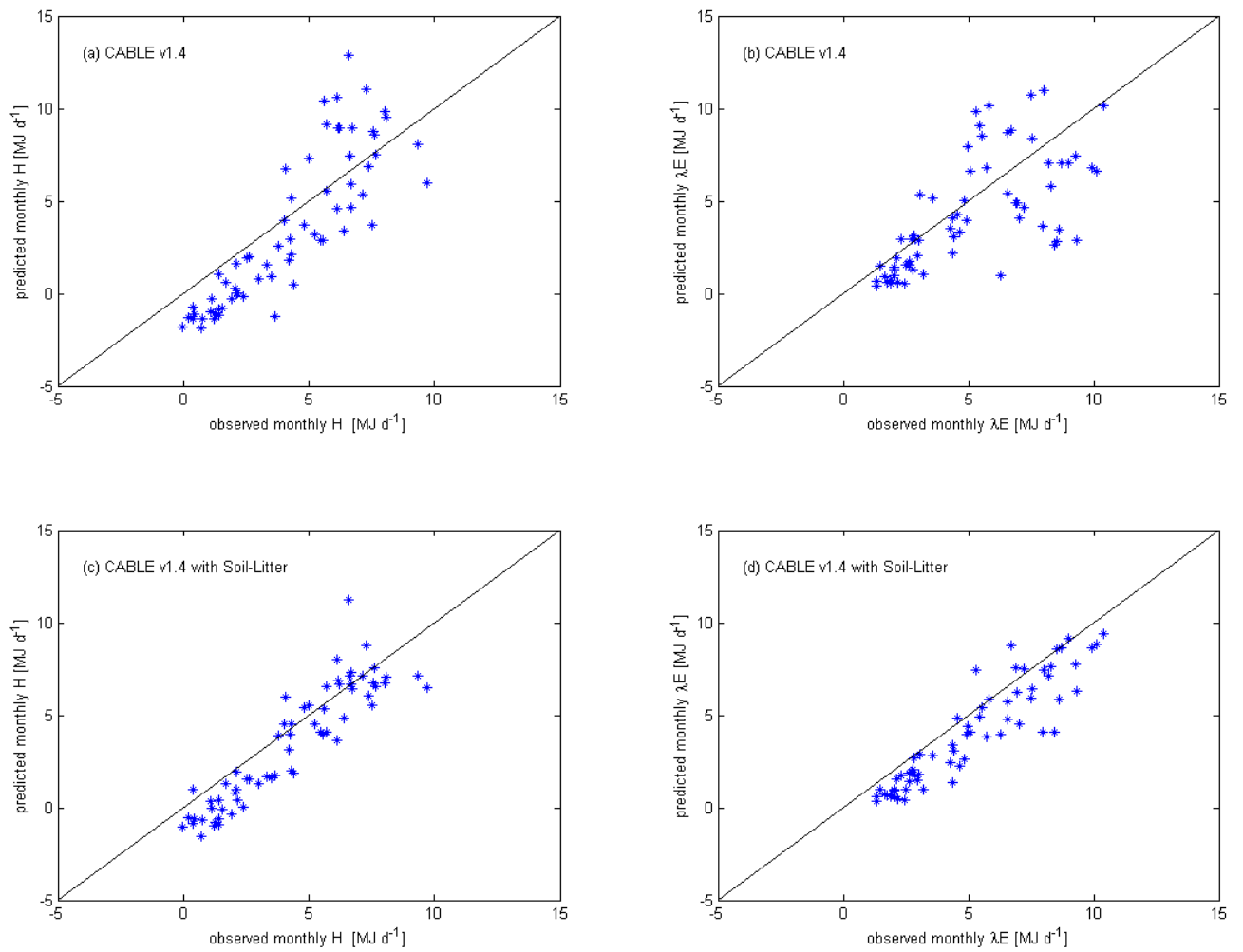
Figure 20: Comparisons of predicted and observed monthly mean *H* and *λE* for simulations using CABLE v1.4 (a) and (b) and CABLE v1.4 with "Soil-Litter" (c) and (d).

9 Conclusion

Through the efforts of all partners, AWAP has achieved its goal of determining the state and trend of the terrestrial water balance of the Australian continent. The project has delivered a robust water balance monitoring and modelling system, providing both operational near-real-time information and histories over more than 100 years for soil moisture and all water fluxes contributing to the terrestrial water balance: rainfall, transpiration, soil evaporation, surface runoff and deep drainage.

The system is now ready for transfer to the Bureau of Meteorology as a long-term operational agency.

Ongoing development of the system is anticipated to continue, with appropriate version control. This development will both take up the scientific opportunities offered by progress to date, and also further improve the operational system.

Appendix A: Dynamic Model

WaterDyn is a simple two-store dynamic water balance model, with a submodel for leaf carbon which may be used optionally to specify the vegetation cover fraction or green-leaf cover (v).

This Appendix summarises the equations currently used in the dynamic model (August 2008, WaterDyn25M). Section A1 describes the water balance model and A2 the leaf carbon submodel.

A1: Water balance model

State variables: The two state variables of the water balance model are soil water stores (W_1, W_2) [m-water] in fast and slow compartments corresponding to upper and lower soil layers. The layers together encompass the whole soil profile from which water is extracted by plant transpiration. Corresponding dimensionless variables are the relative soil water (w_1, w_2) in the two stores, between 0 and 1 and related to W_1 and W_2 by

$$w_i = W_i / (\theta_{Si} Z_{Wi}) \qquad (i = 1, 2) \tag{A1}$$

where θ_{Si} [m^3 m^{-3}] is the saturated volumetric water content and Z_{Wi} [m] is the depth of layer i.

Balance equations: The dynamic equations governing W_1 and W_2 are the mass conservation equations for soil water, Equations (M1) and (M2), repeated here:

$$\frac{dW_1}{dt} = \theta_{S1} Z_{W1} \frac{dw_1}{dt} = \underset{\text{Precipitation}}{F_{WPrec}} - \underset{\substack{\text{Transpiration} \\ \text{from layer 1}}}{F_{WTra1}} - \underset{\substack{\text{Soil} \\ \text{Evaporation}}}{F_{WSoil}} - \underset{\substack{\text{Surface} \\ \text{Runoff}}}{F_{WRun}} - \underset{\substack{\text{Leaching from} \\ \text{layer 1 to 2}}}{F_{WLch1}}$$

$$\frac{dW_2}{dt} = \theta_{S2} Z_{W2} \frac{dw_2}{dt} = \underset{\substack{\text{Leaching from} \\ \text{layer 1 to 2}}}{F_{WLch1}} - \underset{\substack{\text{Deep} \\ \text{Drainage}}}{F_{WLch2}} - \underset{\substack{\text{Transpiration} \\ \text{from layer 2}}}{F_{WTra2}} \tag{A2}$$

where all water fluxes (F_W) are in metres of water per day [m-water day^{-1}].

Phenomenological equations: The phenomenological equations for water fluxes are as follows.

(1) *Precipitation* (F_{WPrec}) is an external input.

(2) *Transpiration* (F_{WTra}) is defined for each soil layer ($i = 1, 2$) as the lesser of an energy-limited transpiration rate $F_{WTra(\text{ELim})i}$ and a water-limited transpiration rate $F_{WTra(\text{WLim})i}$:

$$F_{WTra\,i} = \min\left(F_{WTra(\text{ELim})i}, F_{WTra(\text{WLim})i}\right) \tag{A3}$$

The total energy-limited transpiration rate (summed over two soil layers) is $F_{WTra(\text{ELim})} = F_{WTra(\text{ELim})1} + F_{WTra(\text{ELim})2}$. This total is partitioned among soil layers using the water-limited

transpiration for each layer under prevailing (energy-limited) conditions, so that $F_{WTra(ELim)i} = F_{WTra(ELim)} \times [F_{WTra(WLim)i} / (F_{WTra(WLim)1} + F_{WTra(WLim)2})]$. This means that:

$$F_{WTra\,i} \;=\; \min\left(F_{WTra(ELim)}, F_{WTra(WLim)}\right) \frac{F_{WTra(WLim)i}}{\sum F_{WTra(WLim)i}} \tag{A4}$$

where the sum runs over layers ($i = 1,2$). The total energy-limited transpiration rate, $F_{WTra(ELim)}$, and the water-limited transpiration for each layer, $F_{WTra(WLim)i}$, are defined as follows.

- The total energy-limited transpiration rate is the evaporation rate from surface without water constraints. It is often defined using the Penman-Monteith equation, but for reasons of both physics (Raupach 2000, Raupach 2001) and simplicity, it is defined here as

$$F_{WTra(ELim)} \;=\; v F_{W(PT)} \tag{A5}$$

where v is the vegetation cover fraction (between 0 and 1) and $F_{W(PT)}$ is the Priestley-Taylor evaporation rate [m-water day^{-1}], a thermodynamic estimate of the energy-limited evaporation rate for the whole surface (vegetation plus soil). The factor v relates energy-limited total evaporation to the plant component only.

From (Raupach 2000) and (Raupach 2001), $F_{W(PT)}$ is

$$F_W(PT) \;=\; c_{PT}\Phi_{Eq}\big/(\rho_W\lambda_W) \tag{A6}$$

where ρ_W [mol-water m^{-3}] is the density of liquid water, λ_W [J mol-water^{-1}] is the latent heat of vaporisation of water, Φ_{Eq} [J m^{-2} day^{-1}] is the thermodynamic equilibrium latent heat flux, and c_{PT} is the Priestley-Taylor coefficient, a number which is well constrained at about 1.26 (Priestley and Taylor 1972; Raupach 2001). The equilibrium latent heat flux is given by

$$\Phi_{Eq} \;=\; p\varepsilon\Phi_A^*\big/(p\varepsilon+1) \tag{A7}$$

where Φ_A^* is the isothermal available energy flux, ε is the ratio of latent to sensible heat content of saturated air (2.2 at 20 degC, roughly doubling with each 13 degC temperature increase) and p is a number slightly less than 1 accounting for radiative coupling, defined in the next equation. The isothermal available energy flux Φ_A^* is given by

$$\Phi_A^* \;=\; (1-a)\Phi_{S\downarrow} \;+\; e\left(\Phi_{L\downarrow}-\sigma T_a^4\right); \qquad p \;=\; \frac{G_a}{G_a+G_r} \tag{A8}$$

where $\Phi_{S\downarrow}$ and $\Phi_{L\downarrow}$ are the downward solar (shortwave) and thermal (longwave) irradiances; a and e are whole-surface albedo and emissivity, respectively; σ is the Stefan-Boltzmann constant; T_a [degK] is the air temperature at a reference height; G_a is the aerodynamic conductance for heat and water vapour transfer; $G_r = 4e\sigma T_a^3/(\rho_A c_{PA})$ is the radiative conductance; ρ_A is the density of air; and c_{PA} is the specific heat of air at constant pressure.

Energy fluxes (Φ) are calculated as averages over daylight hours only, since it is assumed that total evaporation ($F_{WE} = F_{WTra} + F_{WSoil}$) and its components are all zero at night. Downward daytime longwave irradiance is estimated with the Swinbank formula, $\Phi_{L\downarrow} = 335.97(T_a/293)^6$ (Swinbank 1963), using average daytime T_a estimated as $0.75T_{a\max} + 0.25T_{a\min}$.

- The water-limited transpiration rate in layer i is given by

$$F_{WTra(\mathrm{WLim})i} = vk_{Ei}\theta_{Si}Z_{Wi}w_i = vk_{Ei}W_i \tag{A9}$$

where k_E is a rate [day^{-1}] for the decay of water extraction by roots from a drying soil under water-limited transpiration and full vegetation cover. The vegetation cover fraction v is included as a multiplier to scale the water extraction by the amount of vegetation present.

(3) *Soil evaporation* (F_{WSoil}) is given by

$$F_{WSoil} = (1-v)w_1^{\beta}F_{W(\mathrm{PT})} \tag{A10}$$

where β is an exponent specifying the response of soil evaporation to upper-layer soil water (w_1).

(4) *Surface runoff* (F_{WRun}) is given by

$$F_{WRun} = F_{WPrec}\,\mathrm{Step}(w_1 - 1) \tag{A11}$$

All precipitation runs off when the upper-layer soil is saturated, and there is no runoff otherwise.

(5) *Leaching* (F_{WLch}) or drainage downward out of soil layer i is given by

$$F_{WLch\,i} = K_{Si}w_i^{\gamma} \tag{A12}$$

where γ is an exponent specifying the response of drainage to relative soil water w_i, and K_{Si} [m day^{-1}] is the saturated hydraulic conductivity of soil layer i.

A2: Vegetation cover fraction and leaf carbon submodel

External specification of vegetation cover fraction: The vegetation cover fraction (v) is given either externally or from a leaf carbon submodel. When externally prescribed, it is given by the smooth curve

$$v = \frac{1-\exp(c_{PAR}\,\mathrm{FAPAR})}{1-\exp(c_{PAR})} \tag{A13}$$

where FAPAR is a remotely-sensed Fraction of Absorbed Photosynthetically Active Radiation and c_{PAR} is a coefficient of order -2. Both v and FAPAR are constrained to the interval from 0 to 1. All results in this report use this method to determine v.

Leaf carbon submodel for vegetation cover fraction: The following submodel was used in early versions of WaterDyn (version 20 and earlier, as used in AWAP Phases 1 and 2) to determine v. This submodel yielded realistic long-term average values of v but incorrect amplitudes and phases for seasonal cycles. Therefore, from WaterDyn version 21 onwards, we have used externally prescribed values of v from remote sensing as above. The leaf carbon submodel is still run but its predictions for v are not coupled to the water balance model and therefore do not influence water balance outputs. All results in this report use externally prescribed values of v.

The state variable is the green-leaf carbon store C_L [molC m^{-2}]. The vegetation cover fraction or green-leaf cover v (dimensionless, between 0 and 1) is related to C_L by

$$v = 1 - \exp(-c_{Ext}\Lambda) = 1 - \exp(-c_{Ext}C_L/C_{L0}) \tag{A14}$$

where c_{Ext} is the exponential light extinction coefficient in the canopy, Λ the leaf area index and C_{L0} the green-leaf carbon store at $\Lambda = 1$. This is given by $C_{L0} = d_L\rho_{CL}$, where d_L is the leaf thickness and ρ_{CL} the density of carbon in green leaf [molC m^{-3}].

The dynamic equation governing C_L is the mass conservation equation

$$\frac{dC_L}{dt} = a_L \underbrace{F_{CP}}_{\text{NPP}} - \underbrace{k_L C_L}_{\substack{\text{Leaf} \\ \text{decay}}} \tag{A15}$$

where F_{CP} is the plant carbon production flux or net primary productivity [molC m^{-2} day^{-1}], a_L the allocation coefficient for growth carbon to leaf, and k_L the decay rate for leaf carbon [day^{-1}]. The phenomenological equation for the plant carbon production flux or net primary productivity (F_{CP}) is (Raupach 2005):

$$F_{CP} = \left[\left(\alpha_Q v F_Q\right)^{-1} + \left(\alpha_W \rho_W F_{WT}\right)^{-1}\right]^{-1} \tag{A16}$$

where F_Q is the incident quantum flux of photosynthetically active radiation (PAR) on the surface [mol-quanta m^{-2} day^{-1}], and α_Q and α_W are respectively a PAR use efficiency [molC mol-quanta^{-1}] and a transpired-water use efficiency [molC mol-water^{-1}]. Of these, α_Q is a prescribed parameter, and α_W is either prescribed or calculated as

$$\alpha_W = m_\alpha \left([CO_2]_a - [CO_2]_c\right)/\left(1.6 D_s\right) \tag{A17}$$

where m_α is a dimensionless multiplier, $[CO_2]_a$ is the atmospheric CO_2 concentration, $[CO_2]_c$ is the CO_2 compensation point [molC molAir^{-1}] calculated using the (von Caemmerer 2000) algorithm, and D_s is the surface saturation deficit [molWater molAir^{-1}], calculated from the air saturation deficit as in (Raupach 1998)

The leaf allocation coefficient a_L responds to soil water through (Raupach 2005):

$$a_L = \sqrt{w}/\left(\sqrt{w} + \sqrt{w_0}\right) \tag{A18}$$

where w_0 is the relative soil water at which $a_L = 0.5$.

Appendix B: Observation Models

This Appendix summarises the equations currently used in the WaterDyn observation models for catchment outflow and land surface temperature (August 2008, WaterDyn25M).

The purpose of an observation model is to produce a model-based estimate h_i of an observed quantity z_i, for model-data fusion. The model-based estimate is a function of model state variables, model forcing variables and parameters. Model-data fusion involves minimisation of a weighted sum of squared differences $(h_i - z_i)^2$ (the model-measurement discrepancy) over a set of observations (i), by adjusting "target variables" which may be model state variables or parameters (Raupach *et al.* 2005b; Trudinger *et al.* 2007; Trudinger *et al.* 2008).

B1: Catchment outflow

The total outflow from an unimpaired catchment (a catchment from which there is negligible water extraction for human use or retention by dams) is a lagged sum of surface runoff and drainage from the lower soil layer, for all grid cells in the catchment. To avoid difficulties with water extractions (irrigation, offtakes etc) and retention (farm dams, river reservoirs etc) we use only data from nominally unimpaired catchments as identified by Dr Francis Chiew (CSIRO Land and Water) (personal communication).

Total catchment outflow is computed in three steps. First, daily surface runoff and deep drainage for the whole catchment ($F_{WRun(C)}$ and F_{WLch2C}) are computed by averaging over all grid cells in the catchment, with area weighting:

$$F_{WRun(C)} \; = \; A_{(C)}^{-1}\sum_j A_{(j)}F_{WRun(j)} \; ; \qquad F_{WLch2(C)} \; = \; A_{(C)}^{-1}\sum_j A_{(j)}F_{WLch2(j)} \tag{B1}$$

where the subscript (j) denotes an individual cell, (C) denotes a whole-catchment average and $A_{(j)}$ and $A_{(C)}$ are the respective areas (with $A_{(C)}$ the sum of all $A_{(j)}$ in the catchment).

Optionally, recursive lowpass filters are applied to $F_{WRun(C)}$ and $F_{WLch2(C)}$ to account for time lags between local runoff, local drainage and catchment outflow as gauged at the catchment outlet. Lowpass-filtered versions of $F_{WRun(C)}$ and $F_{WLch2C)}$, denoted $Z_{WRun(C)}$ and $Z_{WLch2C)}$, are defined by

$$Z_{WRun(C)}\left(t_i\right) \; = \; \left(1 \; - \; \frac{\Delta t}{\tau_{Run(C)}}\right)Z_{WRun(C)}\left(t_{i-1}\right) \; + \; \frac{\Delta t}{\tau_{Run(C)}}F_{WRun(C)}\left(t_i\right)$$

$$\tag{B2}$$

$$Z_{WLch2(C)}\left(t_i\right) \; = \; \left(1 \; - \; \frac{\Delta t}{\tau_{Lch2(C)}}\right)Z_{WLch2(C)}\left(t_{i-1}\right) \; + \; \frac{\Delta t}{\tau_{Lch2(C)}}F_{WLch2(C)}\left(t_i\right)$$

where t_i is a time step, $\tau_{Run(C)}$ and $\tau_{Lch2(C)}$ are the respective smoothing times for $F_{WRun(C)}$ and $F_{WLch2(C)}$, and Δt is the sampling time interval (1 day). The filters are initialised at $Z_{Run(C)} = 0$ and $Z_{Lch2(C)} = 0$. The filters are deactivated (that is, $Z_{WRun(C)} = F_{WRun(C)}$ and $Z_{WLch2(C)} = F_{WLch2(C)}$) when $\tau_{Run(C)} = \Delta t$ and $\tau_{Lch2(C)} = \Delta t$. The approximation in this approach is

that a single time lag is used for all cells in the catchment, irrespective of their location with respect to the catchment outlet.

Finally, the total catchment outflow or discharge is calculated as the sum of runoff and deep drainage for the whole catchment:

$$Z_{WDis(C)} = Z_{WRun(C)} + Z_{WLch2(C)} \tag{B3}$$

B2: Land surface temperature

The observation model for Land Surface Temperature (LST, T_s) is the relationship between the LST at satellite overpass time (t_p) and the air temperature (T_a) and sensible heat flux (Φ_H) at that time. Thus is Equation (M10): $T_s = T_a + \Phi_H(t_p)/(\rho_A c_{PA} G_a(t_p))$. Determination of the aerodynamic conductance (G_a) is described in Section 7.

It is necessary to account for the difference between conditions at the overpass time (t_p) and the average diurnal conditions described by the dynamic model (Appendix A). To do this, the instantaneous (t_p) values of Φ_H and T_a are expressed in terms of diurnally averaged values with the following assumptions:

$$\Phi_H(t_p) = \Phi_H(\text{daylight average}) \max\left(2\cos\left(\frac{\pi(t_p - t_{noon})}{t_{dusk} - t_{dawn}}\right), 0\right) \tag{B4}$$

$$T_a(t_p) = 0.5(T_{a\max} + T_{a\min}) + 0.5(T_{a\max} - T_{a\min})\cos\left(\frac{\pi(t_{Ta\max} - t_p)}{2(t_{Ta\max} - t_{dawn})}\right) \tag{B5}$$

where $t_{Ta\max}$ is the time of maximum temperature, and t_{dawn}, t_{noon} and t_{dusk} are respectively the times of dawn, noon and dusk. Equation (B4) assumes that the time course of heat flux is a cosine curve, and uses the fact Φ_H is averaged over daylight hours only (see Equation (A8) and associated text). Equation (B5) assumes that $T_{a\min}$ (minimum air temperature) occurs at dawn, $T_{a\max}$ (maximum) occurs at a specified time $t_{Ta\max}$, and that the temperature during the day varies cosinusoidally but not in phase with heat flux. Finally, the (diurnally averaged) sensible heat flux is related to the other energy fluxes in the surface energy balance (Raupach 2001):

$$\Phi_A^* = \Phi_E + \frac{\Phi_H}{p}; \qquad \Phi_H = p(\Phi_A^* - \Phi_E) \tag{B6}$$

where notation follows Equation (A7). The isothermal available energy flux (Φ_A^*) is given by Equation (A8), and the latent heat flux (Φ_E) is related to total evaporation by

$$\Phi_E = \rho_W \lambda_W (F_{WT} + F_{WS}) \tag{B7}$$

Combining Equations (M10) and (B4) to (B7), the end result is an expression for $T_s(t_p)$ in terms of meteorological forcing variables and fluxes and stores available to the dynamic model.

Appendix C: Parameters and Forcing Data

C1: Parameters

Parameters are required for both the dynamic and observation models. Parameters are of two classes, spatially uniform (UU) and spatially explicit (VV), where the notation refers to the generic arrays used to hold the two parameter classes in the code. Tables C1 and C2 provide complete lists of both the UU and VV parameters.

The UU parameters are assigned as numbers which apply to all grid cells in the spatial domain. The VV parameters may vary among grid cells and are assigned either through map files or as spatially uniform default values. An important distinction between UU and VV parameters is that only the UU parameters can be target variables for model-data fusion (either by parameter estimation or data assimilation methods). This is to keep the search space of target variables to a manageable size. The UU parameter values shown in Table C1 are prior estimates if the designated element of the UU parameter vector is a target variable for model-data fusion.

C2: Spatially explicit land surface properties

Three kinds of land surface property are required: surface radiative properties (albedo and emissivity), soil properties (saturated volumetric water contents, soil depths and saturated hydraulic conductivities for the two soil layers) and vegetation properties (vegetation cover fraction and the bulk aerodynamic conductance for heat). All are VV parameters, assigned through map files with optional replacement of map data for any VV element with a single, spatially uniform default value (see Table C2).

Radiative properties: The albedo is specified as a time-independent climatology derived from AVHRR satellite measurements, kindly provided by Dr Ian Grant of BoM (Pers. Comm.). The emissivity at this time is set to a uniform default value.

Soil properties: Spatially explicit soil properties for the two soil layers are based on the McKenzie and Hook (1992) and McKenzie *et al.* (2000) interpretations of the 725 soil profile forms (types) mapped in the Digital Atlas of Australian Soils (DAAS) (Northcote et al. 1960-1968). To match the spatial grid of the forcing meteorology, the 1:2,000,000 scale DAAS is rasterised, assigning the dominant soil type within each 0.05° grid cell, reducing the number of discrete soil types across the continent to 300. Pedotransfer functions (McKenzie and Hook 1992; McKenzie *et al.* 2000) then assign physical soil properties in upper and lower layers (A and B horizons) to each soil type. The translation from soil types to physical soil properties via the pedotransfer functions is done offline beforehand. The properties used here are saturated volumetric water content (θ_{Si}), soil depth (Z_{Wi}) and saturated hydraulic conductivity (K_{Si}) in soil layers 1 and 2 ($i = 1,2$).

Vegetation cover fraction: The vegetation cover fraction (v) is determined either externally or from a leaf carbon submodel. When v is externally prescribed (as for all results in this report) it is given from a remotely-sensed vegetation greenness by Equation (A13). From many possible measures of vegetation greenness we have elected to use a monthly climatology of FAPAR from the SeaWiFS satellite (Appendix E). FAPAR from SeaWiFS is a derived

product available globally at ~0.04 deg spatial and monthly time resolution (Gobron *et al.* 2002), continuously from September 1997 to June 2006. It has been resampled to 0.05 deg resolution for use here.

Two aspects of this choice require justification. First, we used FAPAR from SeaWiFS from among many satellite products (from AVHRR, MODIS, Spot-VGT and AATSR, among others; see Appendix E). SeaWiFS is used because it is a sun-synchronous satellite with on-board sensor calibration and active navigation, so that overpasses occur at the same solar time each day. This removes many of the calibration problems which have complicated interpretation of data from older satellites such as AVHRR. Of the "modern" satellites (launched since the mid-nineties), SeaWiFS provides the longest record. Its FAPAR product is free of problems such as obviously spurious noise in either space or time.

Second, we have used a monthly climatology for 1998 to 2006, rather than individual monthly values. The January climatological FAPAR map is formed as the average of the January maps for 1998 to 2006, and similarly for other months. This choice follows from the fact that nether near-real-time nor pre-1997 data are available from SeaWiFS. Therefore, for both near-real-time and historic AWAP water balance products, we use a monthly climatology over available whole years of SeaWiFS data.

Aerodynamic conductance: The aerodynamic conductance (G_a) is found as in Appendix B2.

Multipliers for spatially explicit parameters: We allow for the possibility that spatially explicit (VV) parameters may require modification. To provide flexibility to perturb the mapped physical properties while retaining the information represented by their spatial patterns, we introduce spatially uniform multipliers (m) which act on prior values (either maps or spatially uniform default values) of the albedo (a), emissivity (e), soil properties (θ_{Si}, Z_{Wi} and K_{Si} for two soil layers, $i = 1,2$), bulk aerodynamic conductance (G_a) and FAPAR.

$$a = m_a a_{(prior)}, \qquad e = m_e e_{(prior)}$$
$$\theta_{Si} = m_{\theta i}\theta_{Si(prior)}, \qquad Z_{Wi} = m_{Zi}Z_{Wi(prior)}, \qquad K_{Si} = m_{Ki}K_{Si(prior)} \qquad \text{(C1)}$$
$$G_a = m_G G_{a(prior)}, \qquad \text{FAPAR} = m_{\text{FAPAR}}\text{FAPAR}_{(prior)}$$

The starting values of these multipliers are $m = 1$ in all cases. The multipliers are spatially uniform and are therefore located in the UU array (Table C1).

The multipliers serve two different purposes. First, spatially explicit parameters provided by available map information may require modification for use in the present water balance model. An example is the soil depth: the Digital Atlas of Australian Soils gives an estimate of the physical depth of a layer in the soil profile, whereas soil depth in the model represents the depth of a layer explored by plant roots. We assume (crudely) that mapped values and model parameters are proportional, with multiplier m.

Second, multipliers provide a facility for sensitivity analysis and parameter searching for VV parameters. Because they are located in the UU array, the multipliers can be varied for sensitivity analysis and are searchable as target variables in model-data fusion.

No	Symbol (math)	Symbol (code)	Unit	Value	Description	Equation
1	c_{PT}	CoeffPT	[-]	1.26	Priestley-Taylor coeff	A6
2	c_{Ext}	CoeffBeer	[-]	0.60	Beer Law extinction coeff	A14
3	C_{L0}	CLea0	[-]	60.0	CLea0 = RhoCLeaf*LeafThick	A14
4	k_L	RateCLea	[1/d]	0.0025	rate constant for CLea decay	A15
5	k_{E1}	RateEW1	[1/d]	0.09	rate constant for water lim evap (1)	A9
6	k_{E2}	RateEW2	[1/d]	0.01	rate constant for water lim evap (2)	A9
7	β	PwrFWSoil	[-]	0.01	FWSoil ~ WRel**(PwrFWSoil+1)	A10
8	γ	PwrFWLch	[-]	2.5	FWLch ~ WRel**(PwrFWLch+1)	A12
9	α_O	alfaQ	[molC/Q]	0.04	Light Use Efficiency	A16
10	α_W	alfaWpri	[molC/W]	+0.01	prior Water Use Efficiency (use if > 0)	A16
11	m_α	alfaWmul	[-]	−0.05	multiplier for WUE from deficit (use if > 0)	A17
12	$[CO_2]_a$	CO2A	[molC/A]	380e−6	air [CO2]	A17
13	w_0	WRelA0	[-]	0.5	scale for AllocLea(WRel)	A18
14	L_{max}	rLAImax	[-]	6.0	maximum rLAI	-
15	c_{PAR}	CoeffPAR	[-]	−2.0	FracV = func(CoeffPAR,FAPAR)	A13
16	m_a	AlbedoMult	[-]	1.0	multiplier for albedo	C1
17	m_e	EmisMult	[-]	1.0	multiplier for emissivity	C1
18	$m_{\theta 1}$	WVolSat1Mult	[-]	1.0	multiplier for WVolSat1	C1
19	$m_{\theta 2}$	WVolSat2Mult	[-]	1.0	multiplier for WVolSat2	C1
20	m_{Z1}	ZSoil1Mult	[-]	1.0	multiplier for ZSoil1	C1
21	m_{Z2}	ZSoil2Mult	[-]	1.0	multiplier for ZSoil2	C1
22	m_{K1}	HySat1Mult	[-]	0.8	multiplier for HySat1	C1
23	m_{K2}	HySat2Mult	[-]	0.8	multiplier for HySat2	C1
24	m_G	GaeroMult	[-]	1.0	multiplier for Gaero	A8, B4
25	m_{FAPAR}	FAPARMult	[-]	1.0	multiplier for FAPAR	C1
26	$t_{Ta\max}$	TimeTxFrac	[-]	0.75	Tmax time as fraction of (TDawn, TDusk)	B6
27	-	cN0	[-]	0.12	ZNDVI = Sum[cNi*FracV^i]	-
28	-	cN1	[-]	0.90	ZNDVI = Sum[cNi*FracV^i]	-
29	-	cN2	[-]	-0.45	ZNDVI = Sum[cNi*FracV^i]	-
30	$\tau_{Run(C)}$	TZRunDef	[d]	1.0	default runoff timescale (use if >0)	B2
31	$\tau_{Lch2(C)}$	TZLchDef	[d]	1.0	default leach timescale (use if >0)	B2

Table C1: Spatially uniform (UU) parameters for the WaterDyn model (version WaterDyn25M).

No	Symbol (math)	Symbol (code)	Unit	Default value	Description	Equation
1	-	CatchMap	[-]	-9999	catchment ID map (must be first VV)	-
2	-	LatDeg	[-]	-36.0	latitude (degrees)	-
3	-	Altitude	[m]	0.0	altitude = elevation	-
4	a	Albedo	[-]	0.1	Albedo	A8
5	e	Emis	[-]	1.0	Emissivity	A8
6	θ_{S1}	WVolSat1	[-]	0.4	saturated volumetric water content (1)	A1
7	θ_{S2}	WVolSat2	[-]	0.4	saturated volumetric water content (2)	A1
8	Z_{W1}	ZSoil1	[m]	0.2	soil depth (1)	A1, C1
9	Z_{W2}	ZSoil2	[m]	1.0	soil depth (2)	A1, C1
10	K_{S1}	HySat1	[m/d]	0.02	saturated hydraulic conductivity (1)	A12, C1
11	K_{S2}	HySat2	[m/d]	0.001	saturated hydraulic conductivity (2)	A12, C1
12	G_a	Gaero	[m/s]	0.02	aerodynamic conductance for heat	A8, B4
13	FAPAR	FAPAR01	[-]	0.5	FAPAR: Jan	A13
14	FAPAR	FAPAR02	[-]	0.5	FAPAR: Feb	A13
15	FAPAR	FAPAR03	[-]	0.5	FAPAR: Mar	A13
16	FAPAR	FAPAR04	[-]	0.5	FAPAR: Apr	A13
17	FAPAR	FAPAR05	[-]	0.5	FAPAR: May	A13
18	FAPAR	FAPAR06	[-]	0.5	FAPAR: Jun	A13
19	FAPAR	FAPAR07	[-]	0.5	FAPAR: Jul	A13
20	FAPAR	FAPAR08	[-]	0.5	FAPAR: Aug	A13
21	FAPAR	FAPAR09	[-]	0.5	FAPAR: Sep	A13
22	FAPAR	FAPAR10	[-]	0.5	FAPAR: Oct	A13
23	FAPAR	FAPAR11	[-]	0.5	FAPAR: Nov	A13
24	FAPAR	FAPAR12	[-]	0.5	FAPAR: Dec	A13

Table C2: Spatially explicit (VV) parameters for the WaterDyn model (version WaterDyn25M). Each parameter is assigned spatially either with a map file or as a spatially uniform value shown in the "default value" column.

C3: Meteorological forcing

The model requires the following gridded meteorological forcing data: precipitation (F_{WPrec}), downward solar irradiance ($\Phi_{S\downarrow}$), maximum and minimum air temperatures ($T_{a\max}$, $T_{a\min}$). The project uses these meteorological data at daily time resolution for the period 1 January 1900 to present, gridded across the Australian continent at 0.05 deg spatial resolution. Data in this form are available from two sources.

1. *BoM gridded weather data archive:* The Bureau of Meteorology (BoM) generates gridded (0.05 deg) daily precipitation, downward solar irradiance and maximum and minimum air temperatures operationally, in a companion AWAP project (Jones *et al.* 2007). Rainfall data are available for 1900 to present, temperatures from 1911 to present and solar irradiance from 1990 to present. The solar irradiance data are obtained using satellite imagery from geostationary meteorological satellites. These data are transferred weekly from BoM (Melbourne) to CMAR (Canberra) and used to generate near-real-time AWAP water balance products. For historic runs from 1900 to present, missing solar irradiance data in the BoM weather archive, including the period 1900 to 1989 and any instrument-related pixel losses after that, are replaced with monthly climatological data for 1990 to 2007. Missing temperatures for 1900 to 1910 are replaced with a monthly temperature climatology from the nearest 30-year period, 1911 to 1940.

2. *SILO gridded weather data archive:* An alternative source of weather data is the SILO dataset (Jeffrey *et al.* 2001), which provides gridded (0.05 deg) daily precipitation, ground-based downward solar irradiance and maximum and minimum air temperatures for 1900 to near-present for all variables (data available for this project terminate in mid-2007).

Appendix D: Land Surface Temperature Algorithm

Land surface temperature (LST) estimation from infrared satellite data is problematic due mainly to atmospheric composition (particularly the water vapour component) and the emissivity of the Earth's surface (Prata 1993; Prata 1994). Of these, emissivity is the larger error source as it can be highly spatially and temporally variable because it is dependent on the type, condition and mix of land cover (see below for justification).

Advances have been made in developing algorithms that calculate an LST that is representative of the pixel size of the satellite data. For AVHRR the approach is the so-called "split-window" method where the differential absorption between two closely spaced channels is used to assess and correct for the water vapour content of the atmosphere. The split window algorithm used in this work is (Sobrino and Raissouni 2000):

$$
\begin{aligned}
\text{LST} = {}& T_{11} + 1.40\left(T_{11} - T_{12}\right) + 0.32\left(T_{11} - T_{12}\right)^2 \\
& + 0.83 + \left(57 - 5W\right)\left(1 - \varepsilon\right) - \left(161 - 30W\right)\Delta\varepsilon
\end{aligned}
\tag{D1}
$$

where T_{11} and T_{12} are the brightness temperatures in the 11 and 12 micron channels, W is the precipitable water content of the atmosphere (in g cm^{-2} or cm liquid water), ε is the channel-average emissivity and $\Delta\varepsilon$ is the difference between channel emissivities. The emissivity and $\Delta\varepsilon$ are obtained by consideration of whether the surface is bare soil, partially vegetated or fully vegetated, as determined from the NDVI (following Sobrino and Raissouni 2000). In principle the water vapour can be derived from the data themselves but in practice this proves to be a relatively noisy determination. Until we have refined this method, the value of W is interpolated from the NCEP 2.5 deg 6 hourly global reanalysis fields (Kalnay *et al.* 1996).

For AATSR, an optimised split-window algorithm is (Coll *et al.* 2006):

$$
\begin{aligned}
\text{LST} = {}& T_{11N} + 0.04 + 0.94\left(T_{11N} - T_{12N}\right) + 0.25\left(T_{11N} - T_{12N}\right)^2 \\
& + 45\left(1 - \varepsilon\right) - 55\Delta\varepsilon
\end{aligned}
\tag{D2}
$$

where T_{11N} and T_{12N} are the 11 and 12 nadir micron channels, and again ε is the channel-average emissivity and $\Delta\varepsilon$ is the difference between channel emissivities. Simulation studies (Coll *et al.* 2006) show that this algorithm has little sensitivity to atmospheric precipitable water (a 1 cm increase caused a decrease in estimated LST of less than 1°C), but that an uncertainty in surface emissivity of ±0.005 resulted in an uncertainty in LST of ±0.4 degC.

For determination of AATSR LST we use the quadratic coefficients in Equation (D2), but we calculate ε and $\Delta\varepsilon$ by the same (Sobrino and Raissouni) method used for AVHRR. The AVHRR NDVI-based thresholds for these fractional cover types were scaled by the ratio of maximum AATSR NDVI to maximum AVHRR NDVI. Our NDVI estimates are taken from monthly composites of both AATSR and AVHRR over Australia in 2003 (Paget and King 2005). The minimum AATSR NDVI used in present ε and $\Delta\varepsilon$ calculations is 0.03 and the maximum is 0.75.

Appendix E: Remote Sensing Data Sources

This section summarises information on several remote sensing data sources used here. These include data from the following sensors: (1) NOAA-AVHRR; (2) MODIS, (3) SeaWiFS, (4) SPOT-VGT and (5) AATSR. Of these, the NOAA time series is the only one operationally supported for the next decade. In addition we have used data from (6) the GlobCarbon project, a compilation by the European Space Agency of satellite-based vegetation data from several sources. Details are summarised in Table E1.

NOAA-AVHRR: The NOAA polar-orbiting satellites have carried AVHRR instruments operationally since the launch of NOAA-6 in 1979. The AVHRR sensor records data in 5 spectral bands of the electromagnetic spectrum: (1) red (580-680 nm); (2) Near Infrared (NIR) (725-1100 nm); (3) 3.55-3.93 μm; (4) 10.5-11.3 μm; and (5) 11.5-12.5 μm. The spacecraft are in sun-synchronous polar orbits of approximately 100 min duration at an altitude of about 700km. Each orbit comprises an ascending and a descending component corresponding to whether the spacecraft is travelling northwards or southwards respectively. The overpass time of the ascending node is nominally around 1330 local solar time but changes slowly with orbital drift (typically at 0.25 to 0.5 h/y). The spatial resolution of AVHRR data is 1.1 km at nadir (the point directly beneath the satellite), increasing to 5.4 km at the edge of the swath where the scan angle is 55°. For details see Cracknell 1997.

The CSIRO AVHRR archive is maintained by CSIRO Marine and Atmospheric Research. Between 1981 and 1986 the basic data are coarse-resolution (about 8 km at nadir) Global Area Coverage (GAC) data Cracknell 1997 provided by NOAA. These data are also used to supplement the limited full resolution data from 1986 until 1992 when the data began to be comprehensively archived from direct broadcasts from the NOAA satellites received in Australia. Since 1992, the data from a number of Australian reception stations have been combined by stitching the different segments from each station to eliminate redundancy and produce a single best-quality scene for each overpass (King 2000; Lovell *et al.* 2003; King 2003). The daily coverage in this archive is an area of approximately 50 million km^2, including the entire Australian land surface and surrounding regions to at least 2000km from the Australian coast. Since 1992, coverage of this area has been obtained four times daily.

The Australian AVHRR archive is available in two forms, both used in this work.

1. The "BPAL AVHRR" archive has been compiled from various sources and processed to produce complete, cloud-free, calibrated, geolocated, continental coverage of all AVHRR channels as seen by the afternoon overpass, at 0.05 deg (about 5 km) spatial resolution, covering land only, for 1981 to present. Compositing (maximum-NDVI), to approximately 10-day time resolution, was used as a first-order means of removing cloud effects. Additional "BISE" (Best Index Slope Extraction) filtering was used to further reduce cloud contamination and the effects of variations in view and sun angles (Lovell and Graetz 2001). The "BPAL" terminology arises because this archive extends a series available from NASA for the period 1981-1994 called the PAL (Pathfinder AVHRR Land) dataset, using BISE filtering. The BPAL AVHRR archive is used here for analysis of land condition.

2. The "CATS" (CSIRO AVHRR Time Series) archive is currently available from 1992 to present. This archive includes all AVHRR channels at a nominal spatial resolution of 1.1 km at nadir and temporal resolution of up to four overpasses per day. The data are

calibrated and geolocated, with other processing in several versions described in Table B2.

MODIS: The Moderate Resolution Imaging Spectroradiometer (MODIS) is a key instrument aboard the Terra and Aqua satellites, launched in December 1999 and March 2002, respectively. The orbit of Terra around the Earth is timed so that it passes from north to south in the morning (about 1030 local solar time), while Aqua passes south to north in the afternoon (about 1330 local solar time). Terra MODIS and Aqua MODIS each view the entire Earth surface every day, acquiring data in 36 spectral bands ranging from 405 nm to 14.4 μm. The spatial resolution of MODIS data is 250 m for one spectral band in the visible and one in the NIR, 500 m in 5 visible to mid-infrared bands and 1000 m in all other bands. The data used in this study are standard global products obtained from NASA by DLT tapes (due to the enormous amount of data) and subsequently uploaded to the CSIRO MODIS Data Storage Cluster. These standard products may also be downloaded by FTP from the NASA website.

SeaWiFS: The Sea-viewing Wide Field-of-view Sensor (SeaWiFS) is carried on the SeaStar satellite launched on August 1, 1997 as part of NASA's "Mission to Planet Earth". The SeaStar maintains a sun-synchronous 705 km altitude orbit, with a north-to-south equatorial crossing at 12:20 local solar time, covering the Earth's surface once a day. The SeaWiFS sensor has 8 bands in the 402 nm (violet) to 885 nm (NIR) range. It differs from the AVHRR sensor in that it can tilt to avoid sunglint on the sea. SeaWiFS transmits local area coverage (LAC) data in real-time at a spatial resolution of 1.1km, with global area coverage (GAC) data archived and transmitted at 4.5 km resolution. The data used in this project are the SeaWiFS level 3 monthly NDVI product at 4.5 km resolution and the FAPAR product of Gobron *et al.* (2002). Information about the SeaWiFS project can be obtained from http://oceancolor.gsfc.nasa.gov/SeaWiFS/

SPOT-VGT: The "Vegetation" (VGT) instrument is a wide-field sensor carried as part of the SPOT 4 and 5 satellite payloads launched on March 24, 1998 and May 4, 2002. The SPOT 4/5 satellites maintain a sun-synchronous polar orbit at ~830 km altitude. The Vegetation instrument has 4 non-contiguous bands in the visible, NIR, and MIR range (430-1750 nm), with a swath width of 2250 km at 1.165 km spatial resolution, allowing 90% global coverage in one day. Several products are available, including daily and ten-day synthesis products (S10) at full resolution as well as 4 km and 8 km reduced resolutions. The VGT images are processed and archived by the Belgian research institute VITO. The data used in this project are the SPOT VGT-S10 NDVI series at 1 km resolution.

AATSR: The Advanced Along Track Scanning Radiometer is a 1km resolution sensor with a relatively narrow (512 km) swath carried on ESA's ENVISAT platform in a sun synchronous polar orbit with an overpass time of 1030 and a revisit time of 35 days. Although three overpasses a day cover Australia, the narrowness of the swath means that complete coverage is only obtained every several days. The sensor has 7 bands ranging from the visible through to the thermal infra-red; in particular it has 11 and 12 micron bands that match those of the AVHRR sensor. Two key characteristics of AATSR are the high quality of its thermal calibration, and that it uses a conical scan to obtain a dual view of the swath, thereby allowing improved correction for angular and atmospheric effects. AATSR is a successor instrument to ATSR and ATSR2 which were flown on earlier ESA missions. The Top Of Atmosphere L1B product has been used here to derive Land Surface Temperature measurements from the 1km brightness temperature channels. Gridded LSTs are available from ESA, but only aggregated to lower spatial resolution. We are investigating the possibility of operational inclusion of these data in near real time.

GlobCarbon: The GlobCarbon project is part of the Global Terrestrial Observing System coordinated by the FAO. GlobCarbon uses data supplied by the European Space Agency to produce a range of fully calibrated satellite estimates of global land surface properties (fire, albedo, fAPAR, LAI, vegetation growth cycle) which are nearly independent of the original data source. The focus of the project is on the seven years 1997 to 2003, a period of overlap between various satellite measurements. GlobCarbon products and services are managed by VITO and various other European agencies, and distributed by VITO at http://geofront.vgt.vito.be/geosuccess/. The GlobCarbon data available for this project were monthly LAI from 1999 to 2002, generated from SPOT VGT and ATSR data.

Sensor	Agency (Country)	Platform (Launch)	Swath (km)	Revisit time (overpass time)	Spectral Bands	Nadir spatial resolution (m)
AVHRR		NOAA (numerous satellites)	2500	1 day (nominal: 0900, 1400)	5 bands (visible, NIR, thermal)	1100
MODIS	NASA (USA)	Terra (Dec 1999) Aqua (May 2002)	2330	1-2 days (Terra: 1030) (Aqua: 1330)	36 bands (visible, NIR, MIR, thermal)	250 to 1000
SeaWiFS	NASA (USA)	SeaStar (Aug 1997)	2801 (LAC), 1502 (GAC)	1 day (1220)	8 bands (visible, NIR)	1100 (LAC) 4500 (GAC)
VGT	CNES (France)	SPOT 4 / 5 (Mar 1998 / May 2002)	2250	1-2 days	4 bands (visible, NIR, MIR)	1165
AATSR	ESA	Envisat (2002/02)	512	35 days (1030)	7 bands (visible, SWIR, MIR, thermal)	1000

Table E1: Details of satellite sensors.

Appendix F: Operational System

Overview: Figure F1 gives a conceptual flow diagram of the AWAP operational system (http://www.csiro.au/awap/). The system runs on a weekly basis to provide near-real-time estimates of continental soil moisture and water fluxes, averaged over the previous week.

For operation in forward mode (without data assimilation), the operational system carries out the following basic steps:

1. Download gridded daily meteorological forcing data (rainfall, solar radiation, maximum and minimum temperature) from the Bureau of Meteorology (BoM). These data are generated operationally by a companion AWAP project.

2. Apply quality assurance checks to BoM meteorological forcing data.

3. Obtain assimilation data as available: satellite imagery of vegetation greenness (AVHRR-NDVI) and surface temperatures (AVHRR), and catchment outflow data from unimpaired, gauged catchments. (In forward mode these data are passed through the model for comparisons with output, but not assimilated).

4. Obtain model initial conditions, from the end of previous run.

5. Set model parameters.

6. Run the WaterDyn model for 1 week, producing daily and weekly-averaged output.

7. Calculate output statistics, mainly percentile ranks referenced to the standard climatological reference period 1961-1990.

8. Convert model output to Arcview-compatible form suitable for transfer to clients, and to graphical forms suitable for web-based display.

9. Update the web interface.

10. Update archives, logging and run documentation files.

Hardware: Two DELL 2950 servers, each with two Dual-core processors, 8GB of ram and 1.5TB of RAID5 disk have been purchased and installed to support the project. These have been configured in parallel to provide simultaneous operational and development systems, with the development system being available to take over immediately in the event of a compromise to the operational machine. Data required for each run are hosted on a number of other servers within CMAR and are archived separately.

Software: The software comprises the WaterDyn model itself, data filters to process spatial input data (daily meteorological fields, satellite observations) into the format required by the model, and an output processor to convert and analyse the results of the model run. Additional code, in the form of multiple Perl scripts, is used to integrate these programs, pull data from network servers, log run parameters and anomalies, archive outputs, and push results to the presentation server. A standardised, automated directory structure is used to manage inputs, outputs, archival and documentation.
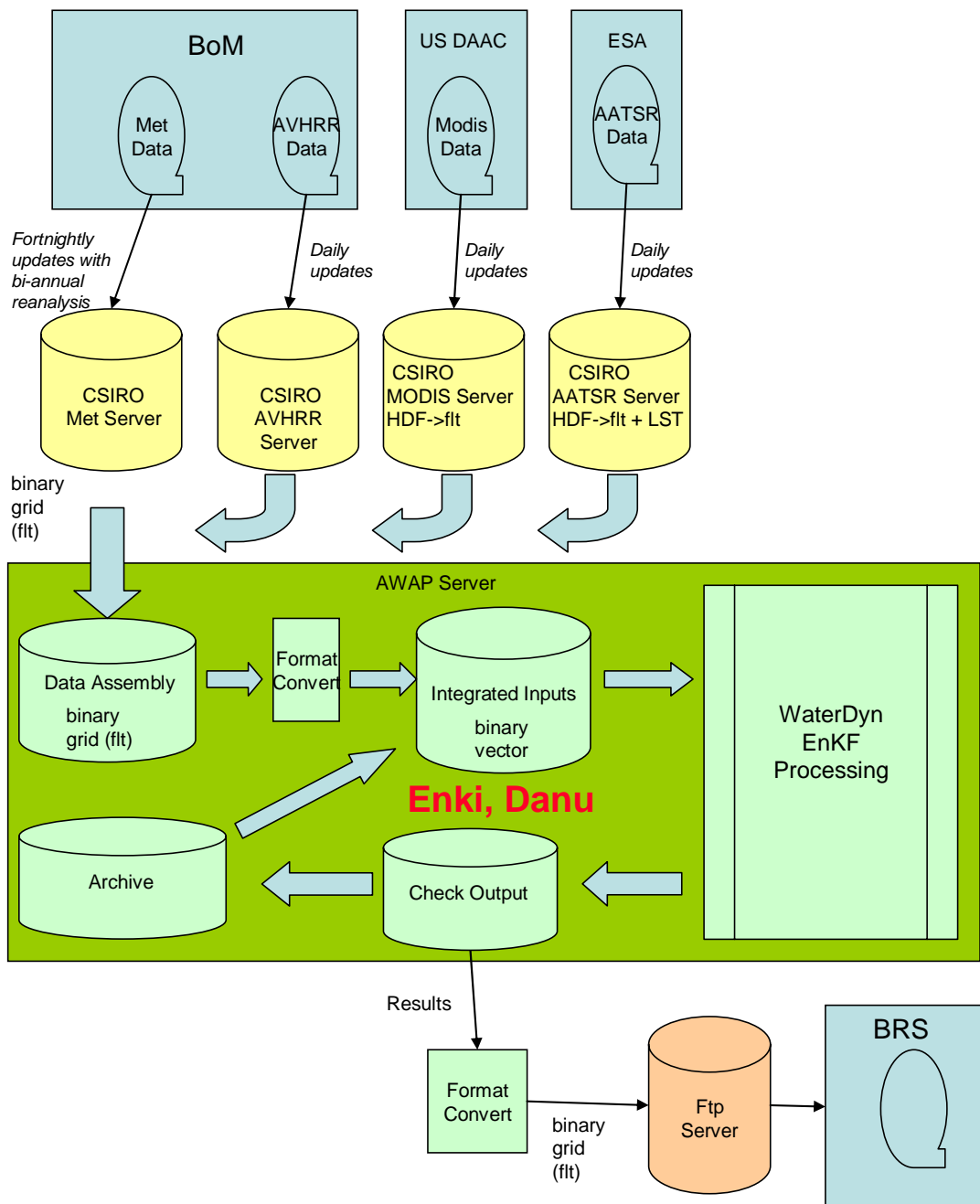
Figure F1: Flow diagram of prototype operational system.

Data: The data streams obtained in near real time are as follows.

1. *Meteorological data:* These are provided by BoM from their website. Since mid-March 2007, daily fields for rainfall, maximum and minimum temperature have been automatically downloaded, reformatted and stored in a local archive on a daily basis.

More recently daily solar radiation has been provided. A script to automatically select, reformat and ingest these data for input to the model has been developed.

2. *AVHRR data:* The NOAA AVHRR instrument provides continental observations of brightness temperature (BT) several times daily. BoM are providing the AVHRR data feed. In CMAR we are developing algorithms to compute land surface temperature (LST) from BT, and are providing support to the BoM with base processing software (CAPS), compositing code, and a system to provide enhanced quality base data in near real time. A 15 year time series of AVHRR BT data has been processed and converted to LST for model testing. It has also been used to successfully develop the ingest pathway for the near real time data feed. A near real time source of atmospheric precipitable water is needed for the LST algorithm. Presently this is obtained from the NCEP global analysis.

3. *AATSR data:* The Advanced Along Track Scanning Radiometer provides highly accurate brightnesss temperature measurements with continental coverage every three days. We have implemented an LST algorithm and processed an historical time series of 3 years of AATSR data for use in the model testing and development. It is ingested into the model by an almost identical route to AVHRR data.

4. *MODIS:* Daily fields of LST are produced by the Land Processes DAAC in the USA. We have automated the process of downloading the 17 separate tiles required to cover Australia each day. Scripts have been developed and tested to mosaic, remap and reformat these tiles into continental fields suitable for ingest into the model.

5. *Runoff:* Stream runoff data is available for many catchments historically. It is possible that the CSIRO Water Resources Observation Network and/or the BoM water monitoring initiative will be able to provide these data in near real time. If so, the model can use them and they will be ingested.

Outputs: The output of the model runs is archived for three purposes: (1) as input to the next run, (2) documentation purposes, and (3) for delivery to BRS. An externally accessible FTP server is in place to enable delivery. As the model development is still continuing and the operational directory structure evolves, it has not yet been practical to automate this stage of the process, though it is under active consideration.

References

Beven KJ (1995) Linking parameters across scales - subgrid parameterizations and scale-dependent hydrological models. *Hydrological Processes* **9**:507-525

Cesaraccio C, Spano D, Duce P, Snyder RL (2001) An improved model for determining degree-day values from daily temperature data. *International Journal of Biometeorology* **45**:161-169

Coll C, Caselles V, Galve JM, Valor E, Niclos R, Sanchez JM (2006) Evaluation of split-window and dual-angle correction methods for land surface temperature retrieval from Envisat/Advanced Along Track Scanning Radiometer (AATSR) data. *J. Geophys. Res. Atmos.* **111**

Cracknell AP (1997) *The advanced very high resolution radiometer (AVHRR)*. Taylor and Francis, London and Bristol, PA,

Gobron N, Pinty B, Mélin F, Taberner M, Verstraete MM (2002) Sea Wide Field-of-View Sensor (SeaWiFS) - an optimized FAPAR algorithm - theoretical basis document. JRC Publication No. EUR 20148 EN, Institute for Environment and Sustainability, Ispra, Italy, 20 pp

Jeffrey SJ, Carter JO, Moodie KB, Beswick AR (2001) Using spatial interpolation to construct a comprehensive archive of Australian climate data. *Environmental Modelling & Software* **16**:309-330

Jones DA, Wang W, Fawcett R (2007) Climate data for the Australian Water Availability Project: final Milestone Report. National Climate Centre, Bureau of Meteorology, Melbourne

Jupp DLB, Culvenor DS, Lovell JL, Newnham GJ, Strahler AH, Woodcock CE (2008) Estimating forest LAI profiles and structural parameters using a ground based laser called "Echidna®". *Tree Physiol.* **In press**

Kalnay E, Kanamitsu M, Kistler R, Collins W, Deaven D, Gandin L, Iredell M, Saha S, White G, Woollen J, Zhu Y, Chelliah M, Ebisuzaki W, Higgins W, JANOWIAK J, Mo KC, Ropelewski C, Wang J, Leetmaa A, Reynolds R, Jenne R, Joseph D (1996) The NCEP/NCAR 40-year reanalysis project. *Bull. Amer. Meteorol. Soc.* **77**:437-471

King EA (2000) Stitching the Australian 1-km archive. Proceedings of the Land EnvSat Workshop, 10th Australasian Remote Sensing and Photogrammetry Conference, Adelaide, Australia, 2000, CSIRO, pp 41-50

King EA (2003) The Australian AVHRR data set at CSIRO/EOC: origins, processes, holdings and prospects. EOC Report 2003/04, CSIRO Earth Observation Centre, Canberra, ACT

Kowalczyk EA, Wang YP, Law RM, Davies HL, McGregor JL, Abramowitz G (2006) The CSIRO Atmosphere Biosphere Land Exchange (CABLE) model for use in climate models and as an offline model. CSIRO Marine and Atmospheric Research Paper 013, CSIRO Marine and Atmospheric Research, Melbourne, Australia

Liu Y, de Jeu RAM, van Dijk AIJM, Owe M (2007) TRMM-TMI satellite observed soil moisture and vegetation density (1998-2005) show strong connection with El Nino in eastern Australia. *Geophys. Res. Lett.* **34**:doi:10.1029/2007GL030311

Lovell JL, Graetz RD (2001) Filtering pathfinder AVHRR land NDVI data for Australia. *Int. J. Remote Sens.* **22**:2649-2654

Lovell JL, Graetz RD, King EA (2003) Compositing AVHRR data for the Australian continent: seeking best practice. *Canadian Journal of Remote Sensing* **29**:770-782

McKenzie NJ, Hook J (1992) Interpretations of the Atlas of Australian Soils. Technical Report 94/1992, CSIRO Division of Soils, Canberra

McKenzie NJ, Jacquier DW, Ashton LJ, Cresswell HP (2000) Estimation of soil properties using the Atlas of Australian Soils. CSIRO Land and Water Technical Report 11/00, CSIRO Land and Water, Canberra, Australia, 24 pp

Nicholls N (2004) The changing nature of Australian droughts. *Climatic Change* **63**:323-336

Nicholls N, Lavery B, Frederiksen C, Drosdowsky W, Torok S (1996) Recent apparent changes in relationships between the El Nino - Southern oscillation and Australian rainfall and temperature. *Geophys. Res. Lett.* **23**:3357-3360

NLWRA (2001a) Australian Agriculture Assessment 2001. National Land and Water Resources Audit, Commonwealth of Australia, Canberra, Australia, 480 pp

NLWRA (2001b) Australian Water Resources Assessment 2000. National Land and Water Resources Audit, Commonwealth of Australia, Canberra, Australia, 160 pp

Northcote KH, with Beckmann GG, Bettenay E, Churchward HM, Van Dijk DC, Dimmock GM, Hubble GD, Isbell RF, McArthur WM, Murtha GG, Nicolls KD, Paton TR, Thompson CH, Webb AA and Wright MJ (1960-1968) Atlas of Australian Soils, Sheets 1 to 10. With explanatory data. CSIRO Australia and Melbourne University Press, Melbourne.

Paget MJ, King EA (2005) Delivering AATSR data to Australian users and an application to Australian NDVI. Proceedings of the MERIS (A)ATSR Workshop 2005 (ESA SP-597), Sep 26, 2005-Sep 30, 2005, ESRIN, pp Published on CDROM, p. 11.1

Power S, Casey T, Folland C, Colman A, Mehta V (1999) Interdecadal modulation of the impact of ENSO on Australia. *Climate Dynamics* **15**:319-324

Prata AJ (1993) Land surface temperatures derived from the advanced very high resolution radiometer and the along-track scanning radiometer 1. Theory. *J. Geophys. Res. Atmos.* **98**:16689-16702

Prata AJ (1994) Land surface temperatures derived from the advanced very high resolution radiometer and the along-track scanning radiometer 2. Experimental results and validation of AVHRR algorithms. *J. Geophys. Res. Atmos.* **99**:13025-13058

Press WH, Teukolsky SA, Vetterling WT, Flannery BP (1992) *Numerical Recipes in Fortran 77: The Art of Scientific Computing*. Cambridge University Press, Cambridge, UK, 934 pp

Priestley CHB, Taylor RJ (1972) On the assessment of surface heat flux and evaporation using large-scale parameters. *Mon. Weather Rev.* **100**:81-92

Prigogine I (1961) *Introduction to Thermodynamics of Irreversible Processes*. Interscience Publishers, New York, 119 pp

Raupach MR (1998) Influences of local feedbacks on land-air exchanges of energy and carbon. *Global Change Biol.* **4**:477-494

Raupach MR (2000) Equilibrium evaporation and the convective boundary layer. *Boundary-Layer Meteorol.* **96**:107-141

Raupach MR (2001) Combination theory and equilibrium evaporation. *Quart. J. Roy. Meteorol. Soc.* **127**:1149-1181

Raupach MR (2005) Dynamics and optimality in coupled terrestrial energy, water, carbon and nutrient cycles. In: Franks SW, Sivapalan M, Takeuchi K, Tachikawa Y (eds) *Predictions in Ungauged Basins: International Perspectives on the State-of-the-Art and Pathways Forward (IAHS Publication No. 301)*. IAHS Press, Wallingford, pp 223-238

Raupach MR (2007) Carbon, Climate and Humans: Australia in the Earth System. In: Hollis A, Jemmeson V (eds) *Physical processes and modelling of the water and carbon cycle: extended abstracts of the first annual CAWCR Modelling Workshop*. Bureau of Meteorology Research Centre Report No. 133, Australian Bureau of Meteorology, Melbourne, pp 75-78

Raupach MR, Barrett DJ, Briggs PR, Kirby JM (2005a) Simplicity, complexity and scale in terrestrial biosphere modelling. In: Franks SW, Sivapalan M, Takeuchi K, Tachikawa Y (eds) *Predictions in Ungauged Basins: International Perspectives on the State-of-the-Art and Pathways Forward (IAHS Publication No. 301)*. IAHS Press, Wallingford, pp 239-274

Raupach MR, Briggs PR (2005) Response of Australian mean evaporation and runoff to long-term variability in precipitation. Technical Report for the Bureau of Rural Science, CSIRO Marine & Atmospheric Research, Canberra, Australia

Raupach MR, Briggs PR, King EA, Paget M, Trudinger CM (2007) Australian Water Availability Project (AWAP), CSIRO Marine and Atmospheric Research Component: Final Report for Phase 2. CSIRO Marine and Atmospheric Research, Canberra, Australia, 38 pp

Raupach MR, Rayner PJ, Barrett DJ, DeFries RS, Heimann M, Ojima DS, Quegan S, Schmullius CC (2005b) Model-data synthesis in terrestrial carbon observation: methods, data requirements and data uncertainty specifications. *Global Change Biol.* **11**:10.1111/j.1365-2486.2005.00917.x

Raupach MR, Trudinger CM, Briggs PR, King EA (2006) Australian Water Availability Project, CSIRO Marine and Atmospheric Research (Earth Observation) Component: Final Report. Report for the Australian Government Department of Agriculture, Fisheries and Forestry, CSIRO Marine and Atmospheric Research, Canberra, Australia, 56 pp

Ross PJ (2003) Modeling soil water and solute transport - Fast, simplified numerical solutions. *Agronomy Journal* **95**:1352-1361

Sobrino JA, Raissouni N (2000) Toward remote sensing methods for land cover dynamic monitoring: application to Morocco. *Int. J. Remote Sens.* **21**:353-366

Swinbank WC (1963) Long-wave radiation from clear skies. *Quart. J. Roy. Meteorol. Soc.* **89**:339-348

Trudinger CM, Raupach MR, Rayner PJ, Enting IG (2008) Using the Kalman filter for parameter estimation in biogeochemical models. *Environmetrics* **19**:doi:10.1002/env.910

Trudinger CM, Raupach MR, Rayner PJ, Kattge J, Liu Q, Pak B, Reichstein M, Renzullo L, Richardson AD, Roxburgh SH, Styles J, Wang YP, Briggs P, Barrett D, Nikolova S (2007) OptIC project: An intercomparison of optimization techniques for parameter estimation in terrestrial biogeochemical models. *Journal of Geophysical Research-Biogeosciences* **112**:Art. No. G02027

von Caemmerer S (2000) Biochemical models of leaf photosynthesis. Techniques in plant sciences, no. 2, CSIRO Publishing, Collingwood, Australia, 165 pp

Wolter K, Timlin MS (1993) Monitoring ENSO in COADS with a seasonally adjusted principal component index. Proc. of the 17th Climate Diagnostics Workshop, Norman, OK, NOAA/N MC/CAC, NSSL, Oklahoma Clim. Survey, CIMMS and the School of Meteor., Univ. of Oklahoma, 52-57. 1993, University of Oklahoma

Wolter K, Timlin MS (1998) Measuring the strength of ENSO - how does 1997/98 rank? *Weather* **53**:315-324